Received: 21 January 2019 | Revised: 13 May 2019 | Accepted: 14 May 2019

DOI: 10.1002/wsbm.1457

ADVANCED REVIEW

WIREs SYSTEMS BIOLOGY AND MEDICINE WILEY

Multiscale modeling of the neuromuscular system: Coupling neurophysiology and skeletal muscle mechanics

Oliver Röhrle[1,2] | Utku Ş. Yavuz[1,3] | Thomas Klotz[1,2] | Francesco Negro[4] | Thomas Heidlauf[5]

[1]Institute for Modelling and Simulation of Biomechanical Systems, University of Stuttgart, Stuttgart, Germany

[2]Stuttgart Center for Simulation Sciences (SC SimTech), University of Stuttgart, Stuttgart, Germany

[3]Biomedical Signals and Systems, Universiteit Twente, Enschede, The Netherlands

[4]Department of Clinical and Experimental Sciences, Università degli Studi di Brescia, Brescia, Italy

[5]EPS5 – Simulation and System Analysis, Hofer pdc GmbH, Stuttgart, Germany

Correspondence
Oliver Röhrle, Institute for Modelling and Simulation of Biomechanical Systems, University of Stuttgart, Pfaffenwaldring 5a, 70569 Stuttgart, Germany.
Email: roehrle@simtech.uni-stuttgart.de

Funding information
Baden Württemberg Stiftung, Grant/Award Number: High Performance Computing II; Deutsche Forschungsgemeinschaft, Grant/Award Number: ExC 310/2 and ExC 2075

Abstract

Mathematical models and computer simulations have the great potential to substantially increase our understanding of the biophysical behavior of the neuromuscular system. This, however, requires detailed multiscale, and multiphysics models. Once validated, such models allow systematic in silico investigations that are not necessarily feasible within experiments and, therefore, have the ability to provide valuable insights into the complex interrelations within the healthy system and for pathological conditions. Most of the existing models focus on individual parts of the neuromuscular system and do not consider the neuromuscular system as an integrated physiological system. Hence, the aim of this advanced review is to facilitate the prospective development of detailed biophysical models of the entire neuromuscular system. For this purpose, this review is subdivided into three parts. The first part introduces the key anatomical and physiological aspects of the healthy neuromuscular system necessary for modeling the neuromuscular system. The second part provides an overview on state-of-the-art modeling approaches representing all major components of the neuromuscular system on different time and length scales. Within the last part, a specific multiscale neuromuscular system model is introduced. The integrated system model combines existing models of the motor neuron pool, of the sensory system and of a multiscale model describing the mechanical behavior of skeletal muscles. Since many sub-models are based on strictly biophysical modeling approaches, it closely represents the underlying physiological system and thus could be employed as starting point for further improvements and future developments.

This article is categorized under:
Physiology > Mammalian Physiology in Health and Disease
Analytical and Computational Methods > Computational Methods
Models of Systems Properties and Processes > Organ, Tissue, and Physiological Models

KEYWORDS

biophysical modeling, continuum mechanics, motor neuron, multiphysics, multiscale, neuromuscular system, skeletal muscle

1 | INTRODUCTION

The complex interplay between the neural system and the musculoskeletal system leads to movement. The muscles act hereby as actuators transforming signals from specialized neurons (motor neurons) into mechanical force and contractile motion. The nervous system is responsible for processing the signals from central (conscious and automatic control) and peripheral (sensory) pathways to consciously control movement. In this sense, the neuromuscular system consists of a complex control system that integrates supraspinal (descending) and sensory (afferent) inflow, and actuators (contracting skeletal muscles).

The *supraspinal control* comprises neural information from higher centers, that is, the motor cortex, the brain stem, cerebellum and the basal ganglia. These higher centers provide voluntary (conscious) movement initiated by thoughts or emotions as a consequence of will (Krakauer & Ghez, 2000), as well as excitation patterns for sequential performance of automated movements (Yuste, MacLean, Smith, & Lansner, 2005). The *sensory controls*, that is, the reflex loops, control the amount of contraction by sensing the length and rate of change of length (contraction velocity) of muscle fibers and tendons to provide information about the position of our body in physical space as well as tactile information about objects and environment enclosing our body. The resulting neural drive is highly adaptable and changes due to aging, fatigue, motor skill or pain, neuromuscular degeneration and spinal cord injury. The *actuators*, that is, the muscle-tendon-complexes, are composed of a hierarchical structure of extracellular matrix, of excitable (active) skeletal muscle cells and of tendinous structures connecting the excitable cells to the skeleton. Body movement is the result of a cascade of molecular processes turning chemical energy, for example, provided by the hydrolysis of adenosine triphosphate (ATP), into mechanical (contraction) and nonmechanical (heat) work.

The overall system, the *neuromuscular system*, is a complex adaptive system, in which the biophysical state of individual elements can change according to various types of tasks and conditions (physiological and pathological). There exist numerous experimental studies that scrutinize the interplay between the neural drive and the corresponding motor output under different conditions, such as aging (Enoka et al., 2003), fatigue (Gandevia, Allen, Butler, & Taylor, 1996), motor skill (Shadmehr, Smith, & Krakauer, 2010) or pain (Yavuz, Negro, Falla, & Farina, 2015), neuromuscular degeneration (Schmied, Pouget, & Vedel, 1999) and spinal cord injury (Shields, 2002). To investigate the neuromuscular system, many experimental studies link force and position control tasks to evaluate the performance of the motor system and its components, such as motor units (De Luca & Hostage, 2010; Negro, Yavuz, & Farina, 2016), spinal cord circuits (Magalhães et al., 2015; Yavuz et al., 2013), and the activity of descending tracts (Kristeva, Patino, & Omlor, 2007; Ushiyama et al., 2012). Despite substantial amount of experimental research, there exist due to the inherent complexity and the many cross-dependencies (feedback system) still substantial gaps in our physiological knowledge. The fact that many biophysical quantities are, from an experimental or ethical point of view, difficult or even impossible to determine (in particular, in human subjects and in vivo) makes our endeavor to gain a deeper understanding of the neuromuscular system an even harder challenge.

Hence, to improve our understanding of the causality relation between neural input and motor output, one can, in addition to the experimental studies, use mathematical models to systematically analyze the physiological system and/or to augment missing data with in silico data. In this respect, mathematical modeling has the advantage to generate data in a controlled environment. This is usually impossible in experiments. Furthermore, detailed biophysical mathematical modeling provides an efficient mean to systematically analyze and reveal complex dependencies and interactions. Although there exist already some (mainly phenomenological) models of the neuromuscular system that significantly contributed to the knowledge of neuromuscular physiology, for example, the works by Fuglevand, Winter, and Patla (1993) and Heckman and Binder (1991), detailed structural and biophysical models of skeletal muscle contraction and the motor neurons innervating the skeletal muscle, that is, the muscle control, are almost nonexistent. However, detailed biophysical models are essential for revealing the full power of an in silico laboratory to investigate the behavior of the modeled system under normal and pathological conditions.

The aim of this advanced review is to ease the barrier of developing and utilizing detailed biophysical, multiscale models of the healthy neuromuscular system. In this sense, we split the review into three parts. The first part (Section 2) is concerned with key aspects of the anatomy and physiology of the neuromuscular system and thus represents the basis for developing biophysical models of the neuromuscular system. The second part (Section 3) provides an extensive overview of existing computational models and modeling approaches of parts of the neuromuscular system. While an integrated physiological model of the neuromuscular system ideally would resolve all structures and phenomena presented in Section 2, the state-of-the-art review section also includes a brief overview on the capabilities and limitations of existing modeling approaches. In the last part (Section 4), we pick specific examples of cutting-edge models of parts of the neuromuscular system and outline how they join together to obtain a comprehensive, biophysically based model of the neuromuscular system. The specific examples, which can also be downloaded or are provided within the Supporting Information, can be considered as a tutorial. They are

chosen to introduce the general concepts of biophysical models, that is, by describing the original model of Hodgkin and Huxley, and how specific biophysical models can be used to model the neuromuscular system. For the integrated neuromuscular system model, we provide detailed descriptions of the motor neuron pool model proposed by Negro & Farina (2011), the muscle fiber model of Shorten, O'Callaghan, Davidson, and Soboleva (2007), the multiscale skeletal muscle model of Röhrle, Davidson, and Pullan (2012) and a model of the muscle spindles proposed by Maltenfort and Burke (2003). The coupled neuromuscular system model should serve as an example how we envision the next level of systemic models of complex physiological systems.

2 | ANATOMY AND PHYSIOLOGY OF THE NEUROMUSCULAR SYSTEM

2.1 | The neural system

Nerves are cord-like bundles. They are mainly made up of nerve fibers connecting the central nervous system with other parts of the body as well as with the other nerves of the peripheral network (Kleinedler, 2008). Cortical and spinal motor neurons control muscle contraction and, thus, movement. The spinal motor neurons are located in the ventral horn of the spinal cord, where they receive neural information mediated by the sensory and supraspinal systems. Each spinal motor neuron (alpha motor neuron, αMN) innervates a number of extrafusal muscle fibers and initiates contractions through a train of electrical signals called action potentials. This excitation-contraction unit consisting of one αMN and its innervated fibers is termed motor unit.

However, αMNs are not the only lower motor neuronal system involved in motor control. The striated portion of intrafusal muscle fibers are innervated by the so-called gamma motor neuron (γMN) or fusimotor neuron. The explicit assignment of γMNs is to control the tension of intrafusal muscle fiber. Thus, the γMN tunes the sensitivity of muscle spindle, which are special receptors sensing the intrafusal muscle fiber length change and therefore provide stretch feedback to the muscle. On the other hand, γMNs does not directly contribute to muscle force generation (Michael-Titus, Revest, & Shortland, 2010). There are two different types of γMNs that relate to fast (dynamic) and slow (static) muscle stretches (Taylor, Ellaway, Durbaba, & Rawlinson, 2000). The γMNs are the final neural pathway that merely innervates the intrafusal muscle fibers. In addition, a third class of spinal motor neurons, the so-called beta motoneurons (βMNs), exists that provides both intra- and extrafusal innervation (Manuel & Zytnicki, 2011). Similar to the γMN, the βMNs have two distinct sub-classes: they control the dynamic and static sensitivity of intrafusal fibers and innervate extrafusal fibers. In this selective skeleton-intrafusal organization, the dynamic βMNs innervate bag1 intrafusal and slow contracting (S-type) muscle fibers while the static ones innervate the longest of the intrafusal chain fibers and fast contracting extrafusal muscle fibers (Bessou, Emonet-Denand, & Laporte, 1963; Boyd, Gladden, McWilliam, & Ward, 1977).

The muscle fibers themselves are embedded within a matrix of extracellular connective tissue. Each muscle fiber is a long, cylindrical, biological cell. For each joint within a musculoskeletal systems, there exist more skeletal muscles that influence the joint motion than degrees of freedom of the respective joint, that is, the system exhibits muscle redundancy. Moreover, since skeletal muscle can only contract, joint movement is achieved through the interplay between agonist and antagonist muscles. The resulting final multidirectional joint torque is therefore the output of a firm neural association between multiple muscle, where supraspinal centers control the sequential activity of the muscles acting on the joint. Within the muscular tissue, there exist sensory receptors, for example, muscle spindles and Golgi tendon organs, translating the muscle's state into neural signals, which are carried back along afferent fibers to the central nervous system. Each muscle transmits its current state to the motor neuron pool of their synergistic and antagonistic muscles via sensory afferent signals.

Figure 1 illustrates the concept of motor units and neural inflow to αMNs from some of the sensory afferent and supraspinal tracks.

2.1.1 | Action potentials

One of the main triggers of electro-physiological processes are action potentials (APs). If the membrane, which is relatively impermeable to Na^+-ions in its resting state, becomes due to a stimulus more permeable to Na^+-ions, a strong Na^+-ion influx occurs. The resulting difference between the membrane potential and the equilibrium potential of Na^+ drives the current, which is particularly strong if Na^+ is far away from its equilibrium potential. The process of changing the membrane potential to restore Na^+ equilibrium is called depolarisation. If the membrane potential exceeds a certain threshold value (approximately −55 mV), that is, the depolarisation is strong enough, voltage-gated ion-channels open and result in a large inward flux of

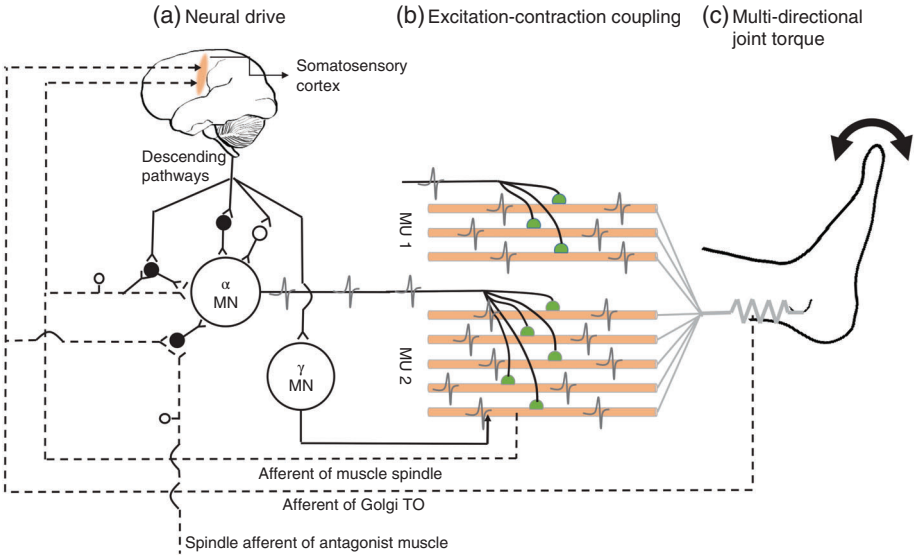

FIGURE 1 The neuromuscular pathway of movement: The figure illustrates the simplified flow of neuromuscular interaction with its three essential components: (a) neural drive comprises projection from supraspinal centers (solid lines), afferent feedbacks (dashed lines) from two exemplary proprioceptive sensory cells, that is, muscle spindle and Golgi tendon organs (Golgi TO) on spinal motor neurons (αMN) and gamma motor neurons (γMNs). The scheme includes ascending branches of sensory afferents which contribute primary somatosensory cortex (orange shade on the brain figure). (b) The excitation-contraction part shows excitation of extrafusal and intrafusal muscle fibers by αMN and γMNs, respectively. (c) The multidirectional joint torque is depicted as a resultant of the neuromuscular interaction

Na^+-ions and an outward flux of K^+-ions. Due to the dominating Na^+-flux, the membrane potential changes towards the equilibrium potential of Na^+ resulting in an inversion of the membrane voltage. As a consequence, the raised membrane voltage causes the voltage-gated Na^+-channels to close. The K^+ outward flux, which is still ongoing, repolarizes the membrane potential and the potential changes again towards the equilibrium potential of K^+ (repolarisation). After the membrane potential is repolarized, the voltage-gated K^+-channels close and the resting membrane potential is restored. This short (2–5 ms) event, in which the electrical potential of the cell is inverted and restored again, is known as action potential (AP). Figure 2 shows the typical trace of one AP.

In neurons, a short-lasting drop in the membrane potential below the resting membrane potential occurs at the end of the repolarization process. This drop is called afterhyperpolarisation. The afterhyperpolarisation potential (AHP) inhibits the development of subsequent APs by increasing the amount of stimulus required to reach the threshold value for AP generation. Note, the actual concentrations of Na^+ and K^+ hardly change throughout the AP. As a consequence, a cell can fire many thousands of APs without actively pumping Na^+ out of the cell or K^+ into it. This is important, since neurons transmit information only through the AP discharge frequency, and not through the magnitude of the AP, which is similar for each discharge.

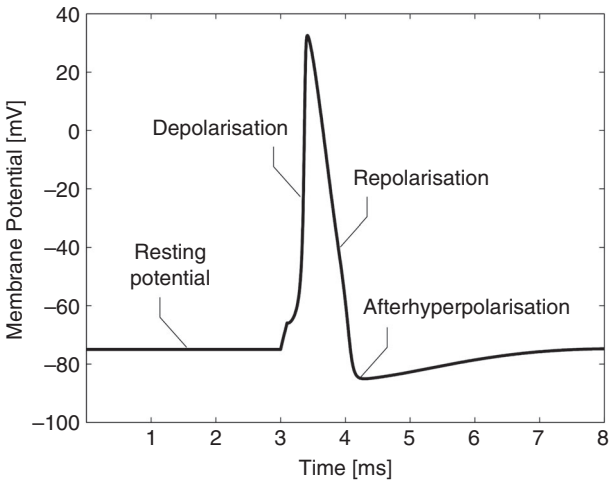

FIGURE 2 Schematic drawing of an action potential

In excitable cells, APs are used in general to transmit signals between different parts of the cell. The mechanism is as follows. The currents flowing locally into the cell while the AP spread out along the length of the cell. This yields a depolarisation of the potential of adjacent patches of the cell membrane. If the depolarisation is strong enough, voltage-gated Na^+-channels open, and the AP is reproduced in this neighboring patch. Subsequent reproductions of the AP on successive patches result in a wave-like propagation of the AP along the membrane of an excitable cell. The propagation of AP is unidirectional since the voltage-gated Na^+-channels fall, after closing, for a short period of time into an inactive state. This defines the absolute refractory period. Moreover, the patch of the axon, which has been depolarized, exhibits a higher concentration of Na^+. Naturally, the Na^+ would diffuse away from the initial stimulation area towards areas with lower Na^+ concentration. These are the two main principles defining the AP dynamics of unilateral AP propagation.

The velocity, at which APs propagate along an axon, depends on physical conditions, for example, temperature, as well as structure, that is, the inactivation duration of the voltage-activated channels, the axon diameter and the presence and extent of myelination. In neurons, for example, AP propagation speeds between 0.1 and 100 m/s have been reported (cf. Hursh, 1939; Kandel, Schwartz, Jessell, et al., 2000). In muscles fibers, Loeb, Pratt, Chanaud, and Richmond (1987) or Lieber and Fridén (2000) report APs propagation speeds of 2–10 m/s. The much faster AP propagation speeds in neurons result from an insulating myelination that is wrapped around the nerve fibers.

The differences in propagation speed are also due to the different functions of the APs. In neurons, APs transmit signals between different parts of the body, while in muscle fibers, the AP triggers cellular processes within the cell, for example, calcium release from the sarcoplasmic reticulum, which eventually leads to force generation.

2.1.2 | Motor neurons

The αMNs are specialized neurons innervating extrafusal muscle fibers. The cell body (or soma) of an αMN is located in the ventral horn of spinal cord, which is part of the central nervous system (Kandel et al., 2000). There, an αMN receives signals from other neurons, such as those of the motor cortex of the brain. Depending on the received signals, the αMN generates action potentials, which are transmitted along the αMN's axon (nerve fiber) to the muscle. At its end, the axon branches profusely, with each end linking to a muscle fiber. When the AP arrives at the neuromuscular junction, the AP propagates along the muscle fiber and commences the contraction chain in the muscle fiber. The αMNs have large and highly myelinated axons resulting in relatively high conduction velocities, which range between 30 and 60 m/s (Kakuda, Nagaoka, & Tanaka, 1992).

As stated above, the entity of an αMN and all the muscle fibers innervated by that αMN is called motor unit (MU). The MU is considered the functional unit of a skeletal muscle, since its αMN stimulates all muscle fibers belonging to the MU co-jointly, and therefore all these fibers contract in response to the stimulation simultaneously. Depending on the size of a muscle and the task assigned to it, the number of its MUs ranges from about one hundred to several thousand. In the human tibialis anterior (TA) muscle, about 300,000 muscle fibers are innervated by approximately 450 αMNs (Buchthal & Schmalbruch, 1980).

All muscle fibers associated with a motor unit are not concentrated in one part of the muscle, but distributes over (a part of) the muscle's cross-sectional area and interdigitates with other muscle fibers stemming from other motor units. The number of fibers within a motor unit can vary even within a single muscle from 10 s to 1000 s. For instance, in the human TA muscle, the number of fibers per motor unit ranges from 50 to 12,000 (Heckman & Enoka, 2004). Moreover, the human TA muscle, as all other muscles, consists of many small and few large MUs, such that the average innervation number (the ratio of the total number of muscle fibers and the number of MUs in a muscle) is about 600 (Feinstein, Lindegård, Nyman, & Wohlfart, 1955). The combination of many parallel-arranged MUs and the wide range in innervation number allows a single muscle to exert a huge spectrum of outputs, ranging from precise movements to large forces. This spectrum of outputs is controlled by the coordinated action of the MUs.

The αMNs innervating a muscle are usually clustered into an elongated motor nucleus often placed within the ventral horn of the spinal cord and potentially extending over one to four spinal cord segments (Kandel et al., 2000). The αMNs receive synaptic input from various sources, such as from the motor cortex via the corticospinal pathway, the brain stem and other descending pathways, as well as from afferent neurons, neighboring motor nuclei, spinal cord interneurons and recurrent pathways. These signals affect the neuron's membrane potential, which is described in detail in the next section.

2.1.3 | Synapses, excitatory and inhibitory postsynaptic potentials

Synapses are connections between cells, at which signals are transmitted from a neuron to another cell, which does not necessarily have to be a neuron. The following description of synapses is restricted to chemical synapses, which are present in the

neuromuscular system, and occur either between neurons or between αMNs and muscle fibers. Besides chemical synapses, electrical and immunological synapses exist in the human body.

Signals are exclusively transmitted from a signal-passing, presynaptic neuron to a signal-receiving, postsynaptic cell. The information is always passed unidirectionally. At the synapse, both the presynaptic and postsynaptic cells contain specialized structures that enable signal transmission. In the presynaptic cell, the synaptic bouton (axon terminal) contains neurotransmitters enclosed in synaptic vesicles. When an AP, which propagates along the membrane of the presynaptic cell, reaches the synapse, the membrane depolarisation causes Ca^{2+}-channels to open. The resulting inward flux of Ca^{2+}-ions increases the Ca^{2+}-concentration in the cell immediately, since the intracellular Ca^{2+}-concentration is kept at a very low level during the resting state. The rise in intracellular Ca^{2+}-concentration causes a release of neurotransmitter into the narrow space between the presynaptic and postsynaptic cells called synaptic cleft. The neurotransmitter binds to receptors embedded in the membrane of the postsynaptic cell, which either open ligand-gated ion channels (in both neurons and muscle fibers) or activate intracellular signaling pathways (only in neurons).

Assuming, first, that the presynaptic cell is an αMN, and the postsynaptic cell is a muscle fiber, the neurotransmitter is acetylcholine (ACh), and the synapse is called neuromuscular junction. The neuromuscular junction is a huge synapse, and an AP discharged by the presynaptic αMN always causes an AP in the postsynaptic muscle fiber. Excluded are pathological cases, which are not within the scope of this review. Due to this one-to-one relation between αMN APs and muscle APs, the term motor unit action potential (MUAP) is commonly used. Following the release of ACh from the αMN at the neuromuscular junction, the ACh molecules bind to ACh receptor channels in the cell membrane of the muscle fiber, which, in response, become permeable to Na^+-ions and K^+-ions. Due to the fact that Na^+-ions have in the nonactivated muscle fiber state a higher electrochemical driving force than K^+-ions, Na^+-ions are the main driver for inducing an end plate potential. Hence, the inward current carried by positive-charged Na^+-ions develops causing a depolarisation of the membrane potential, and an AP is generated at the muscle fiber membrane. The muscle AP propagates along the length of the muscle fiber, from the neuromuscular junction towards the ends of the fiber.

If the presynaptic and postsynaptic cells are neurons, the situation is more complex. First, it is assumed that the input is an ionotropic signal. In this case, the neurotransmitter-binding receptors open ligand-gated channels. Depending on the released neurotransmitter and the type of activated ion channel, the resulting change in the postsynaptic potential is excitatory or inhibitory. If the opened channel is, for example, a Na^+-channel, the resulting inward flux of Na^+-ions will depolarize the membrane of the postsynaptic neuron, that is, an excitatory postsynaptic potential (EPSP) is generated. In general, the amplitude of the EPSP resulting from a single presynaptic AP is not sufficient to exceed the threshold potential, however, postsynaptic potentials can overlap and sum up, both in space (from different nearby synapses) and time (subsequent signals at the same synapse). The most common excitatory neurotransmitter in αMNs is glutamate. In contrast, if the activated channel is a K^+-channel, an outward flux of K^+-ions will hyperpolarize the postsynaptic neuron's membrane, and an inhibitory postsynaptic potential (IPSP) is generated. The most common inhibitory neurotransmitters are γ-aminobutyric acid (GABA) and glycine (Kandel et al., 2000).

If the input, however, is neuromodulatory, the neurotransmitter-binding receptors will activate intracellular signaling pathways to control the state of excitability of the postsynaptic neuron. This is often realized through persistent inward currents that raise or lower the membrane potential relative to the previous resting membrane potential, and can last for hours. The resting membrane potential in αMNs should therefore not be considered as a static quantity, but rather as one that is constantly adjusted through neuromodulatory input to αMNs (Heckman & Enoka, 2012).

2.1.4 | Mechanisms of recruitment and rate coding

The term motor unit pool refers to all MUs in a muscle. Analogously, the term motor neuron pool denotes the entity of the neurons that subserve a single muscle. The size (axonal diameter) and consequently the electrical properties of αMNs vary across an αMN pool. Typically, an αMN pool consists of many small, low-threshold αMNs and much less large, high-threshold αMNs (Powers & Binder, 1985). Note that the size of the αMN is proportional to the size of its corresponding MU, that is, small αMNs innervate small MUs consisting of few fibers, while large αMNs innervate large MUs consisting of many fibers (Heckman & Enoka, 2012).

The αMN pool is subject to signals of different sources, viz. cortical input, afferent signals, for example, from muscle spindles, and signals from interneurons and Renshaw cells. Motor neurons integrate all the excitatory and inhibitory signals that they receive from presynaptic neurons. This causes changes in their membrane potential. Once the input is large enough such that the αMN exceeds its threshold potential, an AP is discharged. The fact that a neuron either discharges an AP or not, but

nothing in between, is known as all-or-none principle and results from the existence of a threshold potential, that is, if and only if the threshold potential is exceeded, then the neuron will discharge an AP. It is not completely understood how the αMN pool in the central nervous system operates as an ensemble to control the force that is exerted by a skeletal muscle. In general, to vary this force, the central nervous system has two mechanisms: (i) recruitment, that is, altering the number of active MUs, and (ii) rate coding, that is, changing the frequency of electrical impulses driving the MUs. It is generally accepted that MUs follow an orderly recruitment according to Henneman's size principle (Henneman, Somjen, & Carpenter, 1965a, 1965b), that is, from the smallest MU (the smallest αMN innervating the fewest muscle fibers) to the largest MU (the largest αMN innervating the largest motor unit). This principle can be simply represented by conformation of Ohm's law. However, there is some evidence that the size principle might not be the only principle applied. In some cases, for example, a differential distribution of synaptic inputs can ether revert or abolish recruitment order enforced by size principle (Miles & Türker, 1986) for biomechanical efficiency (Butler & Gandevia, 2008).

An increased synaptic input to the αMN pool will not only result in an increase of the number of recruited MUs, but it will also increase the discharge rate of all MUs that have already been recruited. Following this, the small, low-threshold MUs always discharge APs at a higher frequency than larger, higher-threshold MUs independent of the synaptic input to the αMN pool. This property is known as onion skin property in De Luca and Hostage (2010), De Luca, LeFever, McCue, and Xenakis (1982b).

2.2 | Skeletal muscle

Muscles turn the neural signals into force. Hereby, one can consider muscles as molecular motors that convert chemical energy into force. As an biological tissue, muscle is classified in three main groups, that is, cardiac, smooth and skeletal muscles, and is constructed by a highly hierarchical structure. The smallest contractile unit of a muscle cell is called sarcomere. Contracting sarcomeres generate in a muscle a pulling force. In skeletal muscle, many in-series connected sarcomeres form a myofribril, whereas bundles of myofibrils form a skeletal muscle fiber. The muscle fibers are embedded within an extracellular matrix such that the exerted force can be transferred to the joint via the passive collagenous structure and the tendon(s). The musculotendinous structure manifests viscoelastic behavior.

2.2.1 | Skeletal muscle architecture

Skeletal muscles are composed of muscle fibers that are mechanically coupled to each other by a network of extracellular connective tissue. The extracellular connective tissue is mainly composed of collagen and elastin, and it is hierarchically organized in different structures called endomysium, perimysium, and epimysium. The endomysium is a dense sheath of collagen fibers that envelops each muscle fiber and is connected to the basement membrane, which is part of the muscle fiber's cell membrane. The perimysium divides the muscle into bundles of fibers, called fascicles. Its tough and relative thick structure keeps the individual fibers together and provides the pathway for the major blood vessels and nerves running through the muscle. The muscle as a whole is coated by the epimysium, which is a particularly tough woven network of thick collagen fibers. The epimysium separates muscles from each other and is connected to the perimysium, cf. Figure 3.

The connective tissue serves several functions. Besides holding the fibers together and giving the muscle its shape, it contains blood vessels and nerves. Furthermore, the connective tissue resists excessive stretching of the muscle and distributes forces to minimize damage to the muscle fibers. The elasticity of the elastin and the wavy collagen bundles enable the muscle belly to regain its shape when external forces are removed. Furthermore, the extracellular connective tissue plays a key role in the force transmission from the muscle fibers to the tendons, for example, Huijing (1999, 2003), Monti, Roy, Hodgson, and Edgerton (1999), Street (1983), Street and Ramsey (1965), Yucesoy, Koopman, Baan, Grootenboer, and Huijing (2003), Yucesoy, Koopman, Huijing, and Grootenboer (2002).

Although all skeletal muscles are made up of the same components, viz. muscle fibers and extracellular connective tissue, they come in different forms and sizes depending on their specific task. The muscles in the human body range from very small, consisting of only a few hundred muscle fibers, to very large, consisting of more than a million fibers. The direction of the muscle fibers is characterized by the underlying fascicle direction. Depending on the arrangement of their fascicles, muscles are classified in distinct forms. In parallel-fibred muscles, for example, the fascicles run from tendon to tendon and are aligned with the muscle's force-generating axis. If the directions of the fascicles form an angle to the muscle's line of action, the muscle is called pennate, and the fascicles attach to aponeuroses, which run along each side of the muscle. Pennate muscles can exhibit larger forces than parallel-fibred muscles of the same volume due to their higher effective or physiological

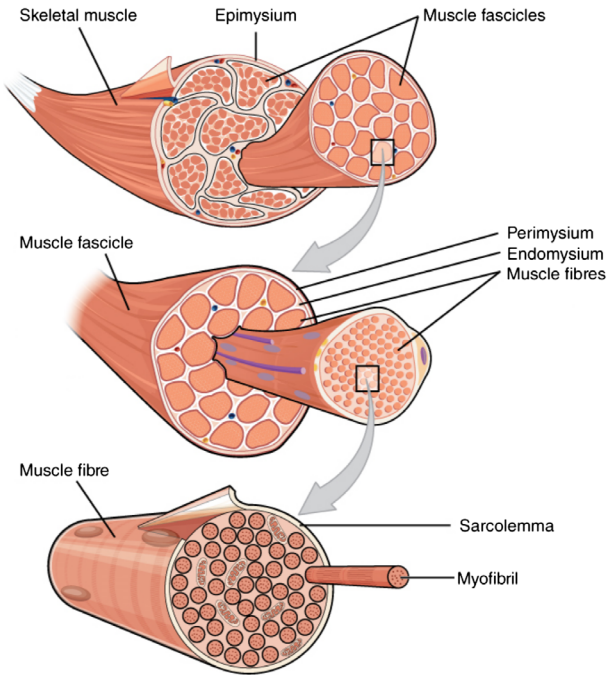

FIGURE 3 Structure of a skeletal muscle. Original image© by OpenStax Anatomy and Physiology

cross-sectional area (PCSA), that is, the cross-sectional area perpendicular to the fascicle direction. However, the pennation angle decreases the amount a muscle can shorten, as well as its contraction velocity. Furthermore, in large mammalian skeletal muscles, muscle fibers might not span the entire length of the fascicle. They might be arranged in series or terminate intrafascicularly (Heron & Richmond, 1993; Loeb et al., 1987; Richmond, MacGillis, & Scott, 1985; Young, Paul, Rodda, Duxson, & Sheard, 2000).

2.2.2 | The structure of a skeletal muscle fiber

Muscle fibers itself are long, cylindrical-shaped cells with a diameter of approximately 50–80 μm. The most prominent structures within the muscle fibers are the myofibrils, which are parallel-aligned, rod-shaped units that are made up of repeating sections called sarcomeres.

The sarcomere, or more precise the half-sarcomere, is the basic contractile unit of a muscle fiber. It contains thick filaments, which consist primarily of the protein myosin, and thin filaments, which consist primarily of the protein actin. The thick filaments are cross-connected by a fine, filamentous structure at one end of the half-sarcomere, the so-called M-disc. The thick filament's other end is connected to titin filaments, which are fine and very elastic macromolecule linking the thick filament to structure at the other end of the half-sarcomere, the so-called Z-disc, see Figure 4. It is believed that the titin filaments act as a molecular spring and keeps the thick filament in its position. A hexagonal lattice of thin filaments surrounds each thick filament. The thick and thin filaments interact via cross-bridges (XBs), that is, myosin molecular heads, which can attach to a neighboring thin filament. The length of a sarcomere is about 2 μm.

2.2.3 | The function of a skeletal muscle fiber

A major contribution of our knowledge about skeletal muscle contraction is based on the observation that skeletal muscle fibers exhibit a periodic microstructure, leading to the formulation of the sliding filament theory (Hanson & Huxley, 1953;

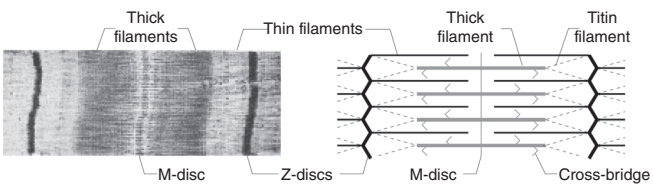

FIGURE 4 Structure of a sarcomere. On the left side, an image of a sarcomere is shown, while the right side shows the schematic structure of a sarcomere including thick, thin, and titin filaments as well as the Z-discs and M-disc (Figure modified from Sameerb at http://en.wikipedia.org/ with permission)

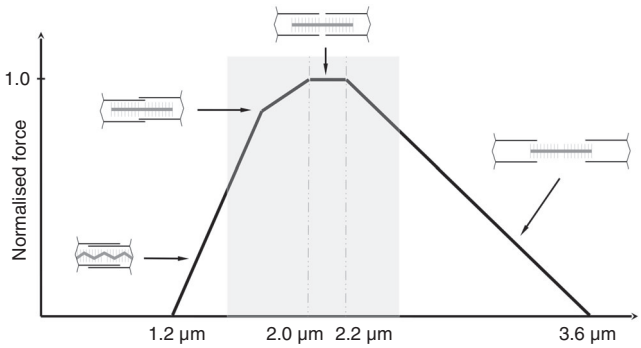

FIGURE 5 Normalized active force-length relationship derived from the geometrical overlap of the thin and the thick filaments (cf. Gordon et al., 1966). The gray color highlights the working range of most of the sarcomeres

Huxley & Hanson, 1954) and the observation the thin filaments and the thick filaments can form cross-links, leading to the formulation of the cross-bridge theory (Huxley, 1957; Huxley, 1958; Huxley, 1969; Huxley, 1974).

In summary, the myosin heads of the thick filaments can attach to specialized binding sites on the thin filament (modulated by Ca^{2+} ions as an second messenger, cf. Section 2.2.5) and form cross-links known as cross-bridges (XBs). After attachment, the catalytic domain of the myosin head (S1 domain) can undergo a conformational change known as the power stroke and which is responsible for active force production and contraction. Finally, the myosin head detaches from the thin filament and the XB returns to the initial detached state. The repeated process of attachment, power-stroke and detachment is known as cross-bridge cycle and is driven by ATP hydrolysis. If the length of the sarcomere is not constrained, the power stroke will result in a relative motion between the thin and the thick filaments and thus leading to muscle contraction. In contrast, during isometric conditions, that is, the length of the sarcomere remains constant despite potential external influences, the power stroke is leading to an displacement of the myosin heads molecular spring (S2 domain) and thus results in active force production. Macroscopically, this behavior can be observed by means of the force-velocity relation (cf. Figure 5), that is, the faster the fiber shortens, the less force it can exert (Hill, 1938). During lengthening contractions, the generated force exceeds the isometric force, cf. Figure 5.

Furthermore, the maximum isometric force a sarcomere can exert depends on the number of possible XB connections between the thick and thin filaments, which is primarily governed by the regions of overlap between the thick and thin filaments, that is, by the length of the sarcomere (Gordon, Huxley, & Julian, 1966). Figure 6 shows the experimentally determined force-sarcomere length relation of Gordon et al. (Gordon et al., 1966). While the classical geometrical filament overlap model is capable to explain the isometric active force production for most sarcomere lengths, it underestimates the active muscle force at very short sarcomere lengths (Ramsey & Street, 1940). More recently, Rode, Siebert, Tomakin, and Blackman (2016) proposed that the isometric active force production at very short sarcomere lengths could be explained by sliding of the thick myosin filaments through the Z-disks, leading to different filament overlap configurations.

The discovery of titin in the mid/late 1970s (Maruyama, 1976; Maruyama et al., 1977; Wang, McClure, & Tu, 1979) was the next major contribution to the current understanding of skeletal muscle fibers function. It is generally accepted that titin contributes to the passive forces of a skeletal muscle fiber and thus stabilize the sarcomeres (Funatsu, Higuchi, & Ishiwata,

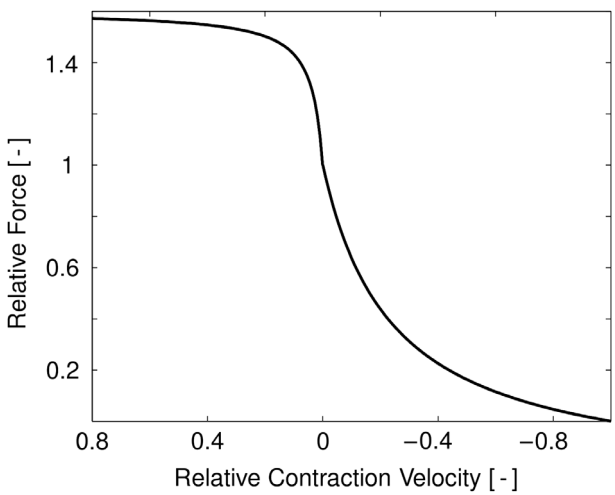

FIGURE 6 The influence of the contraction velocity on the force generation of a skeletal muscle

1990; Leonard & Herzog, 2010; Linke et al., 2002; Maruyama, 1976). While for a long period the active behavior of skeletal muscle fibers was entirely attributed to calcium modulated actin-myosin interactions, more recently it was proposed that titin is an adaptive spring (Labeit et al., 2003; Leonard, DuVall, & Herzog, 2010; Nishikawa et al., 2012; Noble, 1992; Rode, Siebert, & Blickhan, 2009), modulated by the muscle activation, that is, the intracellular calcium concentration. The activation modulated mechanical behavior of titin can explain phenomena like residual force enhancement (Abbott & Aubert, 1952; Edman, Elzinga, & Noble, 1978; Edman, Elzinga, & Noble, 1982; Herzog, Lee, & Rassier, 2006; Herzog & Leonard, 2002) and potentially optimize the metabolic costs of eccentric muscle contraction. The exact physiological behavior of titin is, however, still subject of current research (for a review see Herzog (2018)).

2.2.4 | Passive behavior of skeletal muscle tissue

The mechanical behavior of skeletal muscle tissue in which the tissue is not excited, that is, not active, is termed a skeletal muscle's passive mechanical behavior. It reflects the aggregated mechanical behavior of nonexcited skeletal muscle fiber and the extracellular matrix. Passive muscle tissue exhibits transversely isotropic material behavior (Morrow, Haut Donahue, Odegard, & Kaufman, 2010; Nie, Cheng, Chen, & Weerasooriya, 2011; Takaza, Moerman, Gindre, Lyons, & Simms, 2013). The response of the passive muscle tissue is attributed to both the extracellular connective tissue and the myofilaments, especially titin, within the sarcomeres of the muscle fibers (Prado et al., 2005). While it is often assumed that muscle tissue is stiffer in fiber direction, for example, Morrow et al. (2010), Takaza et al. (2013), Böl, Kruse, Ehret, Leichsenring, and Siebert (2012), and Nie et al. (2011) report a more compliant material behavior in the fiber direction compared to the cross-fiber directions. Furthermore, passive muscle tissue exhibits slightly viscoelastic behavior (Bosboom et al., 2001; Hoyt, Kneezel, Castaneda, & Parker, 2008; Levin & Wyman, 1927; Van Loocke, Lyons, & Simms, 2008; Van Loocke, Simms, & Lyons, 2009). Furthermore, due to its high content of water, it is commonly considered to behave incompressible within the physiological range (Böl, Ehret, Leichsenring, Weichert, & Kruse, 2014; Gindre, Takaza, Moerman, & Simms, 2013; Takaza et al., 2013; Van Loocke, Lyons, & Simms, 2006).

2.2.5 | Excitation-contraction coupling

The complex signaling pathway leading from electrical excitation of a muscle fiber to its contraction is known as excitation-contraction coupling (MacIntosh, Gardiner, & McComas, 2006; Sandow, 1952). The AP of the neuron is transmitted to the muscle fiber at the neuromuscular junction. Starting from there, the AP propagates along the length of the muscle fiber. The propagating signal triggers the release of calcium ions from an intracellular calcium storage called sarcoplasmic reticulum (SR). The released calcium binds, amongst others, to the troponin-tropomyosin regulatory unit, enabling XB cycling (cf. Section 2.2.3), that is, active force production and contraction. The excitation-contraction coupling in skeletal muscle fibers, together with the most prominent structures of the muscle fiber, is schematically represented in Figure 7.

In detail, the AP, generated at the neuromuscular junction, not only propagates along the length of a muscle fiber, but it is also conducted from the surface to the interior of the fiber by numerous, channel-like invaginations of the sarcolemma called T-tubules. Embedded in the membrane of the T-tubules are dihydropyridine receptor (DHPR) channels that are sensitive to changes in the membrane potential. The DHPR channels are mechanically linked via protein structures to the ryanodine receptors (RyR) in the membrane of the SR. The SR is an extensive network of channels in the muscle fibers that stores large amounts of calcium (Ca^{2+}). The RyR is a Ca^{2+}-channel consisting of four subunits. An AP entering the T-tubules activates the DHPR channels, which will then induce the opening of the RyR in the membrane of the SR. When the RyR opens, large amounts of Ca^{2+} will leave the SR and enter the cytosol, following their concentration gradient, since the free concentration of Ca^{2+} in the cytosol is kept at a very low level in the resting state. The Ca^{2+}-ions play a key role in muscle contraction (Melzer, Herrmann-Frank, & Lüttgau, 1995). Once released into the cytosol, Ca^{2+} binds to troponin C, which is part of the troponin-tropomyosin regulatory unit. The binding of two Ca^{2+} ions to troponin C yields a conformational change in the troponin molecule that removes the blocking tropomyosin from the thin filaments. This enables the formation of a XB connection between the thick and thin filaments in the sarcomeres (for a detailed review on the molecular regulation of muscle activity see Gordon, Homsher, and Regnier (2000)), leading to XB cycling (cf. Section 2.2.3).

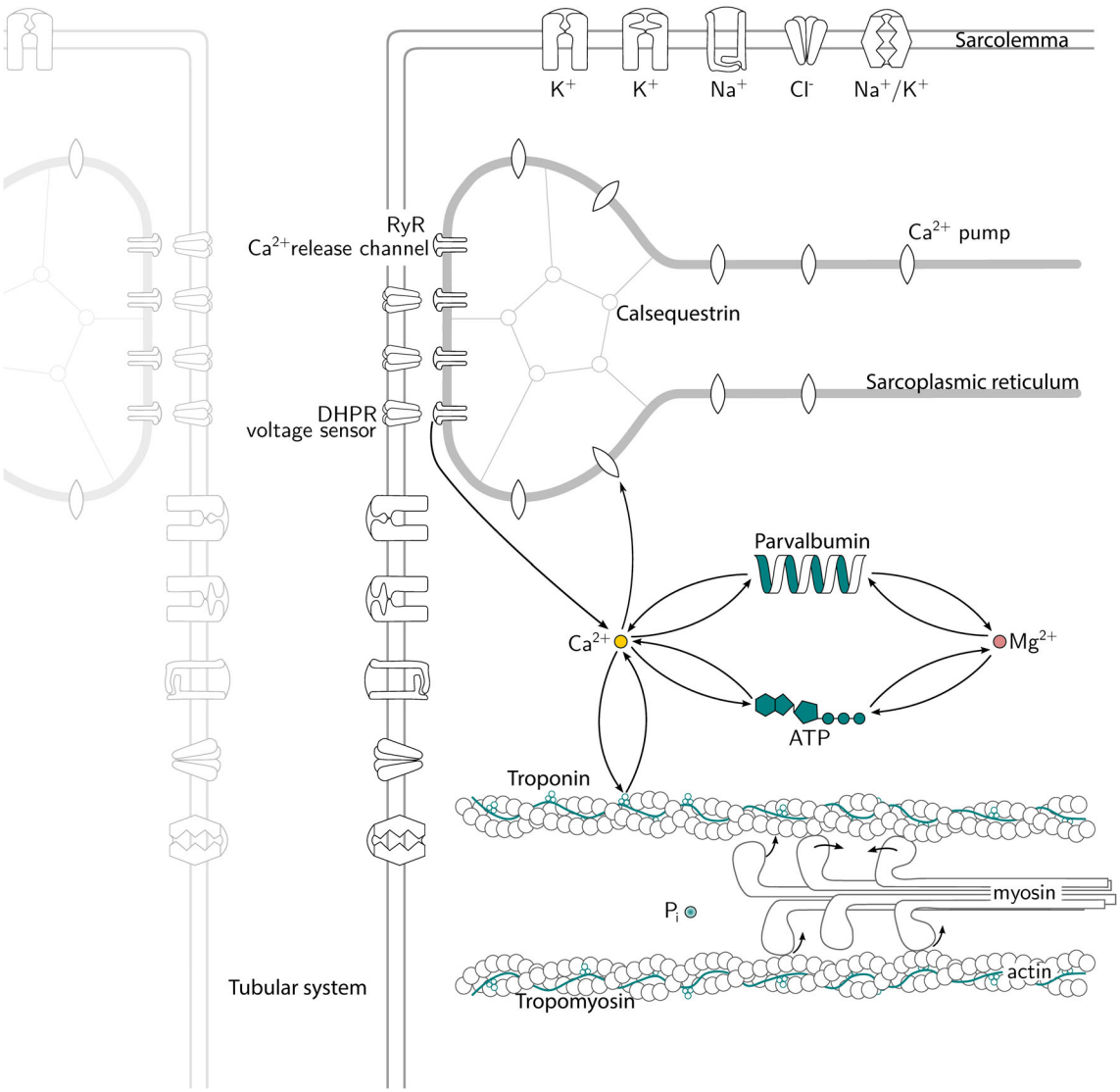

FIGURE 7 Schematic representation of the excitation-contraction coupling in a muscle fiber (Adapted from Röhrle, Neumann, and Heidlauf (2016))

2.3 | The motor unit

After introducing the neural physiology, the skeletal muscle anatomy and the function of individual muscle fibers, this section focuses on the key functional aspects of whole skeletal muscles that are relevant with respect to modeling the neuromuscular system. Most importantly, since electrical activation from one muscle fiber to adjacent ones is not observed in skeletal muscle, each fiber must have its own neuromuscular junction. While it is generally assumed that each fiber is innervated by exactly one αMN, there is some electro-physiological evidence that a few doubly innervated fibers (fibers with multiple motor endplates and polyneuronal innervation) also exist (Lateva, McGill, & Johanson, 2002; McGill & Lateva, 2011). Furthermore, while all muscle fibers belonging to one MU have similar properties, the contractile and metabolic properties of different motor units vary heavily.

2.3.1 | Properties of motor units

The differences observed in the contractile and metabolic properties of skeletal muscle fibers inspired the distinction of different MU types. To this end, MUs have been classified based on their speed of contraction, the handling of intracellular Ca^{2+}-ions, or their resistance to fatigue during prolonged contractions. For example, muscle fibers can be classified based on the expression of certain isoforms of the myosin heavy chain, which determines the rate of XB cycling, and hence, the

speed of contraction. Moreover, based on their metabolic properties, aerobic Type-I (slow-twitch) fibers can be distinguished from their fast-twitch counterparts (Type-II fibers), which, in addition to the oxidation of fats and carbohydrates, use an anaerobic metabolism. Based on a certain stimulation protocol, Burke, Levine, Tsairis, and Zajac (1973) distinguished slow-twitch units (Type S) and fast-twitch units (Type F). The group of Type-F units was further split into fatigue-resistant (Type FR) and fast-fatigable (Type FF) units (Burke et al., 1973).

In general, the smallest MUs, which are recruited first, exert the smallest forces, exhibit the slowest speed of contraction, and show the least amount of fatigue. Conversely, the largest MUs, which are recruited last, exert the largest forces, have the highest speed of contraction, and are most affected by fatigue. However, the physiological properties of human MUs do not cluster into discrete groups, but rather exhibit a continuous distribution from one extreme to the other (Duchateau & Enoka, 2011).

2.3.2 | Types of contractions

The most simple contraction is a single twitch, which is the motor unit's response to a single AP discharged by the MN. The shape of a twitch can be well described by the impulse response to a critically damped second-order system (Fuglevand et al., 1993). The total duration of a muscular AP, from depolarisation to the point where the resting state is restored, is about 2–5 ms. In contrast, the duration of a twitch from the first rise to complete relaxation varies from about 200 ms to more than 500 ms depending on the MU type. Thus, if subsequent stimulations are applied before the actively generated twitch force of the fiber returned to its initial value, a summation of the resulting twitches is observed (fused twitches). Obviously, the increase in force following subsequent stimulations is not unlimited, but after a number of stimulations, a peak force is reached. The value of the peak force depends on the stimulation frequency—it increases with rising frequency up to a certain optimal frequency, beyond which, no further increase in force can be generated. This form of contraction is referred to as tetanic contraction. Peak firing frequencies during isometric contractions of human muscles are approximately 45 Hz (Fuglevand et al., 1993).

2.4 | Motor control

During voluntary movement, the central nervous system controls the activity of the individual motor units in the different muscles by modulation of the synaptic inputs to motor neurons. MN is the controller of a transducer, the motor unit, which converts synaptic currents into contractile force (Heckman & Enoka, 2012). The sources of synaptic inputs to motor neuron pools originate from several supra-spinal and spinal centers, sensory receptors and recurrent pathways (see also Section 2.1.4). For example, a single αMN can receive up to 60,000 synaptic projections from excitatory and inhibitory pathways (Ulf hake & Mulheim, 1988). Due to integrate-and-fire process of the motor neurons and the stochastic nature of these inputs, the MN discharges during natural movements contain a certain degree of variability in the interstimulus interval (time between two successive MN discharges) (Clamann, 1969). This implies that the discharge characteristics of MNs contain information about the neural control signal (Farina, Negro, Muceli, & Enoka, 2016). For these reasons, for example, a significant linear association between the control oscillations in the primary motor cortex and the discharge times of the motor units can be found experimentally (Negro & Farina, 2012). The force generated by the muscles is the result of the summation of the activity of all motor neuron discharges, also called neural drive to the muscles (Farina, Negro, & Dideriksen, 2014). Because of the summation process, in order to provide an efficient motor control, a proportion of the synaptic inputs are shared across MNs in the same and between different motor nuclei (Ishizuka, Mannen, Hongo, & Sasaki, 1979; Lawrence, Porter, & Redman, 1985). The presence of shared synaptic inputs in the motor pools determines a significant level of correlation between the discharge times of different motor units during voluntary contractions (De Luca & Erim, 1994; Negro & Farina, 2012; Semmler, 2002). The quantification of the correlation between motor unit spike trains has been traditionally separated in low-frequency (<8 Hz) common oscillations (common drive) and high frequency components (short-term synchronization). Due to the low-pass characteristics of the muscle contraction (Baldissera, Cavallari, & Cerri, 1998), only the shared low-frequency oscillations are relevant for force generation (Farina & Negro, 2015). Despite the multifunctional roles and control properties of different muscles, it has been shown in particular that their motor pool receives a similar and large proportion of (>60%) common low-frequency components in their synaptic inputs (Negro et al., 2016). Therefore, the majority of the synaptic inputs to the motor neuron pools in the functional bandwidth of muscle contraction is shared and this provides a simple scheme for motor control (Thompson et al., 2018). On the other hand, shared synaptic input in higher bandwidths and independent inputs do not have significant implications in the generation of force, in particular at moderate to high force levels (Castronovo,

Negro, Conforto, & Farina, 2015; Dideriksen, Negro, Enoka, & Farina, 2012; Farina et al., 2014; Negro et al., 2016). For these reasons, variations in the accuracy of the generated force during challenging task and/or activation of sensory inputs is reflected mainly in the correlation of the low-frequency oscillations of the motor neuron discharges (Laine, Yavuz, & Farina, 2014; Yavuz et al., 2015).

2.5 | Further reading

An elaborate description of the nervous system and its components, the neurons, can be found, for example, in Kandel et al. (2000). MacIntosh et al. (2006) give full account on the anatomy and physiology of skeletal muscles and provides some details on the motor neurons (αMNs). Extensive reviews of the motor unit as the functional unit of the neuromuscular system have been carried out by Heckman and Enoka (2004, 2012). Furthermore, the mechanisms involved in human movement, from neural control to muscle mechanics, are comprehensively described in Enoka (2008).

3 | REVIEW ON STATE-OF-THE-ART APPROACHES IN MODELING THE NEUROMUSCULAR SYSTEM

The above constitutes a short summary of the complex anatomy and physiology of the neuromuscular system and provides the context for the respective computational models. From a modeling perspective, there exist two different modeling approaches, that is, phenomenological and biophysical approaches.

Phenomenological models are based on experimentally determined input–output relations. They are often simpler, computationally more efficient, and rely on fewer parameters than their biophysical counterparts, which aim to directly model the biophysical processes by taking into account the underlying anatomy and physiology. Within the range, in which the phenomenological model has been fitted to experiments, phenomenological models can accurately reproduce the system's behavior. However, as they are fitted to input–output relations, phenomenological models cannot provide a full understanding of the underlying physiology. This is true, irrespectively of the system. In contrast, biophysical models are built on the existing knowledge of the physiology of the respective system, and hence, have the ability to be utilized within in silico laboratories to investigate the behavior of the modeled system under normal and pathological conditions. To mimic the macroscopic system behavior in a comprehensive way, biophysical models need to represent all relevant components and structures through biophysically meaningful (state) variables. Therefore, biophysical models often depend on a multitude of parameters, some of which are difficult or even impossible to determine accurately. Note, that (constitutive) relations between different state variables can still be modeled in a phenomenological way, for example, representing the mechanical behavior of a protein by a nonlinear spring or modeling an ion channel as an variable resistor.

While each modeling approach has its own advantages and disadvantages, deriving or postulating a model requires assumptions. These have to be kept in mind at all times. No model should ever be used to make predictions for cases that violate any of the assumptions made within the derivation process.

Based on the constitution of the neuromuscular system, existing mathematical models either focus on the generation of force in the muscle fibers or the muscle's control through the coordinated operation of the motor neurons as an ensemble. Hence, we will first provide a review on modeling approaches for the individual components of the neuromuscular system, for example, the motor neuron pool, the skeletal muscles, musculoskeletal system models, or the electrical state of a muscle (here, EMG), before selecting particular models and stitching them together to a neuromuscular system model.

3.1 | Motor neuron pool model

Several phenomenological and biophysical models have been proposed for the simulation of the motor neuron pool. Phenomenological models are based on the characteristics of motor neuron discharges that have been found experimentally. For example, based on the relation between the synaptic input to a motor neuron and its output discharge rate, Heckman and Binder (1991) and Fuglevand et al. (1993) have proposed powerful phenomenological models for animal and human motor neurons, respectively. These models have been used extensively for the testing of neurophysiological hypotheses or for interpreting experimental data (Dideriksen et al., 2012; Dideriksen, Negro, Enoka, & Farina, 2011; Dideriksen & Farina, 2013; Dideriksen, Farina, Bækgaard, & Enoka, 2010; Jones, Hamilton, & Wolpert, 2002; Enoka et al., 2003; Yao, Fuglevand, & Enoka, 2000). However, one important limitation of phenomenological motor neuron models is the fact that they are not capable of naturally describing the membrane dynamics of the motor neurons, where nonlinear behavior of αMNs predominantly originates.

To overcome these limitations, several biophysical models have been proposed (Booth, Rinzel, & Kiehn, 1997; Cisi & Kohn, 2008; Elias, Chaud, & Kohn, 2012; Elias & Kohn, 2013; Negro & Farina, 2011; Taylor & Enoka, 2004). These are capable of integrating synaptic and/or common inputs on the motor neuron membrane level. This is done by adopting the Hodgkin and Huxley formalism, derived from their experiments on the giant axon of the squid (Hodgkin & Huxley, 1952). Using this formalism, it has been possible to progressively increase the type and the number of the ion channels in multiple compartments of these realistic motor neuron models. Interestingly, the biophysical description of the motor neuron behavior inherently accounts for the size principle of motor neuron recruitment (Henneman et al., 1965a, 1965b) (small, low-threshold motor neurons are recruited before larger motor neurons with higher excitation threshold) and the "onion-skin" property (De Luca & Hostage, 2010; De Luca, LeFever, McCue, & Xenakis, 1982a) (for a certain level of synaptic input to the motor neuron pool, low-threshold motor neurons have higher discharge rates than high-threshold motor neurons). Additionally, these complex motor neuron descriptions were able to reproduce and help to interpret important results in animal (Miles, Dai, & Brownstone, 2005) and human (Powers & Heckman, 2015) experiments. Under the favor of the increased computational power and the flexibility of the simulator environments, it has been possible to create models based on the three-dimensional reconstructed morphology of experimentally recorded motor neurons (Elbasiouny, Amendola, Durand, & Heckman, 2010). These models provide the unique possibility to investigate the neural alterations arising from pathologies of the neuromuscular system.

More recently, biophysical neuromuscular models have been proposed to describe the link between neural activity and force generation (Allen & Elbasiouny, 2018; Dideriksen, Negro, & Farina, 2015; Farina et al., 2016; Nagamori, Laine, & Valero-Cuevas, 2018; Negro et al., 2016; Watanabe et al., 2013; Williams & Baker, 2009). Such models are an evolution of the previously proposed alpha motor neuron models and usually include additionally the simplified simulations of supraspinal pathways (motor cortex, brain stem, etc.), detailed spinal cord networks (excitatory and inhibitory interneurons, gamma motor neuron, afferent projections, etc.) and the musculotendon unit (proprioception, joint dynamics, etc.). Recent applications of these biophysical neuromuscular models include the analysis of the force variability during steady isometric contractions (Dideriksen et al., 2015; Farina et al., 2014; Farina & Negro, 2015; Negro et al., 2016; Negro & Farina, 2011; Watanabe et al., 2013), postural sway (Elias, Watanabe, & Kohn, 2014) and nonlinear control of force oscillations (Watanabe & Kohn, 2015, 2017).

3.2 | Skeletal muscle models

The APs generated by the motor neurons trigger the force generation in the skeletal muscle fibers. There exist various different methods to predict the skeletal muscle activity due to neural stimulation, that is, motor control, for example, analytical methods (Section 3.2.1), phenomenological Hill-type (Section 3.2.2) or continuum-mechanical (Section 3.2.3) approaches, biophysical Huxley-type (Section 3.2.4), or multiscale, multiphysics (Section 3.2.5) skeletal muscle models. Note, although we distinguish modeling skeletal muscle mechanics into these categories, a clear separation between these models does not exist.

3.2.1 | Analytical models and superposition

Heckman and Binder (1991) proposed a phenomenological model based on the input–output behavior of motor units (the muscle fibers innervated by a single motor neuron) during an isometric contraction (the force-frequency relation). Fuglevand et al. (1993) proposed probably the most popular model for linking motor control with muscle force generation of a single motor unit. They use the impulse response of a critically damped, second-order system to represent the twitch force and provide for their system an analytical solution. This simplified motor unit force model has been adopted and enhanced by several researchers, see, for example, Cisi and Kohn (2008) or Dideriksen et al. (2010, 2011, 2012). The resulting overall skeletal muscle force is then obtained by simply adding the individual muscle force units, that is, linearly superimposing the MU forces and hereby entirely ignoring the underlying heterogeneity and its functionality.

3.2.2 | Hill-type skeletal muscle models

In contrast to the models described in Section 3.2.1, Hill-type muscle models focus on describing the dynamics of muscle contraction (Delp et al., 2007; Günther, Schmitt, & Wank, 2007; Häufle, Günther, Bayer, & Schmitt, 2014; Lloyd & Besier, 2003a; Pandy, 2001a; Siebert, Rode, Herzog, Till, & Blickhan, 2008; Till, Siebert, Rode, & Blickhan, 2008; van Ingen

Schenau, Bobbert, Ettema, de Graaf, & Huijing, 1988; Zajac, 1989). Hill-type models are based on the description of Hill (1938). Hill-type models are phenomenological formulations of the macroscopic muscle physiology that superpose a length-dependent passive force (stress–strain relation in the absence of neural stimulation) with a force that results from the neural activation of the muscle (in the following termed active force) and depends on the muscle's length and contraction velocity. Due to their simplicity, computational effectiveness, and the low number of involved parameters, Hill-type muscle models are commonly used to interpret experimental data or describe movement and forces of (parts of) the muscular system within the framework of multibody dynamics.

Hill-type muscle models are typically used to describe whole muscle behavior (Zajac, 1989), although they have also been used to model single sarcomeres, and, by in-series arranging multiple Hill-type models, also myofibrils and muscle fiber segments (Günther, Röhrle, Haeufle, & Schmitt, 2012; Morgan, Mochon, & Julian, 1982; Stoecker, Telley, Stüssi, & Denoth, 2009). While these approaches can describe local changes in sarcomere length, they cannot capture the behavior of a fiber within a three-dimensional muscle tissue. This is due to the fact that the passive forces in isolated myofibrils and single muscle fibers are mainly attributed to the titin filament (Denoth, Stüssi, Csucs, & Danuser, 2002; Horowits, 1992), unlike in muscle tissue, where the extracellular matrix contributes additional passive forces (Prado et al., 2005). Furthermore, in isolated myofibrils and single muscle fibers, force transmission can only take place along their length. In whole muscle, however, force transmission also occurs in lateral direction (Huijing, 1999).

Hill-type models, as well as analytical models, exhibit significant drawbacks, since they lump together all functional and structural properties of a muscle into a few parameters and essentially ignore any spatial heterogeneity. Hill-type models, for example, are described at a point in space through spring constants, damper properties, and one activation level, and the calculated muscle force acts along a predefined line of action. Furthermore, since these models lack a volumetric representation of the skeletal muscle, they are not capable of properly taking into account structural properties, for example, complex fiber architectures, motor unit fiber distributions, or the interaction of a skeletal muscle with surrounding tissue, for example, bones, adjacent muscles, or fat tissue. Moreover, activation history, fatigue, post-tetanic potentiation, doublet potentiation, and serial dependence of twitch responses are—although not necessarily—typically only integrated in a phenomenological way (Fuglevand et al., 1993; Perreault, Heckman, & Sandercock, 2003; Sandercock & Heckman, 1997).

In summary, for an adequate representation of fibers within the muscle tissue and its mechanical implications on the behavior of the whole muscle, a three-dimensional model based on continuum-mechanical principles is required.

3.2.3 | Continuum-mechanical models

Based on the argument that Hill-type models inaccurately predict muscle forces in complex geometries, continuum-mechanical models based on the finite-elasticity theory have been proposed (Blemker, Pinsky, & Delp, 2005; Böl & Reese, 2008; Ehret, Böl, & Itskov, 2011; Meier & Blickhan, 2000; Röhrle & Pullan, 2007; Sánchez, Lloyd, Fels, & Abolmaesumi, 2014; Zuurbier & Huijing, 1992). The need for continuum-mechanical models can be seen in particular when modeling complex muscular structure like the tongue with its complex and interwoven fiber structure (Kieser et al., 2014; Stone et al., 2018; Wang, Nash, Pullan, Kieser, & Röhrle, 2013).

Any continuum-modeling approach requires constitutive relations, mathematically representing the original mechanical material behavior. Thereby, like many other biological tissues skeletal muscles are assumed to be incompressible. Furthermore, the mathematical description of the passive material behavior is typically based on a transversely isotropic, hyperelastic/viscoelastic macroscopic continuum-mechanical constitutive framework (Blemker et al., 2005; Böl, Sturmat, amd Weichert, & Kober, 2011; Johansson, Meier, & Blickhan, 2000). Note that the passive material description often neglects viscoelastic effects (Bosboom et al., 2001; Van Loocke et al., 2008; Van Loocke et al., 2009). Partial justification for doing so is given by Tian, Hoang, Gandevia, Herbert, and Bilston (2011), who demonstrated that the viscous effects in passive muscle tissue are rather small.

While the passive behavior certainly plays a significant role in skeletal muscle tissue, the key mechanical contribution is, however, provided by the active (contractile) material behavior. To adequately model the active behavior of skeletal muscle tissue, there exist two different modeling frameworks in the literature. These are the active stress approach, for example, Blemker et al. (2005), Johansson et al. (2000), Martins, Pires, Salvado, and Dinis (1998), McCulloch, Waldman, Rogers, and Guccione (1992), Nash and Hunter (2000), and the active strain approach, for example, Kondaurov and Nikitin (1987), Nardinocchi and Teresi (2007), Taber and Perucchio (2000). Historically, constitutive modeling of skeletal muscle tissue has been decisively inspired by the cardiac tissue modeling community. Currently similar constitutive modeling approaches are applied to simulate all types of muscle tissue (i.e., skeletal, cardiac and smooth muscle tissue), however, care should be taken, since

even though different muscle tissues are constituted by similar classes of proteins, all muscle types still show significant structural and functional differences.

The most common constitutive modeling framework for modeling active contractile behavior of skeletal muscles is the active stress approach (Blemker et al., 2005; Johansson et al., 2000; Martins et al., 1998; Röhrle, Davidson, & Pullan, 2008). In detail, it is assumed that the overall stress-tensor can be obtained by adding an active contribution to the hyperelastic/viscoelastic passive stress tensor. The active stress tensor is thereby constituted by a scalar-valued stress component (depending on the local activation, the current length and velocity) and a structural tensor taking into account the direction of stress generation, for example, to contribute for the biophysical property that the active stress predominantly acts along the muscle fiber direction.

Alternatively, the active strain approach is based on a multiplicative split of the deformation gradient tensor, which has been initially developed in the field of elasto-plasticity (Lee, 1969). This approach has been utilized to simulate actively contracting skeletal muscles, for example, by Ehret et al. (2011), Hernández-Gascón, Grasa, Calvo, and Rodríguez (2013), or Sharifimajd and Stålhand (2013) Within the active strain approach, the deformation gradient tensor is multiplicatively decomposed into an active (inelastic) component and an elastic part. Note that the active deformation gradient tensor can be interpreted as a shift of the reference configuration and thus stores no energy. As the active stress tensor, the constitutive description of the active deformation gradient tensor has to incorporate the local activation, length, velocity and anisotropy of the tissue. Both the active stress approach and the active strain approach are valid from a macroscopic and phenomenological point of view, that is, both methods can be fitted in such a way that they reproduce the same macroscopic data. While some authors pointed out that the active stress approach might be beneficial from a mathematical point of view, since it is more straight forward to enforce convexity and thus guarantee the existence of a unique solution of the mathematical problem (Ambrosi & Pezzuto, 2012; Rossi, Ruiz-Baier, Pavarino, & Quarteroni, 2012), the active stress approach is more intuitive and has, for example, proven to be a useful method to study knock-out conditions (Heidlauf, Klotz, Rode, Siebert, & Röhrle, 2017).

Key advantages of continuum-mechanical models are, for example, the ability to take into account complex muscle fiber distributions (Blemker & Delp, 2005; Ramasamy et al., 2018), to integrate regional activation properties, or to dynamically generate lines of action (Röhrle & Pullan, 2007). The existence of relatively simple constitutive equations makes phenomenological continuum-mechanical modeling frameworks an elegant tool for predicting the mechanical behavior of skeletal muscles subject to external constraints such as its embedding (other muscles or bones), activation, or impact. This is true even for complex biological tissues. However, the accuracy of phenomenological continuum models always depends on the quality of the available macroscopic (experimental) data. Macroscopic data should ideally consider mixed loading conditions and different levels of activation. This is essential to reproduce the original mechanical tissue properties for (all) different modes of deformation.

Obtaining a comprehensive set of experimental data suitable for fitting material parameters of constitutive equations, however, is extremely challenging—even under in vitro conditions. Designing experiments to obtain sufficient experimental data in vivo poses numerous challenges (Bilston & Tan, 2015). While shearwave elastography (Ateş et al., 2015; Ateş et al., 2018; Bilston & Tan, 2015), intramuscular pressure (Ateş et al., 2018), or measurements during surgical interventions (Ateş, Temelli, & Yucesoy, 2013) can provide some insights into mechanical behavior of skeletal muscles in vivo and in humans, most experimental data, if available, stem from animal experiments, are often restricted to uniaxial loading conditions, for example, Hawkins and Bey (1994), Zajac (1989), or only consider the passive state of the tissue, for example, Böl et al. (2012), Takaza et al. (2013), Van Loocke et al. (2006). Furthermore, biological tissue generally exhibits a high degree of inter- and intra-subject variability. This is in contrast to classical engineering materials. Due to the high variability of the mechanical properties a single set of material parameters is essentially useless as it is not representative at all.

While continuum-mechanical skeletal muscle models have certain advantages with respect to incorporating complex structural properties, they also have disadvantages. For example, phenomenological constitutive relations typically lump together the mechanical properties of different structures such as the myofilament skeleton or the extracellular connective tissue. Thus, the material parameters obtained by fitting the constitutive equations have no direct biophysical meaning and, hence, cannot be related to the underling microstructure.

3.2.4 | Biophysical models of excitation-contraction coupling

Biophysical modeling of muscle cells has been pioneered by Huxley (1957, 1974) by summarizing the ideas of the sliding filament theory and the XB theory (Hanson & Huxley, 1953; Huxley & Hanson, 1954; Huxley & Niedergerke, 1954; Huxley,

1957) within a mathematical model. The model of Huxley (1957) assumes a population of (independent) cross-bridges that can be either in a detached state or an attached, force producing state. Thereby the kinetics of the state transitions depend on the mechanical strains of the cross-bridges, mathematically resulting in a set of coupled partial differential equations (PDEs). Subsequent work refined Huxley's modeling approach, for example, by increasing the number of cross-bridge states and refining the strain dependent kinetic state transitions (a review can, for example, be found within Smith, Barclay, and Loiselle (2005)). Furthermore, the work of Hill (1989), Hill, Eisenberg, Chen, and Podolsky (1975) provided a thermodynamically self-consistent framework, which enabled to relate the kinetic behavior of cross-bridges to muscle energetics. Therefore, biophysical Huxley-type models have been successfully applied to study the molecular mechanisms of force development and transient effects caused by length perturbations. Furthermore, to avoid the complexity of solving PDEs, approximations can be formulated in terms of ordinary differential equations (ODEs) in time, see, for example, the distributed moments approach of Zahalak (1981).

Besides biophysical descriptions of cross-bridge dynamics, biophysical models of other parts of the complex signaling pathway from electrical stimulation to force generation in skeletal muscle fibers have been developed. For example, based on the ground-breaking work of Hodgkin and Huxley (1952), Adrian and Peachey (1973) proposed a model of the membrane electrophysiology of muscle fibers. This model was extended by Wallinga et al. (1999) to a multicompartment model of the ionic currents crossing the T-tubule membrane and the sarcolemma of a muscle fiber. Based on a similar approach, Cannon, Brown, and Corey (1993) utilized a Hodgkin–Huxley model to simulate myotonia and paralysis caused by incomplete inactivation of sodium channels.

Within the excitation-contraction pathway, the intracellular calcium concentration serves as an second messenger enabling cross-bridge cycling. Calcium is also expected to modulate remodeling within the muscle fibers (Bassel-Duby & Olson, 2006). Mathematical models of the intracellular calcium dynamics have been introduced in the 1980s (Cannell & Allen, 1984; Gillis, Thomason, Lefèvre, & Kretsinger, 1982) and subsequently refined/adopted (Baylor & Hollingworth, 1998; Konishi, 1998; Shorten et al., 2007).

While there exist multiple biophysical models focusing on specific aspects of muscle contraction, only few models consider the entire excitation-contraction pathway and typically represent cardiac myocites (Hilgemann & Noble, 1987; Winslow, Rice, Jafri, & Marban, 1999). To simulate the entire excitation-contraction pathway in skeletal muscle fibers, Shorten et al. (2007) coupled a simplified version of Wallinga's model of the membrane electrophysiology (Wallinga et al., 1999) to a model of calcium release from the sarcoplasmic reticulum (Ríos, Karhanek, Ma, & González, 1993), a model of intracellular calcium dynamics (Baylor & Hollingworth, 1998), and an extended version of the cross-bridge dynamics model of Razumova, Bukatina, and Campbell (1999). Furthermore, the model of Shorten et al. (2007) includes a description of metabolic fatigue based on the accumulation of inorganic phosphate in the sacroplasm.

Note that there exists a wide class of similar (sub-) cellular, biophysical muscle models focusing on aspects like metabolism, the behavior of individual ion channels or gene regulation. However, a detailed review of all existing models is beyond the scope of this manuscript (for an overview see, e.g., the models repository on a platform like www.cellml.org).

3.2.5 | Multiscale, multiphysics models

To incorporate such detailed biophysical descriptions into macroscopic volumetric models, multiscale, multiphysics models, which link macroscopic continuum mechanics to the microstructure and molecular kinetics, need to be considered. In contrast to single-scale phenomenological models, biophysical multiscale models are capable to relate microstructural changes and macroscopic deformation. If in addition, one incorporates AP-induced cross-bridge dynamics within active stresses, for example, by solving Huxley-type myofilament models (Heidlauf & Röhrle, 2014; Röhrle et al., 2008) and coupling them to macroscopic deformations, that is, macroscopic mechanics, one obtains as for the case of the chemo-electro-mechanical models proposed by Röhrle et al. (2008) multiscale, multiphysics skeletal models.

The list of applications benefiting from multiscale models is long. For example, anatomically-accurate electrophysiological models can be used to investigate the electro-physiological properties of denervated muscles following functional electrical stimulation (Kin, Trew, Pullan, & Röhrle, 2012). Furthermore, microstructural informed multiscale approaches, which, for example, incorporate microscopic properties of connectives tissues, such as the ones highlighted by Lanir (1979, 1983), are desirable for investigating, for example, experimentally observed changes in the mechanical properties due to distrophies (Hu & Blemker, 2015) or Botulinum toxin type A injections (Ateş & Yucesoy, 2014; Ateş & Yucesoy, 2018).

Macroscopic continuum-mechanical models (no matter if phenomenological or biophysically informed) are only capable of predicting the average deformations of a smeared homogenized material. Applications like predicting muscle injuries, however, might also require local maxima of the displacement field within the heterogeneous microstructure. To overcome such limitations in continuum models, micromechanical continuum models have been developed (Sharafi & Blemker, 2010; Sharafi & Blemker, 2011; Virgilio, Martin, Peirce, & Blemker, 2015). The work by Virgilio et al. (2015) uses, for example microstructural finite-element models of skeletal muscle tissue to study pathological conditions such as muscular dystrophies. In these models, the different constituents, that is, the muscle fibers and the extracellular matrix, are spatially resolved and coupled to each other. While these models provide valuable insights into the mechanics of the underlying microstructure, they also require constitutive material descriptions for each constituent. This often poses additional challenges in obtaining suitable experimental data.

The integration of such microstructural properties can be achieved by employing homogenization theories. Macroscopic and microscopic continuum models, for example, can be unified by means of the FE^2-method (Miehe, Schröder, & Schotte, 1999; Schröder, Schröder, & Hackl, 2014; Smit, Brekelmans, & Meijer, 1998). To the best knowledge of the authors, this methodology, however, has not been applied to model the mechanics of skeletal muscle tissue. The FE^2-method is computationally very expensive such that novel homogenization techniques need to be investigated. Such methods are challenging and subject of current research (Bleiler, Ponte Castañeda, & Röhrle, 2019; Spyrou, Agoras, & Danas, 2017).

For modeling the neuromuscular system, it is important to consider the entire physiology (cf. Section 2.2) and not only mechanical aspects. To do so, the excitation-contraction pathway of Shorten et al. (2007) has been coupled to bioelectrical field equations and a continuum-mechanical constitutive equation by Röhrle and co-workers (Röhrle, 2010; Röhrle et al., 2008; Röhrle et al., 2012; Röhrle, Sprenger, Ramasamy, & Heidlauf, 2013) to simulate the propagation of APs along muscle fibers and the force generation and deformation of muscle, respectively. The resulting model is a multiscale, multiphysics skeletal muscle model that can be linked to a motor neuron model; for example the model of Fuglevand et al. (1993) has been used to drive the simulated muscle contractions by assuming a one-by-one relation between αMN APs and muscle fiber APs (Röhrle et al., 2012). In order to simulate functional electrical stimulation, Kim, Davidson, Röhrle, Soboleva, and Pullan (2007) established an anatomical detailed model of the nerve trunk connecting the MNs and the muscle fibers, and which considers the spatial propagation of APs along the nerve. While the original model of Röhrle and co-workers was limited to isometric contractions, subsequent works established a fully coupled and flexible modeling framework (Heidlauf & Röhrle, 2013; Heidlauf & Röhrle, 2014) embracing neural inputs, feedback mechanisms, and force generation and EMG generation during nonisometric conditions. Furthermore, the overall modeling framework is easily extensible to include additional biophysical details or physiological hypothesis and has for example been used to study residual force-enhancement based on calcium modulated actin-titin interactions (cf. Section 2.2.3) (Heidlauf et al., 2016; Heidlauf et al., 2017).

While the works of Röhrle and co-workers tried to establish an integrated physiological model of the neuromuscular system, there exist other multiscale, multiphysics models focusing on individual aspects of skeletal muscle physiology. For example, Hernández-Gascón et al. (2013) coupled a continuum mechanical muscle model to a phenomenological description of the excitation-contraction coupling pathway, however, neglected muscle recruitment on the motor unit level and the spatial propagation of action potentials. Furthermore, Fernandez, Buist, Nickerson, and Hunter (2005) and Böl, Weikert, and Weichert (2011) used similar modeling approaches, additionally taking into account the spatial propagation of action potentials. However, those models still fail to simulate realistic recruitment scenarios, since they do not resolve individual motor units.

Considering volumetric muscle models, neural control has only been considered by unidirectional coupling and by employing phenomenological models, for example, by using the Fuglevand model to predetermine the motor unit firing times (Röhrle et al., 2012). The bidirectional coupling of the multiscale chemo-electro-mechanical muscle models (Heidlauf & Röhrle, 2014) and biophysical models of the motor neuron pool (Negro & Farina, 2011), that is, including sensory feedback, is feasible, yielding an integrated multiscale and multiphysics model of the neuromuscular system (Heidlauf, Negro, Farina, & Röhrle, 2013).

3.3 | Musculoskeletal system modeling

Almost all simulations of (parts of) the musculoskeletal system appeal to multibody simulation frameworks. In these frameworks, the mechanical behavior of skeletal muscles and the corresponding tendons are typically modeled with spatially lumped Hill-type skeletal muscle models (cf. Section 3.2.2). The respective lines of action are typically defined through a straight line between the muscle-tendon unit's insertion and its origin. To appropriately capture the muscle lever arms, in particular of muscle-tendon units wrapping around a joint, the respective lines of action are diverted through wrapping surfaces

or via points (Charlton & Johnson, 2001; Garner & Pandy, 2000; Scholz, Sherman, Stavness, Delp, & Kecskeméthy, 2016; Zarifi & Stavness, 2017). Multibody musculoskeletal modeling provides a method to investigating movement statics and dynamics by also considering the underlying muscle forces (Damsgaard, Rasmussen, Christensen, Surma, & De Zee, 2006; Pandy, 2001a). Multibody musculoskeletal simulations are mostly based on inverse dynamics using an optimization criteria, for example, minimal squared muscle activation sum or minimal metabolic cost of transport, to determine muscle activation and force distribution given a particular motion (Anderson & Pandy, 2001; Rasmussen, Damsgaard, & Voigt, 2001). These models aim to understand movement disorders or to estimate muscle activation strategies and force distributions for specific conditions (Sartori et al., 2017). Although this approach provides repeatable muscle force patterns that may be valid in specific conditions, its optimization approach omits the nonlinear and context-dependent (time, training, fatigue, pathology, etc.) dynamics of the neuro-musculoskeletal system as a whole. Those vary strongly across subjects/patients. Alternatively, one can also integrate into the musculoskeletal model formulations unique muscle activation captured, for example, from experimental EMG recordings, that is, to employ forward-dynamics simulations to predict motion from neural input. Such EMG-driven musculoskeletal models were used to blindly estimate the multimuscle joint torque function, that is, without any tracking mechanism that accounts for prediction errors (Lloyd & Besier, 2003a; Sartori, Reggiani, Farina, & Lloyd, 2012; Sartori, Yavuz, & Farina, 2017). It is noteworthy that these modeling approaches uses experimental data to simulate muscle force under specific conditions while providing the possibility for real time analysis of neuro-musculoskeletal functions in vivo (Durandau, Farina, & Sartori, 2018).

If musculoskeletal system modeling frameworks that appeal to volumetric skeletal muscle representations do exist at all, then they are typically found in computer animations (Lee, Sifakis, & Terzopoulos, 2009). The main aim of these models is to achieve realistically looking movement fast. They do that by ignoring most of the underlying biophysical principles of skeletal muscle mechanics. Three-dimensional (continuum-mechanical) musculoskeletal system models that aim to resolve the underling physical behavior are extremely rare. Fernandez and Hunter (2005), for example, investigated the wrapping of muscles around the knee joint using a continuum-mechanical musculoskeletal muscle model following an inverse-dynamics approach, that is, prescribing the motion of the skeleton as well as the respective muscle activations to determine contact forces due to muscle wrapping around the knee. One of the first forward-dynamics simulation of a musculoskeletal system, that is, determining the deformations of the soft tissues due to muscular activity, was proposed by Wu, Hung, Hunter, and Mithraratne (2013). They aimed to study facial expressions as a result of prescribing different muscle activations. Ramasamy et al. (2018) developed a pipeline for a simulation-analysis workflow for finite element simulations of the socket and stump of above knee amputees. Although that workflow can be used for forward- or inverse-dynamics simulations, they did not pursue the prediction of motion in that study. The only model predicting the motion of an agonist–antagonist musculoskeletal system (here a two-muscle-one-degree-of-freedom upper limb model) was proposed by Röhrle, Sprenger, and Schmitt (2017). This model was also the basis for developing a novel surrogate approach to achieve forward and inverse simulations in real time (Valentin, Sprenger, Pflüger, & Röhrle, 2018).

Note that accurate musculoskeletal system models require an adequate representation of surrounding connective tissues such as the tendons and aponeuroses, that is, resolving both the three-dimensional geometry as well as the mechanical material behavior. This is essential because connective tissues have a significant influence on the transmission of active muscle stresses to the skeleton and thus on control strategies as well as the energetic efficiency of motion.

Finally, continuum-mechanical musculoskeletal system models, in which skeletal muscles are modeled with chemo-electro-mechanical skeletal muscle models, or which are linked to motor neuron pool models, do not exist. In particular, motor neuron driven musculoskeletal system models combined with chemo-electro-mechanical skeletal muscle models could provide significant impact, as one would be able to predict the resulting electrical potential on the surface, that is, the electromyographic (EMG) signals (cf. Section 3.5). With the help of these simulations and the comparison with measured EMG signals, in particular high-density EMG signals (Staudenmann, Roeleveld, Stegeman, & van Dieen, 2010), one could obtain entirely new insights into the underlying biophysical processes of the neuromuscular system.

3.4 | Sensory feedback modeling

Coupling musculoskeletal system models (cf. Section 3.3) to models of the neural system (cf. Section 3.1), that is, yielding a coupled neuromuscular system model, also requires the consideration of signals stemming from sensory feedback mechanism. The sensory signals evoked by muscle spindles and Golgi tendon organs are the two major feedback signals involved in muscular control and therefore modeling and integration of these two signals should also be considered within computational models. The signals stemming from the muscle spindles and Golgi tendon organs hereby modulate the activity of the αMNs

by feeding back to the αMNs information about the local stretch, the rate of deformation and the mechanical stress within the muscle. Moreover, the sensory activity can be adjusted by specialized γMNs and βMNs (cf. Section 2.1).

The most simplistic approaches for modeling sensory feedback signals, which originate from muscle spindles, are black-box approaches that provide a function simply capturing the (experimentally determined) input–output relation between the afferent firing rate and mechanical perturbations. A comparison between different spindle models is provided, for example, in Prochazka and Gorassini (1998).

Such phenomenological modeling approaches have significant limitations. While they implicitly include the fusimotor drive as well as the contribution from primary and secondary spindle feedback mechanism, they fail to predict the influence of static and dynamic fusimotor inputs stemming from the γMNs and βMNs. Furthermore, phenomenological models are not capable of separating the influence of primary and secondary spindles. Therefore, more detailed (physiologically informed) muscle spindle models haven been proposed that include the modulation of the sensory feedback caused by the fusimotor drive of the γMNs (Lin & Crago, 2002a; Mileusnic, Brown, Lan, & Loeb, 2006) or from both γMNs and βMNs motoneurons (Maltenfort & Burke, 2003).

The Golgi tendon organ is the reciprocal partner of the muscle spindles and plays an important role as it senses changes of the muscle tension. Similar as for the muscle spindles, there exist simplistic phenomenological Golgi tendon organ models that are calibrated to reproduce experimental data from animal experiments (Crago, Houk, & Rymer, 1982; Fukami & Wilkinson, 1977; Houk & Henneman, 1967; Lin & Crago, 2002b; Song, Lan, Loeb, & Gordon, 2008). Furthermore, a more detailed, comprehensive model of the Golgi tendon organ, which is capable of predicting the nonlinear response of the Golgi tendon organs caused by the activity of a heterogeneous MU population, has been proposed by Mileusnic and Loeb (2006).

Realistic modeling predictions of such models, however, are challenging, because the current knowledge on the activity of the mixed fusimotor drive is still poor. Thus, predictions obtained from simulations are based on modeling assumptions that try to estimate the fusimotor activity and therefore yield a high degree of uncertainty. For example, the neuromusculoskeletal model of Elias et al. (2014) considers the static and dynamic fusimotor activities. They do so by appealing to a Gaussian random process with an empirically chosen variance.

3.5 | Simulating electromyographic signals

The impact of a muscle on the electrical potential of its environment, that is, the body, is a consequence of the depolarisation of the muscle fiber membranes. Hence, measuring the overall electrical potential by means of electromyography (EMG), for example, by placing electrodes on the surface of the skin close to a muscle, provides a way of investigating a skeletal muscle's electrical state, and hence can provide deep insight into the functioning of the neuromuscular system (Staudenmann et al., 2010). EMG signals are typically easy to record, for example, using either noninvasive surface electrodes or invasive needle electrodes. However, one of the major drawbacks of EMG signals is that they are hard to interpret and analyze (Farina, Holobar, Merletti, & Enoka, 2010). Thus, mathematical models have a great potential to improve signal interpretation. EMG signals are usually simulated by means of volume conductor models (see Mesin (2013) for a detailed review). Thereby, skeletal muscle tissue is assumed to be an (anisotropic) ohmic conductor and the bio-electrical activity arising from the depolarisation of the muscle fiber membranes is represented by spatially distributed current sources/sinks. Purely phenomenological models simulate EMG signals by prescribing the shape of action potentials and the corresponding conduction velocity (Farina & Merletti, 2001; Farina, Mesin, Martina, & Merletti, 2004; Lowery, Stoykov, Taflove, & Kuiken, 2002; Merletti & Parker, 2004). A biophysically more detailed description of the propagation of action potentials along muscle fibers can be obtained by solving the monodomain model (Mordhorst, Heidlauf, & Röhrle, 2015), which can be considered to be an one-dimensional extension of Hodgkin–Huxley type models. Thereby, the biophysical models can account for changes in the amplitude and propagation velocity of the AP that result, for example, from membrane fatigue. While most of the existing (single-physics) EMG models do not take into account tissue deformation, and hence are restricted to isometric conditions, cf. Mesin, Joubert, Hanekom, Merletti, and Farina (2006), multiphysics models coupling EMG models to continuum mechanical models (Mordhorst et al., 2015), can also simulate EMG generation during nonisometric conditions. To speed up the computation of the electrical signals and the EMG, one can also apply model order reduction techniques (Mordhorst, Strecker, Wirtz, Heidlauf, & Röhrle, 2017).

3.6 | Further reading

With regard to theoretical and mathematical descriptions of biophysical models, the reader is referred to Keener and Sneyd (2009a, 2009b), Tuckwell (2005), and Herzog (2000). As far as fundamentals of mechanical properties of living tissues and continuum mechanics are concerned, the reader is referred to Fung (2013) and Holzapfel (2000).

4 | MODELING THE NEUROMUSCULAR SYSTEM

The aim of this section is to provide for each of the components one sample model and to link them together in one overall systemic model. The framework is hereby set up in a modular way such that individual components of the overall neuromuscular model can be exchanged in a straight forward way. Thereby note that this review focuses on multiscale neuromuscular modeling and not on aspects of validating individual components or even the entire model. This would be beyond the scope of this review. However, one of the advantages of having a multiscale models of the neuromuscular system available is the ability to systematically investigate the impact of specific components with respect to the other components and phenomena on different scales—something that might be challenging to achieve from an experimental point of view. By estimating parameters or changing modeling assumptions on one specific scale and validating against output from another scale, one can also further increase the confidence into the predictive power of multiscale models. The latter is of particular importance for scales on which only sparse and/or poor data exist, that is, on data-poor scales.

After providing a review on the state of the art of different components of the neuromuscular system, this section provides the underlying mathematical equations for one particular neuromuscular model. Hence, after introducing some fundamentals of biophysical modeling by outlining the pioneering work of Hodgkin and Huxley (1952) on the membrane behavior of excitable cells (Section 4.1), this Section follows the structure of Section 3. Starting with the introduction of the individual components of the neuromuscular model, that is, the mathematical description of the biophysical motor neuron model by Negro and Farina (2011) (Section 4.2), the mathematical description of the biophysical muscle fiber model by Shorten et al., (2017) (Section 4.3), the mathematical description of the skeletal muscle model by Röhrle et al. (Section 4.4, the mathematical description of the muscle spindle model by Maltenfort and Burke (2003) (Section 4.5) and finally a fully coupled model of the whole neuromuscular system is presented by combining all sub-models (Section 4.6).

The models have not been chosen arbitrary. The MN pool model of Negro and Farina (2011) was selected because it is capable of integrating excitatory and inhibitory signals from various sources and because it is based on a biophysical modeling approach that implicitly reflects many important characteristics of real MN pools such as, for example, the well established size principle (Henneman et al., 1965a, 1965b). Furthermore, considering the functional organization of the neuromuscular system into MUs, a three-dimensional multiscale continuum modeling approach such as the on proposed by Röhrle et al. (2012) is almost indispensable. In particular, the fact that the physiologically detailed skeletal muscle model can predict both the mechanical system response as well as the corresponding EMG signal during dynamic contractions is needed for the link to the feedback system (mechanical part) and for integrating chemo-electromechanical principles from the (sub-)cellular space. Employing the biophysical muscle fiber model of Shorten et al. (2007) provides us with the ability to link the electrical properties of skeletal muscle fibers with the mechanical properties of the overall muscle tissue, that is, resulting in a multiscale model that is capable of relating macroscopic findings to the cellular state of the tissue. Thereby, the organ-scale skeletal muscle model is implicitly capable of capturing multiple complex phenomena such as, for example, the nonlinear summation of twitches, decrease in the muscle fiber stresses caused by the insufficient activity of the SERCA pumps or membrane fatigue caused by the accumulation of potassium ions in the T-tubule system. Finally, the muscle spindle model of Maltenfort and Burke (2003) has been chosen because it provides the possibility to modulate the sensory feedback based on the activity of a γMN pool. Note, all models are also available for download.

4.1 | Fundamentals—the Hodgkin–Huxley model of the membrane electrophysiology

The Hodgkin and Huxley model (HH-model) simulates the electrical behavior of the membrane of excitable cells by employing an electrical equivalent circuit (Hodgkin & Huxley, 1952). It considers the behavior of a small patch of a membrane and represents ionic currents for sodium and potassium as well as a leakage current. Furthermore, voltage-dependent gating properties are introduced to represent the currents flowing through a large population of ion channels (Nelson, 2005). The form of this description has been used as the basis for almost all other ionic current models of excitable tissues. As such, the HH-model also builds the basis for the motor neuron model and the biophysical skeletal muscle model. Although already nicely presented in their original work (Hodgkin & Huxley, 1952), we briefly introduce it here once more, as it is the basis for many—if not all—biophysical models.

Cell membranes are selectively permeable to (charged) ions, and consequently they are able to separate electrical charges. Within a mathematical model, this can be represented by assigning a capacitance to the cell membrane. The law of capacitance states that the electric charge of a capacitor equals the voltage difference across the capacitor times its capacitance. Taking the time derivative of the law of capacitance and assuming that the membrane capacitance, C_m, is constant with respect to time, then C_m times the temporal change of the membrane potential, V_m, equals the (negative) sum of the ionic currents crossing the membrane, I_{ion}, that is,

$$I_{\mathrm{m}} = C_{\mathrm{m}} \frac{\partial V_{\mathrm{m}}}{\partial t} + I_{\mathrm{ion}} = 0, \tag{1}$$

where I_{m} denotes the total current flow across the cell membrane. The HH-model considers currents through sodium and potassium channels, I_{Na} and I_{K}, respectively, and a leakage current I_{L} representing the natural permeability of the membrane to, for example, Cl^{-}-ions. Furthermore, a current I_{stim} is considered that allows to stimulate the model from outside, that is,

$$I_{\mathrm{ion}} = I_{\mathrm{Na}} + I_{\mathrm{K}} + I_{\mathrm{L}} - I_{\mathrm{stim}}. \tag{2}$$

Herein, a positive sign indicates an outward current with the exception of I_{stim}, where a positive sign indicates an inward current. Based on Ohm's law, the membrane current of a given ion type i, with $i \in \{\mathrm{Na, K, L}\}$, is proportional to the membrane's conductance for this ion species and to a driving force in the form of the difference between the membrane potential and the ion's equilibrium potential, E_i, that is,

$$I_i = g_i (V_{\mathrm{m}} - E_i), \tag{3}$$

where g_i denotes the conductance per unit area for ion species i and is the inverse of the resistance. While the leakage conductance, g_L, is assumed to be constant, the conductances for the potassium and sodium channels depend on the membrane potential, that is,

$$g_{\mathrm{K}} = \bar{g}_{\mathrm{K}} n^4 \text{ and } g_{\mathrm{Na}} = \bar{g}_{\mathrm{Na}} m^3 h, \tag{4}$$

respectively. Therein, $\bar{g}_{\mathrm{K}}$ and $\bar{g}_{\mathrm{Na}}$ denote the maximum values of the respective conductances, and n, m, and h are gating variables resembling probabilities associated with the potassium channel activation, sodium channel activation, and sodium channel inactivation, respectively (Hodgkin & Huxley, 1952).

The evolution equations of the gating variables are based on first-order kinetics and can either be expressed using relaxation time constants (Hodgkin & Huxley, 1952), or take the form

$$\frac{\partial \omega}{\partial t} = \alpha_\omega (V_{\mathrm{m}})(1-\omega) - \beta_\omega (V_{\mathrm{m}})\omega, \tag{5}$$

for $\omega \in \{n, m, h\}$. Hereby, $(1 - \omega)$ and ω represent two states, for example, ω is the probability that a channel is open and, hence, $(1 - \omega)$ is the probability that the channel is closed. The dependence of the forward and backward reaction rates $\eta_\omega \in \{\alpha_\omega(V_{\mathrm{m}}), \beta_\omega(V_{\mathrm{m}})\}$, respectively, on the membrane voltage can be generalized using the form

$$\eta_\omega = \frac{a_\omega + b_\omega V_{\mathrm{m}}}{c_\omega + d_\omega \exp\left(\frac{V_{\mathrm{m}} + e_\omega}{f_\omega}\right)}, \tag{6}$$

with constants a_ω, b_ω, c_ω, d_ω, e_ω, and f_ω (Nelson, 2005). For the sake of brevity, further details are omitted here but can be found, for example, in Hodgkin and Huxley (1952), Nelson (2005).[1] Figure 8 shows the electrical circuit used in the Hodgkin–Huxley model to represent the cell membrane.

Based on the same formalism, more detailed models have been proposed in the literature. These models typically distinguish more ionic currents, and/or subdivide the modeled membrane into multiple compartments, but which are coupled to each other (Adrian & Peachey, 1973; Segev, Fleshman, & Burke, 1989; Wallinga et al., 1999). Moreover, the same ideas of having transition variables between different states have also been utilized for other models than membrane models of excitable cells.

4.2 | Modeling motor neurons and the motor neuron pool

Based on the Hodgkin–Huxley formalism, Cisi and Kohn (2008) proposed a compartmental model for the simulation of spinal cord MNs. While Hodgkin and Huxley simulated a small patch of a membrane, the MN model of Cisi and Kohn (2008) represents the entire cell. To limit the computational load, Cisi and Kohn (2008) simplified the spatial propagation

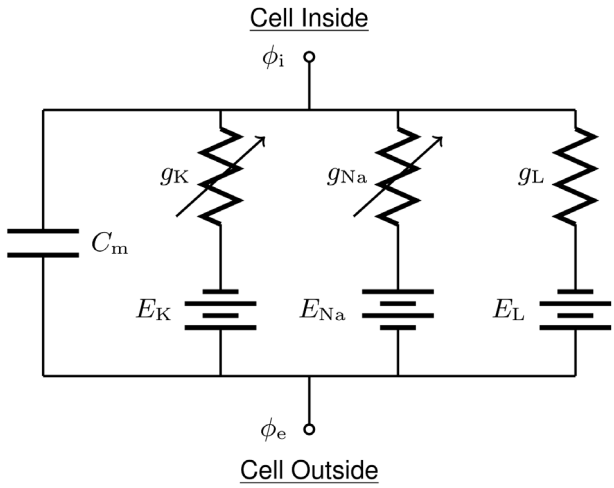

FIGURE 8 Illustration electrical equivalent circuit, which was used by Hodgkin and Huxley (1952) to mimic the electrical behavior of the membrane of the squid giant axon. Resistors with an arrow indicate voltage-dependent conductances. The membrane potential, V_m, equals the difference between the intracellular potential, ϕ_i, and the extracellular potential, ϕ_e. The driving forces in the model are the differences between the membrane potential and the corresponding equilibrium potentials, which are represented by batteries

of the AP by considering two spatially lumped compartments, that is, one representing the dendrites and one representing the soma. Both compartments are connected by an ohmic conductor. They assume that the dendrites and the soma can be geometrically represented by a cylinder. Thus, the electrical properties of the compartments, for example, the membrane capacity, can be derived from macroscopic and geometrical parameters of the compartment, that is, the length and the radius. To be able to solve the evolution of the gating variables analytically, Cisi and Kohn (2008) approximate the time courses of the reaction rates (cf. Equation (6)) by rectangular pulses. Negro and Farina (2011) discard this approximation and solve the ODEs for the gaiting variables using functions of the form given in Equation (6) and using parameters provided by Traub and Miles (1991). The model of Negro and Farina (2011), including its parameterization, is adopted in this work for the simulation of spinal cord MNs.

4.2.1 | Mathematical description of the motor neuron model of Cisi and Kohn

Due to the two compartment approach, the MN model of Cisi and Kohn (2008) distinguishes the membrane potential in the dendrites and in the soma, $V_m{}^d(t)$ and $V_m{}^s(t)$, respectively, that is,

$$\begin{aligned} C_m^d \frac{\partial V_m^d}{\partial t} &= -I_{ion}^d\left(V_m^d\right) - I_C^d\left(V_m^d, V_m^s\right), \\ C_m^s \frac{\partial V_m^s}{\partial t} &= -I_{ion}^s\left(V_m^s\right) - I_C^s\left(V_m^d, V_m^s\right). \end{aligned} \tag{7}$$

The two equations are linked to each other through coupling currents I_C^d and I_C^s, where $I_C^s = -I_C^d$ due to the conservation of electric charge. Furthermore, in Equation (7), I_{ion}^d and I_{ion}^s are the ionic currents crossing the membrane of the dendrites and the soma, respectively. For the dendrites, only a leakage current I_L^d is considered, while for the soma a leakage current I_L^s, a sodium current I_{Na}, a fast and a slow potassium current, I_{Kf} and I_{Ks}, respectively, and an external current I_{stim} are considered, that is,

$$I_{ion}^d = I_L^d \text{ and } I_{ion}^s = I_L^s + I_{Na} + I_{Kf} + I_{Ks} - I_{stim}. \tag{8}$$

Cisi and Kohn (2008) reduced the number of ionic currents to a minimum while still ensuring that the model is capable of capturing the most important neuronal properties, that is, recruitment and firing rate strategies based on electrical properties of the respective αMN. The slow potassium current, for example, has been included to incorporate the afterhyperpolarisation, which impedes the generation of subsequent APs. Additional properties, like persistent inward currents, have been included in follow-up studies (Elias & Kohn, 2013; Elias et al., 2012). The electrical circuit corresponding to the MN model of Cisi and Kohn (2008) is depicted in Figure 9.

Similar to the approach of Hodgkin and Huxley, the description of the ionic currents is based on Ohm's law, that is, the currents equal a conductance times a potential difference, that is,

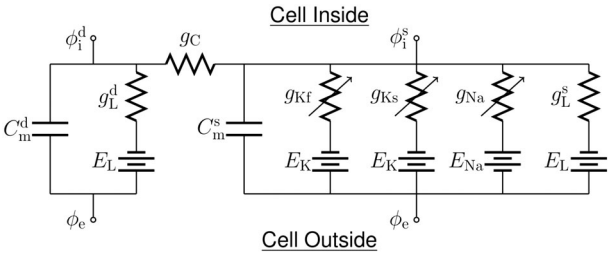

FIGURE 9 Electrical circuit model for the motor neuron model. Again, resistors with an arrow indicate voltage-dependent conductance. The dendritic membrane potential, V_m^d, equals the difference between the dendritic intracellular potential, ϕ_i^d, and the extracellular potential, ϕ_e. The somatic membrane potential, V_m^s, equals the difference between the somatic intracellular potential, ϕ_i^s, and the extracellular potential, ϕ_e. The driving forces in the model are the differences between the membrane potentials and the corresponding equilibrium potentials, which are represented by batteries

$$\begin{aligned} &I_L^d = g_L^d\left(V_m^d - E_L\right),\ I_L^s = g_L^s\left(V_m^s - E_L\right),\\ &I_C^d = g_C\left(V_m^d - V_m^s\right),\ I_{Na} = g_{Na}\left(V_m^s - E_{Na}\right),\\ &I_{Kf} = g_{Kf}\left(V_m^s - E_K\right),\ I_{Ks} = g_{Ks}\left(V_m^s - E_K\right), \end{aligned} \tag{9}$$

where E_L, E_{Na}, and E_K are the equilibrium (or Nernst) potentials, g_C denotes the (constant) coupling conductance, g_L^d and g_L^s are the (constant) dendritic and somatic leakage conductances, respectively, g_{Na} is the sodium channel conductance, and g_{Kf} and g_{Ks} represent the fast and slow potassium channel conductances, respectively. To model the membrane potential dependence of g_{Na}, g_{Kf}, and g_{Ks} gating variables m, n, h, and q are introduced, together with the maximum conductances, $\bar{g}_{Na}$, $\bar{g}_{Kf}$, and $\bar{g}_{Ks}$, the gating variables are defined as

$$g_{Na} = \bar{g}_{Na} m^3 h,\ g_{Kf} = \bar{g}_{Kf} n^4,\ \text{and}\ g_{Ks} = \bar{g}_{Ks} q^2. \tag{10}$$

The evolution of the gating variables, $\omega \in \{m, n, h, q\}$, is given by Equation (5) using the respective forward and backward reaction rates given in Equation (6). Together with the equations for the dendritic and somatic membrane potentials (7), this yields a nonlinear system of six coupled ODEs.

4.2.2 | Mathematical description of the Negro and Farina motor neuron pool model

To simulate the behavior of a MN pool, each MN is described by the equations given above. Note that the equations for one MN can be solved independently of all other MNs, since the modeled MNs are not coupled to each other or do exchange information. The MNs of a pool are only related to each other through synaptic input components common to several MNs and the assigned MN parameters, for example, the excitation threshold. As described in Section 2.1, MN excitation thresholds are distributed across the corresponding MN pool, whereat many low-threshold MNs and few high-threshold MNs are found, cf. for example, Powers and Binder (1985), Thomas, Ross, and Stein (1986). The MN model of Negro and Farina (2011) accounts for this distribution by specifying extreme values for the electrical and geometrical properties of the MNs in a pool, and interpolating exponentially between these extreme values to find the properties of a given MN. To do so, it is convenient to number the MNs in the pool in an ordered sequence, for example, starting from the MN with the lowest excitation threshold (MN number 1) to the highest-threshold MN (MN number N, with N being the number of MNs in the pool). Let δ_l and δ_u denote the lower and upper extreme values of a property, respectively. Following Negro and Farina (2011), the corresponding value of the i-th MN with $i \in \{1, \ldots, N\}$ is determined from

$$\delta_i = \delta_l + \frac{\delta_u - \delta_l}{100} \exp\left(\ln(100)\frac{i}{N}\right). \tag{11}$$

The extreme values of the electrical (soma- and dendrite-specific resistances) and geometrical properties (length and diameter of soma and dendrite) used in the interpolation stem from Cisi and Kohn (2008). It is noteworthy that due to the assigned parameter ranges, a size-ordered MN recruitment pattern is observed, when applying a common stimulation current to the entire MN pool (Cisi & Kohn, 2008). This behavior is also experimentally observed, cf. Henneman et al. (1965a, 1965b). Furthermore, parameters such as equilibrium potentials and membrane capacitance are also adopted from Cisi and Kohn (2008), who utilized for their model a broad range of experimental data available in the literature.

4.2.3 | Input to motor neurons

Spinal cord MNs constantly receive excitatory and inhibitory postsynaptic inputs from various sources, for example, from the motor cortex via the corticospinal tract, from the brain stem, from afferent neurons, and from spinal/supraspinal interneurons. Due to the temporal and spatial summation of these postsynaptic potentials, the MN's membrane potential is permanently subject to random fluctuations (Calvin & Stevens, 1968). In order to account in the model for these fluctuations, the synaptic input current to each MN contains noise components. Furthermore, components in the input signal can be different for each MN or common to (parts of) the MN pool depending on the origin of the input. In detail, a cortical input current I_{CI}, common to the entire MN pool, is considered. This input consists of two parts, a mean component $I_{\mathrm{CI}}{}^{\mathrm{m}}$ and a noise component $I_{\mathrm{CI}}{}^{\mathrm{n}}$. The fluctuating component, $I_{\mathrm{CI}}{}^{\mathrm{n}}$, is modeled as colored Gaußian noise (bandwidth 0.5–40 Hz), cf. Negro and Farina (2011). Gaußian white noise refers to a random signal with zero mean, constant power spectral density, and Gaußian (normal) amplitude distribution. Furthermore, a second common input component I_{SI} is considered representing, for example, signals from the brain stem, interneurons and afferent neurons. This component is modeled as band-limited (0–100 Hz) Gaußian white noise (Negro & Farina, 2011). Additionally, an independent signal $I_{\mathrm{IN}}{}^{i}$, where $i \in \{1, \ldots, N\}$, for each MN is considered representing synaptic noise, which is modeled as band-limited (0–100 Hz) Gaußian white noise (Negro & Farina, 2011). The specific forms of the components are chosen based on literature data, cf. Negro and Farina (2011). The synaptic input signal for each MN is a linear combination of these components, that is, $I_{\mathrm{stim}}{}^{i} = (I_{\mathrm{CI}}{}^{\mathrm{m}} + I_{\mathrm{CI}}{}^{\mathrm{n}}) + I_{\mathrm{SI}} + I_{\mathrm{IN}}{}^{i}$ with $i \in \{1, \ldots, N\}$ (cf. Figure 10). Note that the independent noise component, the secondary common input component, and the fluctuating cortical component contain positive and negative values, representing excitatory and inhibitory signals, and variations from the mean cortical input, respectively. In general, the total variance of the injected synaptic current is modeled as a percentage of the mean synaptic input able to provide a coefficient of variation for the interspike interval (ISI) during steady state contractions of approximately 15% (Maltenfort, Heckman, & Rymer, 1998; Moritz, Barry, Pascoe, & Enoka, 2005).

4.3 | Mathematical description of the skeletal muscle model of Shorten et al.

The signaling pathway from electrical excitation to contraction and force generation in skeletal muscles (see Section 2.2.5) is extremely complex and to date not completely understood (MacIntosh et al., 2006). Even though mathematical models of the excitation-contraction coupling pathway are an essential component for any universal in silico model of the neuromuscular system, the work of Shorten et al. (Shorten et al., 2007) is an exception (cf. Section 3.2.4), providing a model of the entire excitation-contraction coupling pathway. Therefore, within this section, we provide an overview of the model of Shorten et al. (Shorten et al., 2007), including additional modifications to simulate nonisometric contractions.

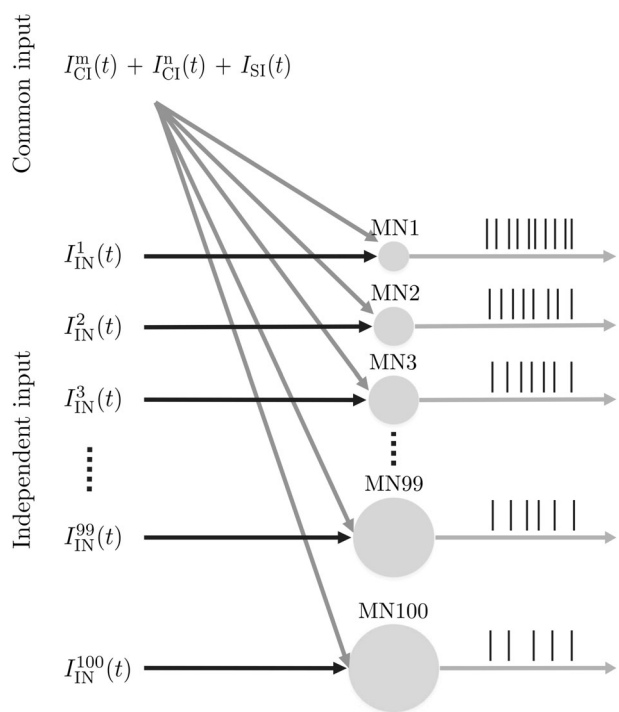

FIGURE 10 Schematic drawing of the motor neuron pool model; the figure illustrates the structure of a model that simulates a pool with 100 αMNs. Thereby the size and thus the electrical properties of the MNs changes through the pool exponentially. Motor neurons receive inputs from different classes of inputs signals. The independent input, that is, $I_{\mathrm{IN}}{}^{i}$, is represented by Gaußian noise with a bandwidth of 0–100 Hz. The common input signal represents the linear combination of a mean component, that is, $I_{\mathrm{CI}}{}^{\mathrm{m}}$, a Gaußian noise component (bandwidth 0.5–40 Hz), that is, $I_{\mathrm{CI}}{}^{\mathrm{n}}$, and the secondary common input, that is, I_{SI}, corresponding to oscillations generated from other structures of the central nervous system and which is also modeled as zero mean Gaußian noise (bandwidth 0–100 Hz). The output of the model is the firing trains of αMNs

In summary, Shorten et al. (2007) combine several published sub-models of the excitation-contraction pathway representing

a. the electrophysiology of the muscle fiber membrane, that is, a HH-model simulating the APs caused by currents in the sarcolemma and T-tubules, cf. Adrian and Peachey (1973), Wallinga et al. (1999),
b. intracellular Ca^{2+} release from the sarcoplasmic reticulum in response to membrane depolarization through ryanodine receptor (RyR) Ca^{2+} release channels, cf. Ríos et al. (1993),
c. intracellular calcium dynamics, that is, the binding of Ca^{2+} to troponin enabling XB cycling and buffers like parvalbumin, adenosine triphosphate, and in the SR to calsequestrin, cf. Baylor and Hollingworth (1998),
d. force generation via cross-bridge cycling, cf. Campbell, Razumova, Kirkpatrick, and Slinker (2001a, 2001b), Razumova et al. (1999), Razumova, Bukatina, and Campbell (2000), and
e. muscle fatigue based on the accumulation of phosphate in the SR.

Figure 11 schematically depicts an overview of the model of Shorten et al. (2007), indicating the individual model components (a–e, see above) and their interactions. Mathematically, the evolution of the state variables, $\boldsymbol{y} = [\boldsymbol{y}_{\text{mem}}^T, \boldsymbol{y}_{\text{RyR}}^T, \boldsymbol{y}_{\text{CaD}}^T, \boldsymbol{y}_{\text{XB}}^T, \boldsymbol{y}_{\text{p}}^T]^T$, can be described by 56 coupled ODEs, that is, $y \in \mathbb{R}^{56}$.

The section is divided into three subsections, providing a brief summary of the individual sub-models and their coupling. While the model of XB cycling was extended to simulate concentric/eccentric contractions (i.e., resolving the force-length relation and the force-velocity relation), the phosphate dynamics model is not described here since the evolution of fatigue in the Shorten et al. (2007) model is not sensitive to the corresponding differential equations (at least for the published parameters). Note that for the sake of brevity, only some important/exemplary differential equations are presented within this manuscript, however, a complete mathematical description and an implementation of the model is available on www.cellml.org.[2]

4.3.1 | Membrane electrophysiology

Based on the Hodgkin–Huxley formalism and geometrical considerations on the shape of the muscle fibers and the T-tubule system, a two-compartment model of membrane electrophysiology is utilized (Wallinga et al., 1999; Adrian & Peachey, 1973). Thereby, ionic currents crossing the sarcolemma (superscript s) and the T-tubule membrane (superscript t) are distinguished. The latter, the current density in the sarcolemma, $I_{\text{ion}}^{\text{s}}$, and the current density in the T-tubule membrane $I_{\text{ion}}^{\text{t}}$, can be calculated as the sum of the individual ion channel current densities, that is,

$$I_{\text{ion}}^{\text{s}} = I_{\text{Na}}^{\text{s}} + I_{\text{DR}}^{\text{s}} + I_{\text{IR}}^{\text{s}} + I_{\text{Cl}}^{\text{s}} + I_{\text{NaK}}^{\text{s}}, \tag{12}$$

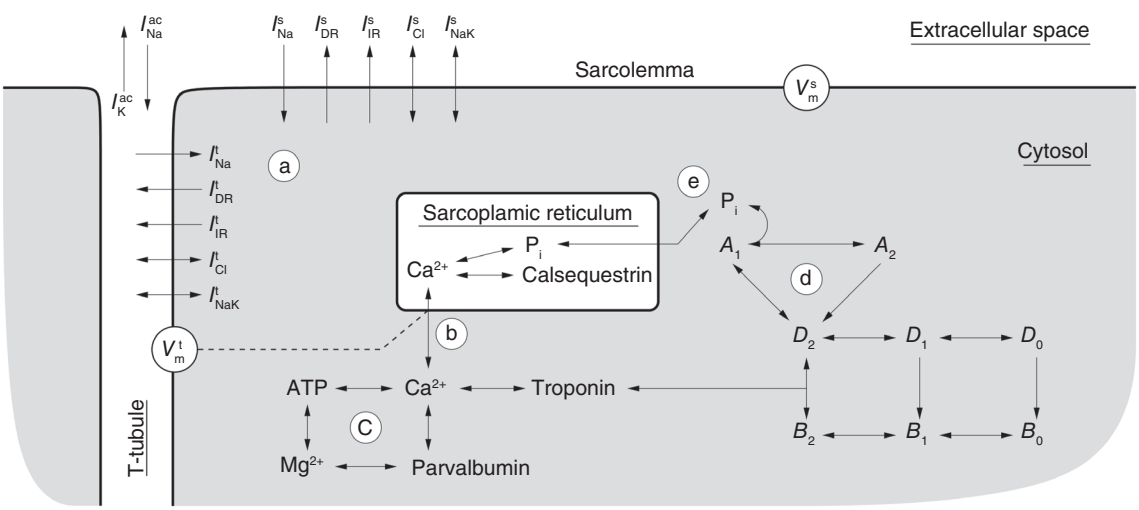

FIGURE 11 Schematic representation of the model of Shorten et al. (2007), indicating its components and their interactions. Therein, (a) indicates the model of the membrane ionic currents, (b) is the Ca^{2+}-release model, (c) denotes the Ca^{2+}-dynamics model, (d) is the model of the XB dynamics, and (e) shows the fatigue model. The figure is taken from Heidlauf (2015)

$$I_{\mathrm{ion}}^{\mathrm{t}} = I_{\mathrm{Na}}^{\mathrm{t}} + I_{\mathrm{DR}}^{\mathrm{t}} + I_{\mathrm{IR}}^{\mathrm{t}} + I_{\mathrm{Cl}}^{\mathrm{t}} + I_{\mathrm{NaK}}^{\mathrm{t}}. \tag{13}$$

In detail, the model considers sodium channels ($I_{\mathrm{Na}}^{\mathrm{s}}$, $I_{\mathrm{Na}}^{\mathrm{t}}$), delayed rectifier potassium channels ($I_{\mathrm{DR}}^{\mathrm{s}}$, $I_{\mathrm{DR}}^{\mathrm{t}}$), inverse rectifier potassium channels ($I_{\mathrm{IR}}^{\mathrm{s}}$, $I_{\mathrm{IR}}^{\mathrm{t}}$), chloride channels ($I_{\mathrm{Cl}}^{\mathrm{s}}$, $I_{\mathrm{Cl}}^{\mathrm{t}}$), and Na^+-K^+ pumps ($I_{\mathrm{NaK}}^{\mathrm{s}}$, $I_{\mathrm{NaK}}^{\mathrm{t}}$). Furthermore, based on Ohm's law, an access current between the T-tubule space and the extracellular space is introduced, electrically coupling the T-tubule space and the extracellular space, that is,

$$I_{\mathrm{T}} = \frac{V_{\mathrm{m}}^{\mathrm{s}} - V_{\mathrm{m}}^{\mathrm{t}}}{R_{\mathrm{a}}}. \tag{14}$$

Therein, R_{a} denotes the access resistance at the T-tubule entrance, taking into account the relative volume of the T-tubule space. Furthermore, $V_{\mathrm{m}}{}^{\mathrm{s}}$ and $V_{\mathrm{m}}{}^{\mathrm{t}}$ are the potential differences across the sarcolemma and the T-tubule membrane, respectively. Finally the evolution of the transmembrane voltage in the sarcolemma and in the T-tubule membrane can be calculated by the following differential equations:

$$\begin{aligned} C_{\mathrm{m}}^{\mathrm{s}} \frac{\partial V_{\mathrm{m}}^{\mathrm{s}}}{\partial t} &= -I_{\mathrm{ion}}^{\mathrm{s}}\left(t, V_{\mathrm{m}}^{\mathrm{s}}\right) - I_{\mathrm{T}}, \\ C_{\mathrm{m}}^{\mathrm{t}} \frac{\partial V_{\mathrm{m}}^{\mathrm{t}}}{\partial t} &= -I_{\mathrm{ion}}^{\mathrm{t}}\left(t, V_{\mathrm{m}}^{\mathrm{t}}\right) + \frac{I_{\mathrm{T}}}{\gamma_{\mathrm{t}}}. \end{aligned} \tag{15}$$

Therein γ_{t} is a geometrical parameter, that is, denoting the ratio between the T-tubule membrane surface are and the sarcolemma membrane surface are. Note that the mathematical modeling of the ion channels, that is, the gating properties and the constitutive relation between the channel conductivity and the gating variables, is similar as in the original Hodgkin–Huxley model, cf. Section 4.1. Further note that the electro-physiological model can be extended to three-dimensional simulations, that is, taking into account the spatial propagation of action potentials, by employing bidomain-type modeling approaches (cf. Section 3.2.5). Thereby, macroscopic quantities, for example, the action potential conduction velocity, are a consequence of the geometrical shape of the muscle fibers (surface-to-volume ratio), the conductivity of the tissue, as well as the (microscopic) membrane properties, and, hence, a predictable outcome of the model. For further details refer to Heidlauf and Röhrle (2013), Röhrle et al. (2008), and Röhrle et al. (2012).

4.3.2 | Intracellular calcium release and calcium dynamics

Incoming APs enter the T-tubule and depolarize the T-tubule membrane ensuring a simultaneous activation of all sarcomeres in the cross-section of a muscle fiber. Changes in the T-tubule membrane potential are sensed by the dihydropyridine receptor. The dihydropyridine receptor in the T-tubule membrane is linked to the RyR complex in the membrane of the SR, which, upon activation, enables the release of Ca^{2+}-ions.

The intracellular release of calcium from the SR to the cytosol is described by a 10-state model originally proposed by Ríos et al. (1993). Therefore, the model takes into account four voltage sensors, which are activated by the T-tubule membrane potential and control the permeability of the Ca^{2+}-channel. In detail, each sensor can be in an activated or a deactivated state, and the Ca^{2+}-channel can be closed or open. The rate at which the Ca^{2+}-channel opens (closes) increases with the number of voltage sensors in the activated (deactivated) state.

In the myoplasma, the released Ca^{2+}-ions activate the thin filament by binding to troponin. Furthermore, Ca^{2+}-ions compete with ions like Mg^{2+} to bind buffers such as parvalbumin and ATP. Mathematically, the transition between the different biochemical states is described by employing first-order kinetics. For example, for the binding of Ca^{2+} to ATP, that is,

$$\mathrm{Ca}^{2+} + \mathrm{ATP} \underset{k_{\mathrm{off}}}{\overset{k_{\mathrm{on}}}{\rightleftharpoons}} \mathrm{CaATP}, \tag{16}$$

this yields the following differential equations:

$$\begin{aligned}
\frac{\partial\left[\mathrm{Ca}^{2+}\right]}{\partial t} &= k_{\mathrm{off}}[\mathrm{CaATP}] - k_{\mathrm{on}}\left[\mathrm{Ca}^{2+}\right][\mathrm{ATP}],\\
\frac{\partial[\mathrm{ATP}]}{\partial t} &= k_{\mathrm{off}}[\mathrm{CaATP}] - k_{\mathrm{on}}\left[\mathrm{Ca}^{2+}\right][\mathrm{ATP}],\\
\frac{\partial[\mathrm{CaATP}]}{\partial t} &= k_{\mathrm{on}}\left[\mathrm{Ca}^{2+}\right][\mathrm{ATP}] - k_{\mathrm{off}}[\mathrm{CaATP}].
\end{aligned} \tag{17}$$

Therein, square brackets indicate concentrations. Note that the calcium-dynamics model considers two myoplasma compartments, that is, one close to the SR and one further away, that are coupled via Fick's law of diffusion. Furthermore, note that since the overall concentration of components as Ca^{2+}-ions is assumed to be constant, the overall model includes additional algebraic constraint equations.

In order to restore the high calcium concentration gradient between the SR and the myoplasma, Ca^{2+}-ions are transported back to the SR via the Ca^{2+}-ATPase (SERCA), where Ca^{2+}- ions bind to calsequestrin. Note that the model of Shorten et al. (2007) fatigue is caused by the inability of the SERCA to maintain the calcium concentration gradient during repeated stimulation. In summary, the calcium dynamics model accounts for 18 ODEs within the biophysical muscle model (Shorten et al., 2007).

4.3.3 | Force generation via cross-bridge dynamics

The binding of two Ca^{2+} ions to troponin C leads to a conformational change in the troponin molecule that removes the blocking tropomyosin from the actin filament, which allows the myosin heads to attach to the actin binding sites to form XBs. Thus, to derive force generation within the sarcomeres from cross-bridge cycling, modulated by Ca^{2+}-ions, Shorten et al. extended the regulatory process of the generic myofilament models of Razumova, Campbell, and co-workers (Campbell et al., 2001a; Campbell et al., 2001b; Razumova et al., 1999; Razumova et al., 2000). In detail, in six of the eight states, XBs are detached with either zero, one, or two Ca^{2+}-ions bound to troponin (denoted by indices 0, 1, and 2, respectively), and tropomyosin in either the blocking (B) or nonblocking (D) position. Only when two Ca^{2+}-ions are bound to troponin, the tropomyosin block can be removed ($B_2 \rightarrow D_2$), and myosin heads can bind to the thin filaments. Furthermore, two attached states are distinguished—the prepower stroke state, A_1, and the postpower stroke state, A_2. Thereby, the transition from the A_1 to the A_2 state represents the power stroke, that is, the force producing step. While in classical Huxley-type myofilament models, for example, Huxley (1957) each XB is associated with an individual elongation of the myosin heads' molecular spring, the applied XB dynamics model (Campbell et al., 2001a, 2001b; Razumova et al., 1999, 2000) is based on mean-field approach, that is, each cross-bridge state is associated with an average cross-bridge elongation. While Shorten et al. (2007) only considered isometric contractions and thus the average XB elongations are constants, the myofilament model of Razumova, Campbell, and co-workers (Campbell et al., 2001a, 2001b; Razumova et al., 1999, 2000) is also capable to simulate concentric/eccentric contractions. The velocity dependency of the prepower stroke XB elongation x_1 and the postpower stroke XB elongation x_2 can be easily incorporated into the model of Shorten et al. (2007) by including two additional differential equations (Heidlauf & Röhrle, 2014). Thereby, XB cycling within the sarcomeres can be simulated by the following differential equations:

$$\begin{aligned}
\frac{\partial[D_2]}{\partial t} &= k_{\mathrm{T}}^{\mathrm{on}}\left[\mathrm{Ca}^{2+}\right][D_1] + k_{\mathrm{Ca}}^{\mathrm{on}}[B_2] + f'[A_1] +\\
&+ g_0[A_2] - \left(k_{\mathrm{T}}^{\mathrm{off}} + k_{\mathrm{Ca}}^{\mathrm{off}} + f_0\right)[D_2],\\
\frac{\partial[A_1]}{\partial t} &= f_0[D_2] + h'[A_2] - (f' + h_0)[A_1],\\
\frac{\partial[A_2]}{\partial t} &= h_0[A_1] - (h' + g_0)[A_2],\\
\frac{\partial x_1}{\partial t} &= -\left(f_0\frac{[D_2]}{[A_1]} + h'\frac{[A_2]}{[A_1]}\right)x_1 +\\
&\quad + h'\frac{[A_2]}{[A_1]}(x_2 - x_0) + \dot{\ell}_{\mathrm{hs}},\\
\frac{\partial x_2}{\partial t} &= -h_0\frac{[A_1]}{[A_2]}(x_2 - (x_1 + x_0)) + \dot{\ell}_{\mathrm{hs}}.
\end{aligned} \tag{18}$$

Therein, k_T^{on} and k_T^{off} are the rate coefficients for the binding and unbinding of Ca^{2+} to troponin, respectively, and k_{Ca}^{on} and k_{Ca}^{off} denote the rate coefficients for switching between the blocking and the nonblocking state of the regulatory unit when two Ca^{2+} ions are bound to troponin. Furthermore, f_0, f', h_0, h', g_0 are reaction rate coefficients for XB cycling and $\dot{\ell}_{hs}$ is the contraction velocity of the half-sarcomere. Assuming constant reaction rates to simulate the XB-cycle would result in a linear force-velocity relation. To reproduce a more realistic hyperbolic force-velocity relation (Hill, 1938), Razumova et al. (1999) introduced additional constitutive relations to modulate the attachment rate, f_0, caused by the interactions between neighboring XBs and the detachment rate, g_0, depending on the average elongation of the postpower stroke XBs, that is,

$$\begin{aligned} f_0 &= \bar{f}\Big(1 + \frac{[A_1]}{T_{tot}}\left[\exp\left(\frac{x_1}{x_0}(\nu - 1)\right) - 1\right] \\ &\quad + \frac{[A_2]}{T_{tot}}\left[\exp\left(\frac{x_2}{x_0}(\nu - 1)\right) - 1\right]\Big), \\ g_0 &= \bar{g}\exp\left(\vartheta(x_2 - x_0)^2\right), \end{aligned} \tag{19}$$

where $\bar{g}$ is the XB-detachment rate of an isometric contraction, ϑ controls the distortion dependence $\bar{f}$ is the forward rate of XB attachment if no neighbor is in the force-bearing state and ν controls the influence of the cooperative effects (for further details see Razumova et al. (1999)).

Furthermore, the number of possible force-producing XBs depends on the overlap between the thin actin and the thick myosin filaments and thus on the half-sarcomere length (cf. Section 2.2.3). The force-length relation, $f_l(\ell_{hs})$, is assumed to be a scalar valued function between 0 and 1 (i.e., $f_l : \ell_{hs} \rightarrow [0, 1]$) and can be included into the model as an additional constitutive relation (Heidlauf & Röhrle, 2014). As f_l is included on the sarcomere level, the piecewise linear relation proposed by Gordon et al. (1966) is employed.

Finally, the normalized active force produced by a half-sarcomere can be expressed as a function of the time, the state variables corresponding to the bound XBs, the sarcomere length ℓ_{hs}, and the contraction velocity $\dot{\ell}_{hs}$, that is,

$$F_{fibre}\left(t, \mathbf{y}, \ell_{hs}, \dot{\ell}_{hs}\right) = f_l(\ell_{hs})\frac{[A_2]x_2 + [A_1]x_1}{\left[A_2^{max}\right]x_0}, \tag{20}$$

where $\left[A_2^{max}\right]$ is the concentration of postpower stroke XBs for an isometric, tetanic contraction and x_0 is the average elongation of postpower stroke XBs for during an isometric contraction.

4.4 | A continuum-mechanical, multiscale skeletal muscle model of Röhrle et al.

With respect to all existing skeletal muscle modeling approaches (cf. Section 3.2.3), continuum-mechanical frameworks provide the greatest flexibility for integrating many physiological details. To establish a biophysically based model of a whole muscle within a continuum-mechanical framework, the microscopic function needs to be linked to the macroscopic (mechanical) behavior of the muscles. This can be achieved through appropriate constitutive models. Within this section, we want to provide a brief overview how the macroscopic active behavior can be derived from the microscopic state of skeletal muscle tissue by utilizing a multiscale constitutive framework.

Any continuum body Ω needs to satisfy the balance of linear momentum, which is given in its' local form by

$$\rho\ddot{\boldsymbol{x}} = \mathrm{div}\left(J^{-1}\boldsymbol{P}\boldsymbol{F}^T\right) + \rho\boldsymbol{b}, \quad \text{in}\,\Omega. \tag{21}$$

Therein $\boldsymbol{x}$ is the actual coordinate of a material point, J is the determinant of the deformation gradient tensor $\boldsymbol{F}$, $\boldsymbol{P}$ is the first Piola-Kirchhoff stress tensor, ρ is the density of the body and $\boldsymbol{b}$ denotes body forces. Equation (21) contains two unknowns, the actual coordinate of a material point and the stress tensor that depends on the deformation and hence on the actual coordinate of a material point. To be able to solve Equation (21), the stress tensor needs to be constitutively defined, that is, relating the stresses to the applied deformations and other state variables, for example, describing the overall active behavior of the muscle. To define the stress tensor, that is, the constitutive law, it is assumed that skeletal muscle tissue is incompressible and

that the overall stress tensor can be obtained through linear superposition of the passive, $\boldsymbol{P}_{\text{passive}}$, and an active contribution, $\boldsymbol{P}_{\text{active}}$, that is,

$$\boldsymbol{P} = \boldsymbol{P}_{\text{passive}} + \boldsymbol{P}_{\text{active}} - pJ\boldsymbol{F}^{-T}. \tag{22}$$

Therein p is the hydrostatic pressure, entering the equation as a Lagrangian multiplier enforcing the incompressibility constraint $J = 1$ (cf., Holzapfel (2000) for more details). From a mechanical point of view, the superposition of the overall stress tensor implies that passive elastic energy and the active elastic energy are stored in two independent mechanical components acting in parallel. Justification can be obtained from the assumption that the filament skeleton is (nearly) rigid (Huxley, 1957), that is, the mechanical interactions between the active XBs and other elastic constituents like collagen or titin are negligible. Note that the overall stress tensor can be easily extended to include additional stress contributions, for example, induced by the sarcomere protein titin (Heidlauf et al., 2016; Heidlauf et al., 2017).

Taking into account the organized fiber arrangement of the microstructure and assuming that the passive mechanical behavior of skeletal muscle tissue is hyperelastic (cf. Section 3.2.3), the passive stress tensor, $\boldsymbol{P}_{\text{passive}}$, can be derived from any suitable transversally isotropic strain energy function W_{passive} (i.e., one that is capable to match macroscopic data):

$$\boldsymbol{P}_{\text{passive}}(\boldsymbol{F}, \boldsymbol{a}_0) = \frac{\partial W_{\text{passive}}(\boldsymbol{F}, \boldsymbol{a}_0)}{\partial \boldsymbol{F}}. \tag{23}$$

Therein $\boldsymbol{a}_0$ is a unit vector pointing in the fiber direction in the reference configuration. Popular constitutive laws for skeletal muscle tissue are Mooney-Rivlin- or Ogden-based, fiber-reinforced, hyperelastic constitutive laws (Blemker et al., 2005; Johansson et al., 2000; Röhrle & Pullan, 2007). Note that a generic transversally isotropic material could be either stiffer in the fiber direction or in the cross-fiber direction. Moreover, as discussed in Section 3.2.3, the constitutive laws are always only as good as the available experimental data.

Constitutive laws for passive materials are straight forward and essentially appeal to the same principles and theories as the ones developed for man-made materials. This is not necessarily any longer true for a skeletal muscles active behavior. However, within Section 4.3.3, we introduced a myofilament model of XB cycling on the sarcomere level that is capable of simulating the force produced by a single muscle fiber (cf. Equation (20)). Due to the normalization, that is, $F_{\text{fibre}}(t, y, \ell_{\text{hs}}, \dot{\ell}_{\text{hs}}) \in [0, 1]$, one can interpret the microscopic forces as normalized stresses. Thus, upscaling methods could be applied to directly derive the active stress tensor from the single muscle fiber force. However, from a smeared/homogenized macroscopic point of view the active muscle stress at a specific material point, depends on the contribution of different MUs. Therefore, we introduce a (generic) homogenization operator, T_{H}, to evaluate the local activation at the material point $\boldsymbol{x}$, that is,

$$T_{\text{H}} : \left(\boldsymbol{x}, F^1_{\text{fibre}}, F^2_{\text{fibre}}, \ldots, F^N_{\text{fibre}}\right) \mapsto \bar{\gamma}, \tag{24}$$

where $\bar{\gamma} \in [0, 1]$ is the normalized active stress at the material point $\boldsymbol{x}$ and N is the number of MUs. Note that the muscle fiber models need to be coupled to the continuum model by the deformation and the rate of deformation in the muscle fiber direction. For example, the normalized active stress $\bar{\gamma}$ can be calculated by the arithmetic mean of the single muscle fiber stresses weighted by their volume fraction in an referential elementary volume, that is,

$$\bar{\gamma}(\boldsymbol{x}) = \sum_{i=1}^{N} w^i_{\text{MU}}(\boldsymbol{x}) F^i_{\text{fibre}}(\boldsymbol{x}), \tag{25}$$

where ${w_{\text{MU}}}^i$ is the volume fraction of the i-th MU at a specific material point, cf. Heidlauf and Röhrle (Heidlauf & Röhrle, 2014), Heidlauf et al. (Heidlauf et al., 2016; Heidlauf et al., 2017). Note that in the work of Heidlauf and co-workers (Heidlauf et al., 2016; Heidlauf et al., 2017; Heidlauf & Röhrle, 2014) additionally complexity arises from coupling the cellular muscle model to a model of the action potential propagation (cf. Section 3.2.5). Finally the active stress tensor can be calculated by.

$$\boldsymbol{P}_{\text{active}}(\bar{\gamma}, \boldsymbol{F}, \boldsymbol{a}_0) = p_{\max} \bar{\gamma} \boldsymbol{F}(\boldsymbol{a}_0 \otimes \boldsymbol{a}_0), \tag{26}$$

where $p_{\max}$ is a material parameter denoting the maximum stress during an isometric contraction.

4.5 | The muscle spindle model of maltenfort and burke

Muscle spindles are proprioceptive sensory cells detecting changes of the muscle length. Muscle spindles are functionally divided into two specific endings that are sensitive to jerk (fast) and static (slow) perturbations. The primary and secondary axons from mammalian muscle spindles transmit those information to the central nervous system. The sensitivity of the muscle spindles is controlled/adjusted by the fusimotor neurons, that is, the γMNs. In correlation with spindle feedback γMNs are conventionally divided into two groups (static and dynamic) that bias the activity of primary and secondary spindle cells. While there exist multiple models to simulate skeletal muscle mechanics and activation (i.e., both phenomenological and biophysical), only few (mostly phenomenological) models consider sensory systems such as the muscle spindles (cf. Section 3.4).

Herein, we provide a brief introduction of the muscle spindle model of Maltenfort and Burke (Maltenfort & Burke, 2003), consisting of a model describing the material behavior in response to an external perturbation, that is, which is based on a phenomenological transfer function, and a sensory model. From a mathematical point of view, the sensory response can be described by a set of algebraic equations and thus, a function can be provided mapping the current deformation, velocity and γ-activation (cf. Sections 2.1 and 2.1.4) to the firing rate of the muscle spindle, that is, R_{spindle}. Thereby, it is assumed that the overall spindle response can be calculated by the superposition of a passive contribution, R_{passive}, and a mm modulated contribution, R_γ, that is,

$$R_{\text{spindle}}\left(\lambda,\dot{\lambda},\gamma_{\text{s}},\gamma_{\text{d}}\right)=R_{\text{passive}}\left(\lambda,\dot{\lambda}\right)+R_{\gamma}\left(\lambda,\dot{\lambda},\gamma_{\text{s}},\gamma_{\text{d}}\right), \tag{27}$$

where λ is the applied stretch, $\dot{\lambda}$ denotes the rate of deformation, γ_{s} is the static γMN drive and γ_{d} is the dynamic γMN drive (both in pulses-per-second). Based on the knowledge that there exist different types of muscle spindles, the γMN modulated sensitivity of the muscle spindles can be further split into an static part, R_γ^{s}, that is, increasing the sensitivity to static stretch perturbations, and a dynamic part, R_γ^{d}, that is, increasing the sensitivity to fast length perturbations:

$$\begin{aligned} R_{\gamma}\left(\lambda,\dot{\lambda},\gamma_{\text{s}},\gamma_{\text{d}}\right) &= R_{\gamma}^{\text{s}}\left(\lambda,\dot{\lambda},\gamma_{\text{s}}\right)+R_{\gamma}^{\text{d}}\left(\lambda,\dot{\lambda},\gamma_{\text{d}}\right)+ \\ &+\left(\frac{1}{R_{\gamma}^{\text{s}}\left(\lambda,\dot{\lambda},\gamma_{\text{s}}\right)}+\frac{1}{R_{\gamma}^{\text{d}}\left(\lambda,\dot{\lambda},\gamma_{\text{d}}\right)}\right)^{-1}. \end{aligned} \tag{28}$$

Finally all individual parts, that is, R_{passive}, R_γ^{s} and R_γ^{d}, can be calculated from the following generic equation, separating purely stretch dependent feedback, purely velocity dependent feedback, mixed stretch and velocity dependent feedback and a velocity and stretch independent spindle activity:

$$R=\left[f_{\text{sv}}\left(\gamma,\dot{\lambda}\right)+f_{\text{s}}(\gamma)\right]\lambda+f_{\text{v}}\left(\gamma,\dot{\lambda}\right)+f_{\text{c}}(\gamma). \tag{29}$$

Therein f_{sv}, f_{s}, f_{v} and f_{c} are arbitrary scalar valued functions, for a more detailed description see Maltenfort and Burke (2003). Note that for the passive spindle activity, R_{passive} the dependency from γ vanishes. Finally note that while the model of Maltenfort and Burke (2003) includes a phenomenological description of the βMNs (not described here), it fails to simulate the response of secondary spindles.

4.6 | The neuromuscular model: Coupling the neural and chemo-electromechanical model

After introducing models for all major components of the neuromuscular system, that is, MN pools (cf. Section 4.2), skeletal muscles (cf. Section 4.3 and Section 4.4) and the sensory system (cf. Section 4.5), it is possible to combine them to an integrated physiological in silico model of the neuromuscular system. The coupling between the different sub-models is schematically represented in Figure 12. In detail, the MNs (Cisi & Kohn, 2008; Negro & Farina, 2011) integrate cortical and sensory inputs and thereby dictate the recruitment and firing frequency of the muscle fibers, as well as the γ-activation of the muscle spindles. Note that to the knowledge of the authors there exists currently no suitable model considering γMN pools and

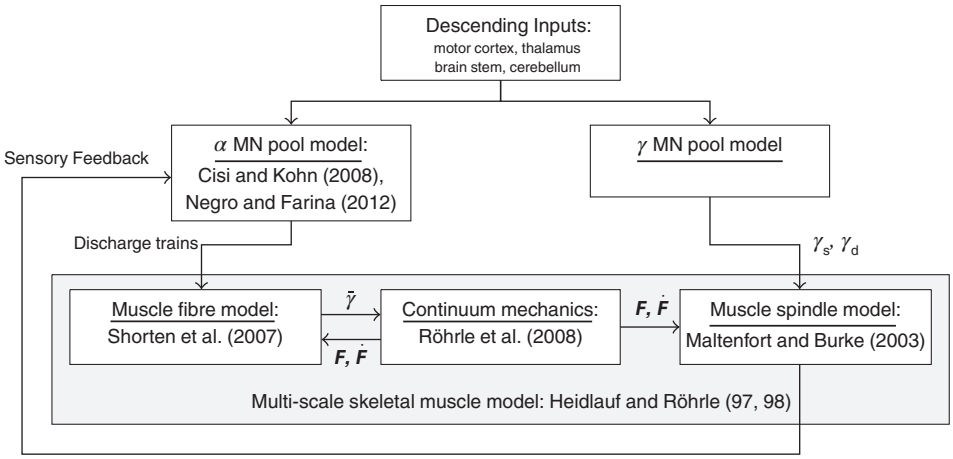

FIGURE 12 Schematic representation of the structure of the biophysical model of the neuromuscular system. The MN pools integrate descending inputs from the central nervous system and feedback signals from sensory organs such as the muscle spindles. Note that currently there exists no suitable model for the γMN pool and thus simulations of the integrated model rely on assumptions such as co-activation between the αMN pool and the corresponding γMN pool. The discharge trains calculated by the motor neuron model are used to drive the multiscale skeletal muscle model by stimulating the membranes of the muscle fibers belonging to the corresponding MU. Thereby both macroscopic quantities such as the overall muscle force output and internal states such as the concentrations of specific ions can be observed. Furthermore, the sensory feedback of the muscle spindles is calculated based on the current deformation, the rate of deformation and the applied γ-activation

therefore assumptions such as co-activation between the αMNs and the γMNs need to be employed (Vallbo, 1974). Furthermore, the amount of physiological realism can be increased by incorporating additional sensory systems such as the Golgi tendon organs as well as modeling the fusimotor drive from the βMNs. The multiscale skeletal muscle model (Heidlauf & Röhrle, 2013; Heidlauf & Röhrle, 2014) is directly driven by the discharge trains of the MN pool, cf., for example, Röhrle et al. (2012), and can thereby, in combination with the applied boundary conditions, predict both quantities that are typically captured by experiments, for example, the overall muscle force or EMG signals, as well as additional internal state variables, for example, ion concentrations or the full displacement field. Note that by employing multiscale constitutive relations, microscopic and macroscopic quantities are directly coupled to each other. Furthermore, the muscle spindle models (Maltenfort & Burke, 2003) are assigned to specific points within the three-dimensional muscle geometry. Input to the spindle models are obtained from the local deformation, that is, the local deformation gradient tensor $\boldsymbol{F}$, the local rate of deformation, that is, $\dot{\boldsymbol{F}}$, and the γ-drive obtained from the γMN pool model. Thereby an additional constitutive equation is needed, mapping the deformation gradient tensor $\boldsymbol{F}$ to the stretch of the muscle spindles. Finally, the perceived changes, that is, encoded by the muscle spindle firing frequency, need to be translated into (electrical) signals that can be integrated by the αMNs. The combination by several of those models, that is, extending the neural connectivity according to physiological hypothesizes, will result in an integrated model of the whole musculoskeletal system (cf. Section 3.3).

4.7 | Numerical considerations

The integrated model of the neuromuscular system (cf. Section 4.6) takes into account physical processes on multiple time and length scales. From a mathematical point of view, this yields highly heterogeneous and coupled sets of equations, that is, by coupling different types of PDEs and ODEs representing different processes on different spatial and temporal scales. From a numerical point of view, this leads to multiple challenges. While it would theoretically be possible to solve the fully coupled model in one framework and in a monolithic way, it is often more convenient to employ staggered solution schemes for such large-scale, multiscale, multiphysics problems. Thereby, specialized solution methods and optimized numerical discretizations

schemes (both in space and time) can be applied to each of the sub-problem. For example, the system of PDEs originating from the governing equations of the three-dimensional, continuum-mechanical framework describing the mechanical behavior of skeletal muscles is usually best discretized using the finite element method (FEM) with Taylor-Hood basis functions. For solving the equations describing the bioelectrical state of the activated skeletal muscle, one might need to appeal to a much finer mesh resolution while linear Lagrange basis elements are, due to the fine mesh resolution, often fully sufficient. While staggered solution schemes seem to provide an almost natural way of choosing different discretizations and basis functions, one needs to define appropriate transfer functions to exchange variables between the different meshes. Appropriate interpolation or restriction operators are needed. This might, however, not always be trivial and often the starting point to novel homogenization techniques. Furthermore, for choosing a monolithic approach over a staggered solution scheme, one requires an extremely flexible, multiphysics simulation framework that is capable of handling multiple discretizations and equation types. If such flexibility would not be given, but yet one wants to solve the resulting system in a monolithic way, then such large-scale, multiscale, multiphysics skeletal muscle models lead to extremely demanding simulations often exceeding the computational power of the largest supercomputing facilities. However, if the flexibility is given, monolithic solution schemes might be advantageous. Regardless of choosing a monolithic or a staggered solution schemes, parallelization strategies are essential to obtain for such detailed biophysical modeling approaches predictions within reasonable time. This poses entirely new challenges with respect to data communications. Finally note that the development of systemic physiological models is massively facilitated if existing models are easily accessible, for example, by using mark-up languages or sharing models within open-source software projects such as CellML (Lloyd, Lawson, Hunter, & Nielsen, 2008) or FieldML (Christie, Nielsen, Blackett, Bradley, & Hunter, 2009).

4.8 | Further reading

The models of Cisi and Kohn, of Negro and Farina, and the nonisometric extension of Shorten et al., that is, Heidlauf and Röhrle (2014), are provided as CellML models within the Supporting Information. As far as implementation details and numerical aspects, in particular of the continuum-mechanical framework together with the FEM method, are concerned, the reader is referred to the books of Bonet and Wood (2008), Zienkiewicz, Taylor, and Zhu (2005), or Hughes (2012).

5 | SUMMARY AND CONCLUSIONS

In summary, this review focuses on key anatomical and physiological aspects of the neuromuscular system, on an overview of the state of the art in modeling individual parts of the neuromuscular system and on an outline of a specific neuromuscular system model, which closely represents the underlying physiological behavior. Specifically, this neuromuscular system model demonstrates how to couple the biophysically detailed MN pool model of Negro and Farina (2011) to the chemo-electro-mechanical skeletal muscle model of Röhrle et al. (2012). All of the sub-models within the outlined neuromuscular system model have been chosen, because they have been previously developed, used (whereby the authors were capable to validate published simulation results) and/or extended by the authors. While the aim is to develop a fully biophysical-based neuromuscular model, the presented model still appeals for modeling the mechanical behavior of the (passive) skeletal muscle tissue (cf. Section 4.4) and for the muscle spindle model (cf. Section 4.5) phenomenological models.

While the specific neuromuscular system model outlined in Section 4 closely resembles many of the physiological relevant pathways of the neuromuscular system leading to voluntary force generation, for example, as described in Section 2, there exist significant uncertainties regarding its parameters. This is a major challenge for all (multiscale) modeling approaches that aim to simulate biological systems. While all individual (sub-)models are typically calibrated to reproduce data that were measured during specific experimental conditions, one cannot obtain experimental data for all state variables and parameters of the model. Furthermore, the experimental environment does unfortunately often differ from the in vivo conditions, which one aims to model. A further challenge is that most of the experimental studies for the individual models do not stem from the same animal model. While an extensive overview and discussion on the acquisition of experimental data and on parameter estimation methods is far beyond the scope of this review, it is obvious that a fully validated biophysically detailed nueromuscular system model remains hardly feasible. On the other hand, careful identification and isolation of shortcomings are needed as this highlights the requirement for strictly physics-based modeling approaches, that is, eliminating multiple degrees of freedom by employing physical constraints (e.g., based on the laws of thermodynamics). Furthermore, strictly physics-based modeling increases the confidence to produce substantial simulation outputs when using a model for extrapolation, that is, prediction, by simulating conditions the model was not calibrated to—something not (necessarily) possible for

phenomenological models or machine learning approaches. Finally note that the goodness of physics-based models can also be evaluated by it's capabilities to predict phenomena that were not explicitly modeled or assumed within the model itself.

In general, the individual parts of the integrated neuromuscular model, that is, the sub-models, can be replaced with other more elaborate sub-models and further extended to simulate further physiological phenomena. For example, including models capturing metabolism is essential when simulating (various) long-lasting exercises/activities. Moreover, including detailed models of signal transduction on the cellular level (e.g., including the transcription and translation of genes or second messenger systems such as the intracellular calcium concentration), can potentially be used to simulate remodeling processes and thus importantly contribute to investigate degenerative neuromuscular diseases. This, however, also puts strong requirements onto the flexibility of the overall computational framework. One framework, which has been specifically designed to cope with such flexibility and challenges, is, for example, the international open-source software library, OpenCMISS (Bradley et al., 2011; Bradley et al., 2018).

In conclusion, the model described in this review should serve as an excellent example of a multiscale model that is capable of successfully simulating muscle contractions under several different conditions. The reviewed biophysically based, three-dimensional neuromuscular system model should serve researchers as a starting point to further improve individual sub-models, to integrate new physiological aspects, to develop experimental protocols for validating the overall model, or to make predictions and test hypothesis for identifying underlying processes leading to pathologies and, hence, to obtain an advanced in silico testing tool for gaining new insights into neuromuscular diseases.

ACKNOWLEDGMENTS

The review was partially funded by the Cluster of Excellence for Simulation Technology (ExC 310/2 and ExC 2075) and by the Baden-Württemberg Stiftung as part of the DiHu project of the High Performance Computing II program.

CONFLICT OF INTEREST

The authors have declared no conflicts of interest for this article.

ENDNOTES

[1] For an implementation see https://models.physiomeproject.org/workspace/hodgkin_huxley_1952.

[2] For an implementation see https://models.physiomeproject.org/workspace/shorten_ocallaghan_davidson_soboleva_2007.

RELATED WIREs ARTICLES

Advanced Review Systems biology of skeletal muscle: fiber type as an organizing principle
Systems analysis of biological networks in skeletal muscle function

REFERENCES

Abbott, B. C., & Aubert, X. M. (1952). The force exerted by active striated muscle during and after change of length. *The Journal of Physiology*, *117*(1), 77–86.

Adrian, R. H., & Peachey, L. D. (1973). Reconstruction of the action potential of frog sartorius muscle. *The Journal of Physiology*, *235*(1), 103–131.

Allen, J. M., & Elbasiouny, S. M. (2018). The effects of model composition design choices on high-fidelity simulations of motoneuron recruitment and firing behaviors. *Journal of Neural Engineering*, *15*(3), 036024.

Ambrosi, D., & Pezzuto, S. (2012). Active stress vs. active strain in mechanobiology: Constitutive issues. *Journal of Elasticity*, *107*(2), 199–212.

Anderson, F. C., & Pandy, M. G. (2001). Static and dynamic optimization solutions for gait are practically equivalent. *Journal of Biomechanics*, *34*(2), 153–161.

Ateş, F., Andrade, R. J., Freitas, S. R., Hug, F., Lacourpaille, L., Gross, R., … Nordez, A. (2018). Passive stiffness of monoarticular lower leg muscles is influenced by knee joint angle. *European Journal of Applied Physiology*, *118*(3), 585–593.

Ateş, F., Davies, B. L., Chopra, S., Coleman-Wood, K., Litchy, W. J., & Kaufman, K. R. (2018). Intramuscular pressure of tibialis anterior reflects ankle torque but does not follow joint angle-torque relationship. *Frontiers in Physiology*, *9*(22). https://doi.org/10.3389/fphys.2018.00022

Ateş, F., Hug, F., Bouillard, K., Jubeau, M., Frappart, T., Couade, M., … Nordez, A. (2015). Muscle shear elastic modulus is linearly related to muscle torque over the entire range of isometric contraction intensity. *Journal of Electromyography and Kinesiology*, *25*(4), 703–708.

Ateş, F., Temelli, Y., & Yucesoy, C. A. (2013). Human spastic gracilis muscle isometric forces measured intraoperatively as a function of knee angle show no abnormal muscular mechanics. *Clinical Biomechanics*, *28*, 48–54.

Ateş, F., & Yucesoy, C. A. (2014). Effects of botulinum toxin type a on non-injected bi-articular muscle include a narrower length range of force exertion and increased passive force. *Muscle & Nerve*, *49*(6), 866–878.

Ateş, F., & Yucesoy, C. A. (2018). Botulinum toxin type-a affects mechanics of non-injected antagonistic rat muscles. *Journal of the Mechanical Behavior of Biomedical Materials*, *84*, 208–216.

Baldissera, F., Cavallari, P., & Cerri, G. (1998). Motoneuronal pre-compensation for the low-pass filter characteristics of muscle. A quantitative appraisal in cat muscle units. *The Journal of Physiology*, *511*(2), 611–627.

Bassel-Duby, R., & Olson, E. N. (2006). Signaling pathways in skeletal muscle remodeling. *Annual Review of Biochemistry*, *75*, 19–37.

Baylor, S. M., & Hollingworth, S. (1998). Model of Sarcomeric Ca^{2+} movements, including ATP Ca^{2+} binding and diffusion, during activation of frog skeletal muscle. *The Journal of General Physiology*, *112*(3), 297–316.

Bessou, P., Emonet-Denand, F., & Laporte, Y. (1963). Occurrence of intrafusal muscle fibres innervation by branches of slow α motor fibres in the cat. *Nature*, *198*(4880), 594–595.

Bilston, L. E., & Tan, K. (2015). Measurement of passive skeletal muscle mechanical properties in vivo: Recent progress, clinical applications, and remaining challenges. *Annals of Biomedical Engineering*, *43*(2), 261–273.

Bleiler, C., Ponte Castañeda, P., & Röhrle, O. (2019). A microstructurally-based, multi-scale, continuum-mechanical model for the passive behaviour of skeletal muscle tissue. *Journal of the Mechanical Behavior of Biomedical Materials*, *97*, 171–186.

Blemker, S. S., & Delp, S. L. (2005). Three-dimensional representation of complex muscle architectures and geometries. *Annals of Biomedical Engineering*, *33*(5), 661–673.

Blemker, S. S., Pinsky, P. M., & Delp, S. L. (2005). A 3D model of muscle reveals the causes of nonuniform strains in the biceps brachii. *Journal of Biomechanics*, *38*(4), 657–665.

Böl, M., Ehret, A. E., Leichsenring, K., Weichert, C., & Kruse, R. (2014). On the anisotropy of skeletal muscle tissue under compression. *Acta Biomaterialia*, *10*(7), 3225–3234.

Böl, M., Kruse, R., Ehret, A. E., Leichsenring, K., & Siebert, T. (2012). Compressive properties of passive skeletal muscle—The impact of precise sample geometry on parameter identification in inverse finite element analysis. *Journal of Biomechanics*, *45*(15), 2673–2679.

Böl, M., & Reese, S. (2008). Micromechanical modelling of skeletal muscles based on the finite element method. *Computer Methods in Biomechanics and Biomedical Engineering*, *11*(5), 489–504.

Böl, M., Sturmat, C., amd Weichert, M., & Kober, C. (2011). A new approach for the validation of skeletal muscle modelling using MRI data. *Computational Mechanics*, *47*, 591–601.

Böl, M., Weikert, R., & Weichert, C. (2011). A coupled electromechanical model for the excitation-dependent contraction of skeletal muscle. *Journal of the Mechanical Behavior of Biomedical Materials*, *4*, 1299–1310.

Bonet, J., & Wood, R. D. (2008). *Nonlinear continuum mechanics for finite element analysis* (2nd ed.). Cambridge, England: Cambridge University Press.

Booth, V., Rinzel, J., & Kiehn, O. (1997). Compartmental model of vertebrate motoneurons for ca2+−dependent spiking and plateau potentials under pharmacological treatment. *Journal of Neurophysiology*, *78*(6), 3371–3385.

Bosboom, E., Hesselink, M., Oomens, C., Bouten, C., Drost, M., & Baaijens, F. (2001). Passive transverse mechanical properties of skeletal muscle under in vivo compression. *Journal of Biomechanics*, *34*(10), 1365–1368.

Boyd, I., Gladden, M. H., McWilliam, P., & Ward, J. (1977). Control of dynamic and static nuclear bag fibres and nuclear chain fibres by gamma and beta axons in isolated cat muscle spindels. *The Journal of Physiology*, *265*(1), 133–162.

Bradley, C., Bowery, A., Britten, R., Budelmann, V., Camara, O., Christie, R., … Hunter, P. (2011). Opencmiss: A multi-physics & multi-scale computational infrastructure for the vph/physiome project. *Progress in Biophysics and Molecular Biology*, *107*(1), 32–47.

Bradley, C. P., Emamy, N., Ertl, T., Göddeke, D., Hessenthaler, A., Klotz, T., … Röhrle, O. (2018). Enabling detailed, biophysics-based skeletal muscle models on hpc systems. *Frontiers in Physiology*, *9*(816). https://doi.org/10.3389/fphys.2018.00816

Buchthal, F., & Schmalbruch, H. (1980). Motor unit of mammalian muscle. *Physiological Reviews*, *60*(1), 90–142.

Burke, R., Levine, D., Tsairis, P., & Zajac, F. E. (1973). Physiological types and histochemical profiles in motor units of the cat gastrocnemius. *The Journal of Physiology*, *234*(3), 723–748.

Butler, J. E., & Gandevia, S. C. (2008). The output from human inspiratory motoneurone pools. *The Journal of Physiology*, *586*(5), 1257–1264.

Calvin, W. H., & Stevens, C. F. (1968). Synaptic noise and other sources of randomness in motoneuron interspike intervals. *Journal of Neurophysiology*, *31*(4), 574–587.

Campbell, K. B., Razumova, M. V., Kirkpatrick, R. D., & Slinker, B. K. (2001a). Nonlinear myofilament regulatory processes affect frequency-dependent muscle fiber stiffness. *Biophysical Journal*, *81*(4), 2278–2296.

Campbell, K. B., Razumova, M. V., Kirkpatrick, R. D., & Slinker, B. K. (2001b). Myofilament kinetics in isometric twitch dynamics. *Annals of Biomedical Engineering*, *29*(5), 384–405.

Cannell, M., & Allen, D. (1984). Model of calcium movements during activation in the sarcomere of frog skeletal muscle. *Biophysical Journal*, *45*(5), 913–925.

Cannon, S., Brown, R., & Corey, D. (1993). Theoretical reconstruction of myotonia and paralysis caused by incomplete inactivation of sodium channels. *Biophysical Journal*, *65*(1), 270–288.

Castronovo, A. M., Negro, F., Conforto, S., & Farina, D. (2015). The proportion of common synaptic input to motor neurons increases with an increase in net excitatory input. *Journal of Applied Physiology*, *119*(11), 1337–1346.

Charlton, I. W., & Johnson, G. R. (2001). Application of spherical and cylindrical wrapping algorithms in a musculoskeletal model of the upper limb. *Journal of Biomechanics*, *34*(9), 1209–1216.

Christie, G. R., Nielsen, P. M., Blackett, S. A., Bradley, C. P., & Hunter, P. J. (2009). Fieldml: Concepts and implementation. *Philosophical Transactions of the Royal Society of London A: Mathematical, Physical and Engineering Sciences*, *367*(1895), 1869–1884.

Cisi, R. R., & Kohn, A. F. (2008). Simulation system of spinal cord motor nuclei and associated nerves and muscles, in a web-based architecture. *Journal of Computational Neuroscience*, *25*(3), 520–542.

Clamann, H. P. (1969). Statistical analysis of motor unit firing patterns in a human skeletal muscle. *Biophysical Journal*, *9*(10), 1233–1251.

Crago, P. E., Houk, J. C., & Rymer, W. Z. (1982). Sampling of total muscle force by tendon organs. *Journal of Neurophysiology*, *47*(6), 1069–1083.

Damsgaard, M., Rasmussen, J., Christensen, S. T., Surma, E., & De Zee, M. (2006). Analysis of musculoskeletal systems in the anybody modeling system. *Simulation Modelling Practice and Theory*, *14*(8), 1100–1111.

De Luca, C., LeFever, R., McCue, M., & Xenakis, A. (1982a). Control scheme governing concurrently active human motor units during voluntary contractions. *The Journal of Physiology*, *329*(1), 129–142.

De Luca, C. J., LeFever, R. S., McCue, M. P., & Xenakis, A. P. (1982b). Behaviour of human motor units in different muscles during linearly varying contractions. *The Journal of Physiology*, *329*(1), 113–128.

De Luca, C. J., & Erim, Z. (1994). Common drive of motor units in regulation of muscle force. *Trends in Neurosciences*, *17*(7), 299–305.

De Luca, C. J., & Hostage, E. C. (2010). Relationship between firing rate and recruitment threshold of motoneurons in voluntary isometric contractions. *Journal of Neurophysiology*, *104*(2), 1034–1046.

Delp, S. L., Anderson, F. C., Arnold, A. S., Loan, P., Habib, A., John, C. T., … Thelen, D. G. (2007). Opensim: Open-source software to create and analyze dynamic simulations of movement. *IEEE Transactions on Biomedical Engineering*, *54*(11), 1940–1950.

Denoth, J., Stüssi, E., Csucs, G., & Danuser, G. (2002). Single muscle fiber contraction is dictated by inter-sarcomere dynamics. *Journal of Theoretical Biology*, *216*(1), 101–122.

Dideriksen, J., Negro, F., Enoka, R., & Farina, D. (2011). Neuromuscular adjustments that constrain submaximal EMG amplitude at task failure of sustained isometric contractions. *Journal of Applied Physiology*, *111*(2), 485–494.

Dideriksen, J., Negro, F., Enoka, R., & Farina, D. (2012). Motor unit recruitment strategies and muscle properties determine the influence of synaptic noise on force steadiness. *Journal of Neurophysiology*, *107*(12), 3357–3369.

Dideriksen, J. L., & Farina, D. (2013). Motor unit recruitment by size does not provide functional advantages for motor performance. *The Journal of Physiology*, *591*(24), 6139–6156.

Dideriksen, J. L., Farina, D., Bækgaard, M., & Enoka, R. M. (2010). An integrative model of motor unit activity during sustained submaximal contractions. *Journal of Applied Physiology*, *108*(6), 1550–1562.

Dideriksen, J. L., Negro, F., & Farina, D. (2015). The optimal neural strategy for a stable motor task requires a compromise between level of muscle cocontraction and synaptic gain of afferent feedback. *Journal of Neurophysiology*, *114*(3), 1895–1911.

Duchateau, J., & Enoka, R. M. (2011). Human motor unit recordings: Origins and insight into the integrated motor system. *Brain Research*, *1409*, 42–61.

Durandau, G., Farina, D., & Sartori, M. (2018). Robust real-time musculoskeletal modeling driven by electromyograms. *IEEE Transactions on Biomedical Engineering*, *65*(3), 556–564.

Edman, K., Elzinga, G., & Noble, M. (1982). Residual force enhancement after stretch of contracting frog single muscle fibers. *The Journal of General Physiology*, *80*(5), 769–784.

Edman, K. A., Elzinga, G., & Noble, M. I. (1978). Enhancement of mechanical performance by stretch during tetanic contractions of vertebrate skeletal muscle fibres. *The Journal of Physiology*, *281*(1), 139–155.

Ehret, A. E., Böl, M., & Itskov, M. (2011). A continuum constitutive model for the active behaviour of skeletal muscle. *Journal of the Mechanics and Physics of Solids*, *59*, 625–636.

Elbasiouny, S. M., Amendola, J., Durand, J., & Heckman, C. (2010). Evidence from computer simulations for alterations in the membrane biophysical properties and dendritic processing of synaptic inputs in mutant superoxide dismutase-1 motoneurons. *Journal of Neuroscience*, *30*(16), 5544–5558.

Elias, L. A., Chaud, V. M., & Kohn, A. F. (2012). Models of passive and active dendrite motoneuron pools and their differences in muscle force control. *Journal of Computational Neuroscience*, *33*(3), 515–531.

Elias, L. A., & Kohn, A. F. (2013). Individual and collective properties of computationally efficient motoneuron models of types s and f with active dendrites. *Neurocomputing*, *99*, 521–533.

Elias, L. A., Watanabe, R. N., & Kohn, A. F. (2014). Spinal mechanisms may provide a combination of intermittent and continuous control of human posture: Predictions from a biologically based neuromusculoskeletal model. *PLoS Computational Biology*, *10*(11), e1003944.

Enoka, R. M. (2008). *Neuromechanics of human movement*. Champaign, IL: Human Kinetics.

Enoka, R. M., Christou, E. A., Hunter, S. K., Kornatz, K. W., Semmler, J. G., Taylor, A. M., & Tracy, B. L. (2003). Mechanisms that contribute to differences in motor performance between young and old adults. *Journal of Electromyography and Kinesiology*, *13*(1), 1–12.

Farina, D., Holobar, A., Merletti, R., & Enoka, R. M. (2010). Decoding the neural drive to muscles from the surface electromyogram. *Clinical Neurophysiology*, *121*(10), 1616–1623.

Farina, D., & Merletti, R. (2001). A novel approach for precise simulation of the EMG signal detected by surface electrodes. *IEEE Transactions on Biomedical Engineering*, *48*, 637–646.

Farina, D., Mesin, L., Martina, S., & Merletti, R. (2004). A surface EMG generation model with multilayer cylindrical description of the volume conductor. *IEEE Transactions on Biomedical Engineering*, *51*(3), 415–426.

Farina, D., & Negro, F. (2015). Common synaptic input to motor neurons, motor unit synchronization, and force control. *Exercise and Sport Sciences Reviews*, *43*(1), 23–33.

Farina, D., Negro, F., & Dideriksen, J. L. (2014). The effective neural drive to muscles is the common synaptic input to motor neurons. *The Journal of Physiology*, *592*(16), 3427–3441.

Farina, D., Negro, F., Muceli, S., & Enoka, R. M. (2016). Principles of motor unit physiology evolve with advances in technology. *Physiology*, *31*(2), 83–94.

Feinstein, B., Lindegård, B., Nyman, E., & Wohlfart, G. (1955). Morphologic studies of motor units in normal human muscles. *Cells, Tissues, Organs*, *23*(2), 127–142.

Fernandez, J. W., Buist, M. L., Nickerson, D. P., & Hunter, P. J. (2005). Modelling the passive and nerve activated response of the rectus femoris muscle to a flexion loading: A finite element framework. *Medical Engineering & Physics*, *27*(10), 862–870.

Fernandez, J. W., & Hunter, P. J. (2005). An anatomically based patient-specific finite element model of patella articulation: Towards a diagnostic tool. *Biomechanics and Modeling in Mechanobiology*, *4*(1), 20–38.

Fuglevand, A. J., Winter, D. A., & Patla, A. E. (1993). Models of recruitment and rate coding organization in motor unit pools. *Journal of Neurophysiology*, *70*(6), 2470–2488.

Fukami, Y., & Wilkinson, R. (1977). Responses of isolated golgi tendon organs of the cat. *The Journal of Physiology*, *265*(3), 673–689.

Funatsu, T., Higuchi, H., & Ishiwata, S. (1990). Elastic filaments in skeletal muscle revealed by selective removal of thin filaments with plasma gelsolin. *Journal of Cell Biology*, *110*(1), 53–62.

Fung, Y.-C. (2013). *Biomechanics: Mechanical properties of living tissues*. New York, NY: Springer Science & Business Media.

Gandevia, S., Allen, G. M., Butler, J. E., & Taylor, J. L. (1996). Supraspinal factors in human muscle fatigue: Evidence for suboptimal output from the motor cortex. *The Journal of Physiology*, *490*(2), 529–536.

Garner, B. A., & Pandy, M. G. (2000). The obstacle-set method for representing muscle paths in musculoskeletal models. *Computer Methods in Biomechanics and Biomedical Engineering*, *3*(1), 1–30.

Gillis, J.-M., Thomason, D., Lefèvre, J., & Kretsinger, R. (1982). Parvalbumins and muscle relaxation: A computer simulation study. *Journal of Muscle Research & Cell Motility*, *3*(4), 377–398.

Gindre, J., Takaza, M., Moerman, K. M., & Simms, C. K. (2013). A structural model of passive skeletal muscle shows two reinforcement processes in resisting deformation. *Journal of the Mechanical Behavior of Biomedical Materials*, *22*, 84–94.

Gordon, A. M., Homsher, E., & Regnier, M. (2000). Regulation of contraction in striated muscle. *Physiological Reviews*, *80*(2), 853–924.

Gordon, A. M., Huxley, A. F., & Julian, F. J. (1966). The variation in isometric tension with sarcomere length in vertebrate muscle fibres. *The Journal of Physiology*, *184*, 170–192.

Günther, M., Röhrle, O., Haeufle, D. F., & Schmitt, S. (2012). Spreading out muscle mass within a hill-type model: A computer simulation study. *Computational and Mathematical Methods in Medicine*, *2012*, 1–13.

Günther, M., Schmitt, S., & Wank, V. (2007). High-frequency oscillations as a consequence of neglected serial damping in Hill-type muscle models. *Biological Cybernetics*, *97*, 63–79.

Hanson, J., & Huxley, H. E. (1953). Structural basis of the cross-striations in muscle. *Nature*, *172*, 530–532.

Häufle, D. F. B., Günther, M., Bayer, A., & Schmitt, S. (2014). Hill-type muscle model with serial damping and eccentric force–velocity relation. *Journal of Biomechanics*, *47*(6), 1531–1536.

Hawkins, D., & Bey, M. (1994). A comprehensive approach for studying muscle-tendon mechanics. *Journal of Biomechanical Engineering*, *116*(1), 51–55.

Heckman, C. J., & Binder, M. D. (1991). Computer simulation of the steady-state input-output function of the cat medial gastrocnemius motoneuron pool. *Journal of Neurophysiology*, *65*(4), 952–967.

Heckman, C. J., & Enoka, R. M. (2004). Physiology of the motor neuron and the motor unit. *Handbook of Clinical Neurophysiology*, *4*, 119–147.

Heckman, C. J., & Enoka, R. M. (2012). Motor unit. *Comprehensive Physiology*, *2*, 2629–2682.

Heidlauf, T. (2015). *Chemo-electro-mechanical modelling of the neuromuscular system.* (PhD thesis). University of Stuttgart.

Heidlauf, T., Klotz, T., Rode, C., Altan, E., Bleiler, C., Siebert, T., & Röhrle, O. (2016). A multi-scale continuum model of skeletal muscle mechanics predicting force enhancement based on actin–titin interaction. *Biomechanics and Modeling in Mechanobiology*, *15*(6), 1423–1437.

Heidlauf, T., Klotz, T., Rode, C., Siebert, T., & Röhrle, O. (2017). A continuum-mechanical skeletal muscle model including actin-titin interaction predicts stable contractions on the descending limb of the force-length relation. *PLoS Computational Biology*, *13*(10), e1005773.

Heidlauf, T., Negro, F., Farina, D., & Röhrle, O. (2013). An integrated model of the neuromuscular system. In *Sixth international IEEE/EMBS conference on Neural Engineering (NER)* (pp. 227–230). Piscataway, NJ: IEEE.

Heidlauf, T., & Röhrle, O. (2013). Modeling the Chemoelectromechanical behavior of skeletal muscle using the parallel open-source software library OpenCMISS. *Computational and Mathematical Methods in Medicine*, *2013*, 1–14.

Heidlauf, T., & Röhrle, O. (2014). A multiscale chemo-electro-mechanical skeletal muscle model to analyze muscle contraction and force generation for different muscle fiber arrangements. *Frontiers in Physiology*, *5*(498), 1–14.

Henneman, E., Somjen, G., & Carpenter, D. O. (1965a). Functional significance of cell size in spinal motoneurons. *Journal of Neurophysiology*, *28*(3), 560–580.

Henneman, E., Somjen, G., & Carpenter, D. O. (1965b). Excitability and inhibitibility of motoneurons of different sizes. *Journal of Neurophysiology*, *28*(3), 599–620.

Hernández-Gascón, B., Grasa, J., Calvo, B., & Rodríguez, J. F. (2013). A 3D electro-mechanical continuum model for simulating skeletal muscle contraction. *Journal of Theoretical Biology*, *335*, 108–118.

Heron, M. I., & Richmond, F. J. R. (1993). In-series fiber architecture in long human muscles. *Journal of Morphology*, *216*(1), 35–45.

Herzog, W. (2000). *Skeletal muscle mechanics: From mechanisms to function*. Hoboken, NJ: John Wiley & Sons.

Herzog, W. (2018). The multiple roles of titin in muscle contraction and force production. *Biophysical Reviews*, 1–13. Heidelberg, Germany.

Herzog, W., Lee, E.-J., & Rassier, D. E. (2006). Residual force enhancement in skeletal muscle. *The Journal of Physiology*, *574*(3), 635–642.

Herzog, W., & Leonard, T. R. (2002). Force enhancement following stretching of skeletal muscle: A new mechanism. *Journal of Experimental Biology*, *205*(9), 1275–1283.

Hilgemann, D., & Noble, D. (1987). Excitation-contraction coupling and extracellular calcium transients in rabbit atrium: Reconstruction of basic cellular mechanisms. *Proceedings of the Royal Society of London B: Biological Sciences*, *230*(1259), 163–205.

Hill, A. V. (1938). The heat of shortening and the dynamic constants of muscle. *Proceedings of the Royal Society of London B*, *126*(843), 136–195.

Hill, T. L. (1989). *Free energy transduction and biochemical cycle kinetics*. New York, NY: Springer Verlag.

Hill, T. L., Eisenberg, E., Chen, Y. D., & Podolsky, R. J. (1975). Some self-consistent two-state sliding filament models of muscle contraction. *Biophysical Journal*, *15*, 335–372.

Hodgkin, A. L., & Huxley, A. F. (1952). A quantitative description of membrane current and its application to conduction and excitation in nerve. *The Journal of Physiology*, *117*(4), 500–544.

Holzapfel, G. A. (2000). *Nonlinear solid mechanics*. Chichester, England: John Wiley & Sons LTD.

Horowits, R. (1992). Passive force generation and titin isoforms in mammalian skeletal muscle. *Biophysical Journal*, *61*(2), 392–398.

Houk, J., & Henneman, E. (1967). Responses of golgi tendon organs to active contractions of the soleus muscle of the cat. *Journal of Neurophysiology*, *30*(3), 466–481.

Hoyt, K. H., Kneezel, T., Castaneda, B., & Parker, K. J. (2008). Quantitative sonoelastography for the in vivo assessment of skeletal muscle viscoelasticity. *Physics in Medicine and Biology*, *53*, 4063–4080.

Hu, X., & Blemker, S. S. (2015). Musculoskeletal simulation can help explain selective muscle degeneration in duchenne muscular dystrophy. *Muscle & Nerve*, *52*(2), 174–182.

Hughes, T. J. (2012). *The finite element method: Linear static and dynamic finite element analysis*. Mineola, NY: Courier Corporation.

Huijing, P. A. (1999). Muscle as a collagen fiber reinforced composite: A review of force transmission in muscle and whole limb. *Journal of Biomechanics*, *32*(4), 329–345.

Huijing, P. A. (2003). Muscular force transmission necessitates a multilevel integrative approach to the analysis of function of skeletal muscle. *Exercise and Sport Sciences Reviews*, *31*(4), 167–175.

Hursh, J. B. (1939). Conduction velocity and diameter of nerve fibers. *American Journal of Physiology*, *127*(1), 131–139.

Huxley, A. F. (1957). Muscle structure and theories of contraction. *Progress in Biophysics and Biophysical Chemistry*, *7*, 255–318.

Huxley, A. F. (1974). Muscular contraction. *The Journal of Physiology*, *243*(1), 1–43.

Huxley, A. F., & Niedergerke, R. (1954). Structural changes in muscle during contraction: Interference microscopy of living muscle Fibres. *Nature*, *173*, 971–973.

Huxley, H. (1958). The contraction of muscle. *Scientific American*, *199*(5), 66–86.

Huxley, H. E. (1969). The mechanism of muscular contraction. *Science*, *164*(3886), 1356–1366.

Huxley, H. E., & Hanson, J. (1954). Changes in the cross-striations of muscle during contraction and stretch and their structural interpretation. *Nature*, *173*, 973–976.

Ishizuka, N., Mannen, H., Hongo, T., & Sasaki, S. (1979). Trajectory of group Ia afferent fibers stained with horseradish peroxidase in the lumbosacral spinal cord of the cat: Three dimensional reconstructions from serial sections. *Journal of Comparative Neurology*, *186*(2), 189–211.

Johansson, T., Meier, P., & Blickhan, R. (2000). A finite-element model for the mechanical analysis of skeletal muscles. *Journal of Theoretical Biology*, *206*(1), 131–149.

Jones, K. E., Hamilton, A. F. d. C., & Wolpert, D. M. (2002). Sources of signal-dependent noise during isometric force production. *Journal of Neurophysiology*, *88*(3), 1533–1544.

Kakuda, N., Nagaoka, M., & Tanaka, R. (1992). Conduction velocities of α-motor fibers innervating human thenar muscles and order of recruitment upon voluntary contraction. *Muscle & Nerve: Official Journal of the American Association of Electrodiagnostic Medicine*, *15*(3), 332–343.

Kandel, E. R., Schwartz, J. H., & Jessell, T. M. (2000). *Principles of neural science* (Vol. 4). New York, NY: McGraw-Hill.

Keener, J., & Sneyd, J. (2009a). *Mathematical physiology I: Cellular physiology* (Vol. 1, 2nd ed.). New York, NY: Springer.

Keener, J., & Sneyd, J. (2009b). *Mathematical physiology II: Systems physiology* (Vol. 2, 2nd ed.). New York, NY: Springer.

Kieser, J. A., Farland, M. G., Jack, H., Farella, M., Wang, Y., & Röhrle, O. (2014). The role of oral soft tissues in swallowing function: What can tongue pressure tell us? *Australian Dental Journal*, *59*(Suppl 1), 155–161.

Kim, J. H., Davidson, J. B., Röhrle, O., Soboleva, T. K., & Pullan, A. J. (2007). Anatomically based lower limb nerve model for electrical stimulation. *Biomedical Engineering Online*, *6*(1), 48.

Kin, J. H., Trew, M. L., Pullan, A. J., & Röhrle, O. (2012). Simulating a dual-array electrode configuration to investigate the influence of skeletal muscle fatigue following functional electrical stimulation. *Computers in Biology and Medicine*, *42*(9), 915–924.

Kleinedler, S. R. (2008). *The American heritage medical dictionary*. Boston: Houghton Mifflin Company.

Kondaurov, V., & Nikitin, L. (1987). Finite strains of viscoelastic muscle tissue. *Journal of Applied Mathematics and Mechanics*, *51*(3), 346–353.

Konishi, M. (1998). Cytoplasmic free concentrations of Ca2+ and Mg2+ in skeletal muscle fibers at rest and during contraction. *The Japanese Journal of Physiology*, *48*(6), 421–438.

Krakauer, J., & Ghez, C. (2000). Voluntary movement. In *Principles of neural science* (Vol. 4, pp. 756–781). New York, NY: McGraw-Hill.

Kristeva, R., Patino, L., & Omlor, W. (2007). Beta-range cortical motor spectral power and corticomuscular coherence as a mechanism for effective corticospinal interaction during steady-state motor output. *NeuroImage*, *36*(3), 785–792.

Labeit, D., Watanabe, K., Witt, C., Fujita, H., Wu, Y., Lahmers, S., … Granzier, H. (2003). Calcium-dependent molecular spring elements in the giant protein titin. *Proceedings of the National Academy of Sciences of the United States of America*, *100*(23), 13716–13721.

Laine, C., Yavuz, U., & Farina, D. (2014). Task-related changes in sensorimotor integration influence the common synaptic input to motor neurones. *Acta Physiologica*, *211*(1), 229–239.

Lanir, Y. (1979). A structural theory for the homogeneous biaxial stress-strain relationships in flat collagenous tissues. *Journal of Biomechanics*, *12*(6), 423–436.

Lanir, Y. (1983). Constitutive equations for fibrous connective tissues. *Journal of Biomechanics*, *16*(1), 1–12.

Lateva, Z. C., McGill, K. C., & Johanson, M. E. (2002). Electrophysiological evidence of adult human skeletal muscle fibres with multiple endplates and polyneuronal innervation. *The Journal of Physiology*, *544*(2), 549–565.

Lawrence, D. G., Porter, R., & Redman, S. J. (1985). Corticomotoneuronal synapses in the monkey: Light microscopic localization upon motoneurons of intrinsic muscles of the hand. *Journal of Comparative Neurology*, *232*(4), 499–510.

Lee, E. H. (1969). Elastic-plastic deformation at finite strains. *Journal of Applied Mechanics*, *36*(1), 1.

Lee, S.-H., Sifakis, E., & Terzopoulos, D. (2009). Comprehensive biomechanical modeling and simulation of the upper body. *ACM Transactions on Graphics*, *28*(4), 99.

Leonard, T. R., DuVall, M., & Herzog, W. (2010). Force enhancement following stretch in a single sarcomere. *American Journal of Physiology-Cell Physiology*, *299*(6), C1398–C1401.

Leonard, T. R., & Herzog, W. (2010). Regulation of muscle force in the absence of actin-myosin-based cross-bridge interaction. *American Journal of Physiology-Cell Physiology*, *299*(1), C14–C20.

Levin, A., & Wyman, J. (1927). The viscous elastic properties of muscle. *Proceedings of the Royal Society of London B*, *101*(709), 218–243.

Lieber, R., & Fridén, J. (2000). Functional and clinical significance of skeletal muscle architecture. *Muscle & Nerve*, *23*, 1647–1666.

Lin, C.-C. K., & Crago, P. E. (2002a). Structural model of the muscle spindle. *Annals of Biomedical Engineering*, *30*(1), 68–83.

Lin, C.-C. K., & Crago, P. E. (2002b). Neural and mechanical contributions to the stretch reflex: A model synthesis. *Annals of Biomedical Engineering*, *30*(1), 54–67. https://doi.org/10.1114/1.1432692

Linke, W. A., Kulke, M., Li, H., Fujita-Becker, S., Neagoe, C., Manstein, D. J., … Fernandez, J. M. (2002). PEVK domain of titin: An entropic spring with actin-binding properties. *Journal of Structural Biology*, *137*(1–2), 194–205.

Lloyd, C. M., Lawson, J. R., Hunter, P. J., & Nielsen, P. F. (2008). The cellml model repository. *Bioinformatics*, *24*(18), 2122–2123.

Lloyd, D. G., & Besier, T. F. (2003a). An emg-driven musculoskeletal model to estimate muscle forces and knee joint moments in vivo. *Journal of Biomechanics*, *36*(6), 765–776.

Loeb, G., Pratt, C., Chanaud, C., & Richmond, F. (1987). Distribution and innervation of short, interdigitated muscle fibers in parallel-fibered muscles of the cat hindlimb. *Journal of Morphology*, *191*(1), 1–15.

Lowery, M. M., Stoykov, N. S., Taflove, A., & Kuiken, T. A. (2002). A multiple-layer finite-element model of the surface EMG signal. *IEEE Transactions on Biomedical Engineering*, *49*(5), 446–454.

MacIntosh, B. R., Gardiner, P. F., & McComas, A. J. (2006). *Skeletal muscle: Form and function* (2nd ed.). Champaign: Human Kinetics.

Magalhães, S. C., Kaelin-Lang, A., Sterr, A., do Prado, G. F., Eckeli, A. L., & Conforto, A. B. (2015). Transcranial magnetic stimulation for evaluation of motor cortical excitability in restless legs syndrome/Willis–ekbom disease. *Sleep Medicine*, *16*(10), 1265–1273.

Maltenfort, M. G., & Burke, R. (2003). Spindle model responsive to mixed fusimotor inputs and testable predictions of β feedback effects. *Journal of Neurophysiology*, *89*(5), 2797–2809.

Maltenfort, M. G., Heckman, C., & Rymer, W. Z. (1998). Decorrelating actions of renshaw interneurons on the firing of spinal motoneurons within a motor nucleus: A simulation study. *Journal of Neurophysiology*, *80*(1), 309–323.

Manuel, M., & Zytnicki, D. (2011). Alpha, beta and gamma motoneurons: Functional diversity in the motor system's final pathway. *Journal of Integrative Neuroscience*, *10*(03), 243–276.

Martins, J., Pires, E., Salvado, R., & Dinis, P. (1998). A numerical model of passive and active behavior of skeletal muscles. *Computer Methods in Applied Mechanics and Engineering*, *151*(3), 419–433 Containing papers presented at the Symposium on Advances in Computational Mechanics.

Maruyama, K. (1976). Connectin, an elastic protein from myofibrils. *The Journal of Biochemistry*, *80*(2), 405–407.

Maruyama, K., Matsubara, S., Natori, R., Nonomura, Y., Kimura, S., Ohashi, K., … Eguchi, G. (1977). Connectin, an elastic protein of muscle. *The Journal of Biochemistry*, *82*(2), 317–337.

McCulloch, A., Waldman, L., Rogers, J., & Guccione, J. (1992). Large-scale finite element analysis of the beating heart. *Critical Reviews in Biomedical Engineering*, *20*(5–6), 427–449.

McGill, K. C., & Lateva, Z. C. (2011). History dependence of human muscle-fiber conduction velocity during voluntary isometric contractions. *Journal of Applied Physiology*, *111*(3), 630–641.

Meier, P., & Blickhan, R. (2000). FEM-Simulation of Skeletal Muscle: The influence of inertia during activation and deactivation. In W. Herzog (Ed.), *Skeletal muscle mechanics: From mechanisms to function*, chapter 12 (pp. 207–233). Hoboken, NJ: John Wiley & Sons.

Melzer, W., Herrmann-Frank, A., & Lüttgau, H. C. (1995). The role of Ca2+ ions in excitation-contraction coupling of skeletal muscle fibres. *Biochimica et Biophysica Acta (BBA)-Reviews on Biomembranes*, *1241*(1), 59–116.

Merletti, R., & Parker, P. (2004). *Electromyography—Physiology, engineering, and noninvasive applications*. Piscataway, NJ: John Wiley & Sons.

Mesin, L. (2013). Volume conductor models in surface electromyography: Computational techniques. *Computers in Biology and Medicine*, *43*(7), 942–952.

Mesin, L., Joubert, M., Hanekom, T., Merletti, R., & Farina, D. (2006). A finite element model for describing the effect of muscle shortening on surface EMG. *IEEE Transactions on Biomedical Engineering*, *53*, 693–600.

Michael-Titus, A., Revest, P., & Shortland, P. (2010). 9—Motor systems i: Descending pathways and cerebellum. In A. Michael-Titus, P. Revest, & P. Shortland (Eds.), *The nervous system* (2nd ed., pp. 159–180). London, England: Churchill Livingstone.

Miehe, C., Schröder, J., & Schotte, J. (1999). Computational homogenization analysis in finite plasticity simulation of texture development in polycrystalline materials. *Computer Methods in Applied Mechanics and Engineering*, *171*(3–4), 387–418.

Miles, G., Dai, Y., & Brownstone, R. (2005). Mechanisms underlying the early phase of spike frequency adaptation in mouse spinal motoneurones. *The Journal of Physiology*, *566*(2), 519–532.

Miles, T., & Türker, K. (1986). Does reflex inhibition of motor units follow the "size principle"? *Experimental Brain Research*, *62*(2), 443–445.

Mileusnic, M. P., Brown, I. E., Lan, N., & Loeb, G. E. (2006). Mathematical models of proprioceptors. i. Control and transduction in the muscle spindle. *Journal of Neurophysiology*, *96*(4), 1772–1788.

Mileusnic, M. P., & Loeb, G. E. (2006). Mathematical models of proprioceptors. Ii. Structure and function of the golgi tendon organ. *Journal of Neurophysiology*, *96*(4), 1789–1802.

Monti, R. J., Roy, R. R., Hodgson, J. A., & Edgerton, V. R. (1999). Transmission of forces within mammalian skeletal muscles. *Journal of Biomechanics*, *32*(4), 371–380.

Mordhorst, M., Heidlauf, T., & Röhrle, O. (2015). Predicting electromyographic signals under realistic conditions using a multiscale chemo-electromechanical finite element model. *Interface Focus*, *5*(2), 20140076.

Mordhorst, M., Strecker, T., Wirtz, D., Heidlauf, T., & Röhrle, O. (2017). Pod-deim reduction of computational emg models. *Journal of Computational Science*, *19*, 86–96.

Morgan, D., Mochon, S., & Julian, F. (1982). A quantitative model of intersarcomere dynamics during fixed-end contractions of single frog muscle fibers. *Biophysical Journal*, *39*(2), 189–196.

Moritz, C. T., Barry, B. K., Pascoe, M. A., & Enoka, R. M. (2005). Discharge rate variability influences the variation in force fluctuations across the working range of a hand muscle. *Journal of Neurophysiology*, *93*(5), 2449–2459.

Morrow, D. A., Haut Donahue, T. L., Odegard, G. M., & Kaufman, K. R. (2010). Transversely isotropic tensile material properties of skeletal muscle tissue. *Journal of the Mechanical Behavior of Biomedical Materials*, *3*(1), 124–129.

Nagamori, A., Laine, C. M., & Valero-Cuevas, F. J. (2018). Cardinal features of involuntary force variability can arise from the closed-loop control of viscoelastic afferented muscles. *PLoS Computational Biology*, *14*(1), e1005884.

Nardinocchi, P., & Teresi, L. (2007). On the active response of soft living tissues. *Journal of Elasticity*, *88*(1), 27–39.

Nash, M. P., & Hunter, P. J. (2000). Computational mechanics of the heart. From tissue structure to ventricular function. *Journal of Elasticity*, *61*, 113–141.

Negro, F., & Farina, D. (2011). Decorrelation of cortical inputs and motoneuron output. *Journal of Neurophysiology*, *106*(5), 2688–2697.

Negro, F., & Farina, D. (2012). Factors influencing the estimates of correlation between motor unit activities in humans. *PLoS One*, *7*(9), e44894.

Negro, F., Yavuz, U. Ş., & Farina, D. (2016). The human motor neuron pools receive a dominant slow-varying common synaptic input. *The Journal of Physiology*, *594*(19), 5491–5505.

Nelson, M. E. (2005). Electrophysiological models. In S. H. Koslow & S. Subramaniam (Eds.), *Databasing the brain: From data to knowledge [Neuroinformatics]* (pp. 285–301). New York, NY: John Wiley & Sons.

Nie, X., Cheng, J.-I., Chen, W. W., & Weerasooriya, T. (2011). Dynamic tensile response of porcine muscle. *Journal of Applied Mechanics*, *78*(2), 021009.

Nishikawa, K. C., Monroy, J. A., Uyeno, T. E., Yeo, S. H., Pai, D. K., & Lindstedt, S. L. (2012). Is titin a 'winding filament'? A new twist on muscle contraction. *Proceedings of the Royal Society of London B: Biological Sciences*, *279*(1730), 981–990.

Noble, M. (1992). Enhancement of mechanical performance of striated muscle by stretch during contraction. *Experimental Physiology: Translation and Integration*, *77*(4), 539–552.

Pandy, M. G. (2001a). Computer modeling and simulation of human movement. *Annual Review of Biomedical Engineering*, *3*, 245–273.

Perreault, E. J., Heckman, C. J., & Sandercock, T. G. (2003). Hill muscle model errors during movement are greatest within the physiologically relevant range of motor unit firing rates. *Journal of Biomechanics*, *36*(2), 211–218.

Powers, R. K., & Binder, M. D. (1985). Distribution of oligosynaptic group I input to the cat medial gastrocnemius motoneuron pool. *Journal of Neurophysiology*, *53*(2), 497–517.

Powers, R. K., & Heckman, C. J. (2015). Contribution of intrinsic motoneuron properties to discharge hysteresis and its estimation based on paired motor unit recordings: A simulation study. *Journal of Neurophysiology*, *114*(1), 184–198.

Prado, L. G., Makarenko, I., Andresen, C., Krüger, M., Opitz, C. A., & Linke, W. A. (2005). Isoform diversity of giant proteins in relation to passive and active contractile properties of rabbit skeletal muscles. *The Journal of General Physiology*, *126*(5), 461–480.

Prochazka, A., & Gorassini, M. (1998). Models of ensemble firing of muscle spindle afferents recorded during normal locomotion in cats. *The Journal of Physiology*, *507*(1), 277–291.

Ramasamy, E., Avci, O., Dorow, B., Chong, S.-Y., Gizzi, L., Steidle, G., … Röhrle, O. (2018). An efficient modelling-simulation-analysis workflow to investigate stump-socket interaction using patient-specific, three-dimensional, continuum-mechanical, finite element residual limb models. *Frontiers in Bioengineering and Biotechnology*, *6*.

Ramsey, R. W., & Street, S. F. (1940). The isometric length-tension diagram of isolated skeletal muscle fibers of the frog. *Journal of Cellular and Comparative Physiology*, *15*(1), 11–34.

Rasmussen, J., Damsgaard, M., & Voigt, M. (2001). Muscle recruitment by the min/max criterion–a comparative numerical study. *Journal of Biomechanics*, *34*(3), 409–415.

Razumova, M. V., Bukatina, A. E., & Campbell, K. B. (1999). Stiffness-distortion sarcomere model for muscle simulation. *Journal of Applied Physiology*, *87*(5), 1861–1876.

Razumova, M. V., Bukatina, A. E., & Campbell, K. B. (2000). Different myofilament nearest neighbor interactions have distinctive effects on contractile bahavior. *Biophysical Journal*, *78*(6), 3120–3137.

Richmond, F. J., MacGillis, D. R., & Scott, D. A. (1985). Muscle-fiber compartmentalization in cat splenius muscles. *Journal of Neurophysiology*, *53*(4), 868–885.

Ríos, E., Karhanek, M., Ma, J., & González, A. (1993). An allosteric model of the molecular interactions of excitation-contraction coupling in skeletal muscle. *The Journal of General Physiology*, *102*(3), 449–481.

Rode, C., Siebert, T., & Blickhan, R. (2009). Titin-induced force enhancement and force depression: A 'sticky-spring' mechanism in muscle contractions? *Journal of Theoretical Biology*, *259*(2), 350–360.

Rode, C., Siebert, T., Tomalka, A., & Blickhan, R. (2016). Myosin filament sliding through the z-disc relates striated muscle fibre structure to function. *Proceedings of the Royal Society B: Biological Sciences*, *283*(1826), 20153030.

Röhrle, O. (2010). Simulating the electro-mechanical behavior of skeletal muscles. *Computing in Science & Engineering*, *12*(6), 48–57.

Röhrle, O., Davidson, J. B., & Pullan, A. J. (2008). Bridging scales: A three-dimensional electromechanical finite element model of skeletal muscle. *SIAM Journal on Scientific Computing*, *30*(6), 2882–2904.

Röhrle, O., Davidson, J. B., & Pullan, A. J. (2012). A physiologically based, multi-scale model of skeletal muscle structure and function. *Frontiers in Physiology*, *3*, 1–14.

Röhrle, O., Neumann, V., & Heidlauf, T. (2016). The role of parvalbumin, sarcoplasmatic reticulum calcium pump rate, rates of cross-bridge dynamics, and ryanodine receptor calcium current on peripheral muscle fatigue: A simulation study. *Computational and Mathematical Methods in Medicine*, *2016*, 1–14.

Röhrle, O., & Pullan, A. J. (2007). Three-dimensional finite element modelling of muscle forces during mastication. *Journal of Biomechanics*, *40*(15), 3363–3372.

Röhrle, O., Sprenger, M., Ramasamy, E., & Heidlauf, T. (2013). Multiscale skeletal muscle modeling: From cellular level to a multi-segment skeletal muscle model of the upper limb. In G. A. Holzapfel & E. Kuhl (Eds.), *Computer models in biomechanics* (pp. 103–116). the Netherlands: Springer.

Röhrle, O., Sprenger, M., & Schmitt, S. (2017). A two-muscle, continuum-mechanical forward simulation of the upper limb. *Biomechanics and Modeling in Mechanobiology*, *16*(3), 743–762.

Rossi, S., Ruiz-Baier, R., Pavarino, L. F., & Quarteroni, A. (2012). Orthotropic active strain models for the numerical simulation of cardiac biomechanics. *International Journal for Numerical Methods in Biomedical Engineering*, *28*(6–7), 761–788.

Sánchez, C. A., Lloyd, J. E., Fels, S., & Abolmaesumi, P. (2014). Embedding digitized fibre fields in finite element models of muscles. *Computer Methods in Biomechanics and Biomedical Engineering: Imaging & Visualization*, *2*(4), 223–236.

Sandercock, T. G., & Heckman, C. (1997). Force from cat soleus muscle during imposed locomotor-like movements: Experimental data versus Hill-type model predictions. *Journal of Neurophysiology*, *77*(3), 1538–1552.

Sandow, A. (1952). Excitation-contraction coupling in muscular response. *The Yale Journal of Biology and Medicine*, *25*(3), 176.

Sartori, M., Fernandez, J., Modenese, L., Carty, C., Barber, L., Oberhofer, K., … Lloyd, D. G. (2017). Toward modeling locomotion using electromyography-informed 3d models: Application to cerebral palsy. *WIREs Systems Biology and Medicine*, *9*(2), e1368.

Sartori, M., Reggiani, M., Farina, D., & Lloyd, D. G. (2012). Emg-driven forward-dynamic estimation of muscle force and joint moment about multiple degrees of freedom in the human lower extremity. *PLoS One*, *7*(12), e52618.

Sartori, M., Yavuz, U. Ş., & Farina, D. (2017). In vivo neuromechanics: Decoding causal motor neuron behavior with resulting musculoskeletal function. *Scientific Reports*, *7*(1), 13465.

Schmied, A., Pouget, J., & Vedel, J.-P. (1999). Electromechanical coupling and synchronous firing of single wrist extensor motor units in sporadic amyotrophic lateral sclerosis. *Clinical Neurophysiology*, *110*(5), 960–974.

Scholz, A., Sherman, M., Stavness, I., Delp, S., & Kecskeméthy, A. (2016). A fast multi-obstacle muscle wrapping method using natural geodesic variations. *Multibody System Dynamics*, *36*(2), 195–219.

Schröder, J. (2014). A numerical two-scale homogenization scheme: The FE^2-method. In J. Schröder & K. Hackl (Eds.), *Plasticity and beyond, volume 550 of CISM international centre for mechanical sciences* (pp. 1–64). Vienna, Austria: Springer.

Segev, I., Fleshman, J. W., & Burke, R. E. (1989). Compartmental models of complex neurons. In C. Koch & I. Segev (Eds.), *Methods in neuronal modeling* (pp. 63–96). Cambridge, MA: MIT Press.

Semmler, J. G. (2002). Motor unit synchronization and neuromuscular performance. *Exercise and Sport Sciences Reviews*, *30*(1), 8–14.

Shadmehr, R., Smith, M. A., & Krakauer, J. W. (2010). Error correction, sensory prediction, and adaptation in motor control. *Annual Review of Neuroscience*, *33*, 89–108.

Sharafi, B., & Blemker, S. S. (2010). A micromechanical model of skeletal muscle to explore the effects of fiber and fascicle geometry. *Journal of Biomechanics*, *43*(16), 3207–3213.

Sharafi, B., & Blemker, S. S. (2011). A mathematical model of force transmission from intrafascicularly terminating muscle fibers. *Journal of Biomechanics*, *44*(11), 2031–2039.

Sharifimajd, B., & Stålhand, J. (2013). A continuum model for skeletal muscle contraction at homogeneous finite deformations. *Biomechanics and Modeling in Mechanobiology*, *12*(5), 965–973.

Shields, R. K. (2002). Muscular, skeletal, and neural adaptations following spinal cord injury. *Journal of Orthopaedic & Sports Physical Therapy*, *32*(2), 65–74.

Shorten, P. R., O'Callaghan, P., Davidson, J. B., & Soboleva, T. K. (2007). A mathematical model of fatigue in skeletal muscle force contraction. *Journal of Muscle Research and Cell Motility*, *28*(6), 293–313.

Siebert, T., Rode, C., Herzog, W., Till, O., & Blickhan, R. (2008). Nonlinearities make a difference: Comparison of two common Hill-type models with real muscle. *Biological Cybernetics*, *98*(2), 133–143.

Smit, R. J. M., Brekelmans, W. A. M., & Meijer, H. E. H. (1998). Prediction of the mechanical behavior of nonlinear heterogeneous systems by multi-level finite element modeling. *Computer Methods in Applied Mechanics and Engineering*, *155*, 181–192.

Smith, N. P., Barclay, C. J., & Loiselle, D. S. (2005). The efficiency of muscle contraction. *Progress in Biophysics and Molecular Biology*, *88* (1), 1–58.

Song, D., Lan, N., Loeb, G. E., & Gordon, J. (2008). Model-based sensorimotor integration for multi-joint control: Development of a virtual arm model. *Annals of Biomedical Engineering*, *36*(6), 1033–1048. https://doi.org/10.1007/s10439-008-9461-8

Spyrou, L. A., Agoras, M., & Danas, K. (2017). A homogenization model of the voigt type for skeletal muscle. *Journal of Theoretical Biology*, *414*, 50–61.

Staudenmann, D., Roeleveld, K., Stegeman, D. F., & van Dieen, J. H. (2010). Methodological aspects of semg recordings for force estimation—A tutorial and review. *Journal of Electromyography and Kinesiology*, *20*(3), 375–387.

Stoecker, U., Telley, I. A., Stüssi, E., & Denoth, J. (2009). A multisegmental cross-bridge kinetics model of the myofibril. *Journal of Theoretical Biology*, *259*(4), 714–726.

Stone, M., Woo, J., Lee, J., Poole, T., Seagraves, A., Chung, M., … Blemker, S. S. (2018). Structure and variability in human tongue muscle anatomy. *Computer Methods in Biomechanics and Biomedical Engineering: Imaging & Visualization*, *6*(5), 499–507.

Street, S. F. (1983). Lateral transmission of tension in frog myofibers: A myofibrillar network and transverse cytoskeletal connections are possible transmitters. *Journal of Cellular Physiology*, *114*(3), 346–364.

Street, S. F., & Ramsey, R. W. (1965). Sarcolemma: Transmitter of active tension in frog skeletal muscle. *Science*, *149*(3690), 1379–1380.

Taber, L. A., & Perucchio, R. (2000). Modeling heart development. *Journal of Elasticity and the Physical Science of Solids*, *61*(1), 165–197.

Takaza, M., Moerman, K. M., Gindre, J., Lyons, G., & Simms, C. K. (2013). The anisotropic mechanical behaviour of passive skeletal muscle tissue subjected to large tensile strain. *Journal of the Mechanical Behavior of Biomedical Materials*, *17*, 209–220.

Taylor, A., Ellaway, P., Durbaba, R., & Rawlinson, S. (2000). Distinctive patterns of static and dynamic gamma motor activity during locomotion in the decerebrate cat. *The Journal of Physiology*, *529*(3), 825–836.

Taylor, A. M., & Enoka, R. M. (2004). Quantification of the factors that influence discharge correlation in model motor neurons. *Journal of Neurophysiology*, *91*(2), 796–814.

Thomas, C. K., Ross, B. H., & Stein, R. B. (1986). Motor-unit recruitment in human first dorsal interosseous muscle for static contractions in three different directions. *Journal of Neurophysiology*, *55*(5), 1017–1029.

Thompson, C. K., Negro, F., Johnson, M. D., Holmes, M. R., McPherson, L. M., Powers, R. K., … Heckman, C. J. (2018). Robust and accurate decoding of motoneuron behaviour and prediction of the resulting force output. *The Journal of Physiology*, *596*, 2643–2659.

Tian, M., Hoang, P. D., Gandevia, S. C., Herbert, R. D., & Bilston, L. E. (2011). Viscous elements have little impact on measured passive length-tension properties of human gastrocnemius muscle-tendon units in vivo. *Journal of Biomechanics*, *44*(7), 1334–1339.

Till, O., Siebert, T., Rode, C., & Blickhan, R. (2008). Characterization of isovelocity extension of activated muscle: A Hill-type model for eccentric contractions and a method for parameter determination. *Journal of Theoretical Biology*, *255*(2), 176–187.

Traub, R. D., & Miles, R. (1991). *Neuronal networks of the hippocampus*. New York, NY: Cambridge University Press.

Tuckwell, H. C. (2005). *Introduction to theoretical neurobiology: Volume 2, nonlinear and stochastic theories* (Vol. 8). Cambridge: Cambridge University Press.

Ulfhake, B., & Cullheim, S. (1988). Postnatal development of cat hind limb motoneurons. Iii: Changes in size of motoneurons supplying the triceps surae muscle. *Journal of Comparative Neurology*, *278*(1), 103–120.

Ushiyama, J., Masakado, Y., Fujiwara, T., Tsuji, T., Hase, K., Kimura, A., … Ushiba, J. (2012). Contraction level-related modulation of corticomuscular coherence differs between the tibialis anterior and soleus muscles in humans. *Journal of Applied Physiology*, *112*(8), 1258–1267.

Valentin, J., Sprenger, M., Pflüger, D., & Röhrle, O. (2018). Gradient-based optimization with b-splines on sparse grids for solving forward-dynamics simulations of three-dimensional, continuum-mechanical musculoskeletal system models. *International Journal for Numerical Methods in Biomedical Engineering*, *34*(5), e2965.

Vallbo, A. (1974). Human muscle spindle discharge during isometric voluntary contractions. Amplitude relations between spindle frequency and torque. *Acta Physiologica Scandinavica*, *90*(2), 319–336.

van Ingen Schenau, G. J., Bobbert, M. F., Ettema, G. J., de Graaf, J. B., & Huijing, P. A. (1988). A simulation of rat EDL force output based on intrinsic muscle properties. *Journal of Biomechanics*, *21*(10), 815–824.

Van Loocke, M., Lyons, C., & Simms, C. (2008). Viscoelastic properties of passive skeletal muscle in compression: Stress-relaxation behaviour and constitutive modelling. *Journal of Biomechanics*, *41*(7), 1555–1566.

Van Loocke, M., Lyons, C. G., & Simms, C. K. (2006). A validated model of passive muscle in compression. *Journal of Biomechanics*, *39*(16), 2999–3009.

Van Loocke, M., Simms, C., & Lyons, C. (2009). Viscoelastic properties of passive skeletal muscle in compression—Cyclic behaviour. *Journal of Biomechanics*, *42*(8), 1038–1048.

Virgilio, K. M., Martin, K. S., Peirce, S. M., & Blemker, S. S. (2015). Multiscale models of skeletal muscle reveal the complex effects of muscular dystrophy on tissue mechanics and damage susceptibility. *Interface Focus*, *5*(2), 1–10.

Wallinga, W., Meijer, S. L., Alberink, M. J., Vliek, M., Wienk, E. D., & Ypey, D. L. (1999). Modelling action potentials and membrane currents of mammalian skeletal muscle fibres in coherence with potassium concentration changes in the T-tubular system. *European Biophysics Journal*, *28*(4), 317–329.

Wang, K., McClure, J., & Tu, A. (1979). Titin: Major myofibrillar components of striated muscle. *Proceedings of the National Academy of Sciences of the United States of America*, *76*(8), 3698–3702.

Wang, Y. K., Nash, M. P., Pullan, A. J., Kieser, J. A., & Röhrle, O. (2013). Model-based identification of motion sensor placement for tracking retraction and elongation of the tongue. *Biomechanics and Modeling in Mechanobiology*, *12*(2), 383–399.

Watanabe, R. N., & Kohn, A. F. (2017). Nonlinear frequency-domain analysis of the transformation of cortical inputs by a motoneuron pool-muscle complex. *IEEE Transactions on Neural systems and Rehabilitation Engineering: A Publication of the IEEE Engineering in Medicine and Biology Society*, *25*(11), 1930–1939.

Watanabe, R. N., & Kohn, A. F. (2015). Fast oscillatory commands from the motor cortex can be decoded by the spinal cord for force control. *Journal of Neuroscience*, *35*(40), 13687–13697.

Watanabe, R. N., Magalhães, F. H., Elias, L. A., Chaud, V. M., Mello, E. M., & Kohn, A. F. (2013). Influences of premotoneuronal command statistics on the scaling of motor output variability during isometric plantar flexion. *Journal of Neurophysiology*, *110*(11), 2592–2606.

Williams, E. R., & Baker, S. N. (2009). Renshaw cell recurrent inhibition improves physiological tremor by reducing corticomuscular coupling at 10 hz. *Journal of Neuroscience*, *29*(20), 6616–6624.

Winslow, R. L., Rice, J., Jafri, S., & Marban, E. (1999). B. O' Rourke. Mechanisms of altered excitation-contraction coupling in canine tachycardia-induced heart failure, ii: Model studies. *Circulation Research*, *84*(5), 571–586.

Wu, T., Hung, A. P.-L., Hunter, P., & Mithraratne, K. (2013). Modelling facial expressions: A framework for simulating nonlinear soft tissue deformations using embedded 3d muscles. *Finite Elements in Analysis and Design*, *76*, 63–70.

Yao, W., Fuglevand, R. J., & Enoka, R. M. (2000). Motor-unit synchronization increases emg amplitude and decreases force steadiness of simulated contractions. *Journal of Neurophysiology*, *83*(1), 441–452.

Yavuz, U. Ş., Mrachacz-Kersting, N., Sebik, O., Berna Ünver, M., Farina, D., & Türker, K. S. (2013). Human stretch reflex pathways reexamined. *Journal of Neurophysiology*, *111*(3), 602–612.

Yavuz, U. Ş., Negro, F., Falla, D., & Farina, D. (2015). Experimental muscle pain increases variability of neural drive to muscle and decreases motor unit coherence in tremor frequency band. *Journal of Neurophysiology*, *114*(2), 1041–1047.

Young, M., Paul, A., Rodda, J., Duxson, M., & Sheard, P. (2000). Examination of intrafascicular muscle fiber terminations: Implications for tension delivery in series-fibered muscles. *Journal of Morphology*, *245*(2), 130–145.

Yucesoy, C. A., Koopman, B. H., Baan, G. C., Grootenboer, H. J., & Huijing, P. A. (2003). Effects of inter- and extramuscular myofascial force transmission on adjacent synergistic muscles: Assessment by experiments and finite-element modeling. *Journal of Biomechanics*, *36*(12), 1797–1811.

Yucesoy, C. A., Koopman, B. H., Huijing, P. A., & Grootenboer, H. J. (2002). Three-dimensional finite element modeling of skeletal muscle using a two-domain approach: Linked fiber-matrix mesh model. *Journal of Biomechanics*, *35*(9), 1253–1262.

Yuste, R., MacLean, J. N., Smith, J., & Lansner, A. (2005). The cortex as a central pattern generator. *Nature Reviews Neuroscience*, *6*(6), 477–483.

Zahalak, G. I. (1981). A distribution-moment approximation for kinetic theories of muscular contraction. *Mathematical Biosciences*, *55*(1), 89–114.

Zajac, F. E. (1989). Muscle and tendon: Properties, models, scaling, and application to biomechanics and motor control. *Critical Reviews in Biomedical Engineering*, *17*(4), 359–411.

Zarifi, O., & Stavness, I. (2017). Muscle wrapping on arbitrary meshes with the heat method. *Computer Methods in Biomechanics and Biomedical Engineering*, *20*(2), 119–129.

Zienkiewicz, O. C., Taylor, R. L., & Zhu, J. Z. (2005). *The finite element method: Its basis and fundamentals* (Vol. 1). Oxford: Butterworth-Heinemann.

Zuurbier, C. J., & Huijing, P. A. (1992). Influence of muscle geometry on shortening speed of fibre, aponeurosis and muscle. *Journal of Biomechanics*, *25*(9), 1017–1026.

SUPPORTING INFORMATION

Additional supporting information may be found online in the Supporting Information section at the end of this article.

How to cite this article: Röhrle O, Yavuz UŞ, Klotz T, Negro F, Heidlauf T. Multiscale modeling of the neuromuscular system: Coupling neurophysiology and skeletal muscle mechanics. *WIREs Syst Biol Med*. 2019;e1457. https://doi.org/10.1002/wsbm.1457